NASA TN D-1789

TECHNICAL NOTE

D-1789

AERODYNAMIC CHARACTERISTICS OF TOWED SPHERES, CONICAL RINGS, AND CONES USED AS DECELERATORS AT MACH NUMBERS FROM 1.57 TO 4.65

By Nickolai Charczenko

Langley Research Center
Langley Station, Hampton, Va.

NATIONAL AERONAUTICS AND SPACE ADMINISTRATION
WASHINGTON
April 1963

NATIONAL AERONAUTICS AND SPACE ADMINISTRATION

TECHNICAL NOTE D-1789

AERODYNAMIC CHARACTERISTICS OF TOWED SPHERES, CONICAL RINGS, AND CONES USED AS DECELERATORS AT MACH NUMBERS FROM 1.57 TO 4.65

By Nickolai Charczenko

SUMMARY

An investigation was made to determine the drag and stability characteristics of spheres, conical rings, cones, and modified cones when towed in the wake of several space-vehicle configurations. The tests were made over a Mach number range of 1.57 to 4.65 with variation in the following parameters: Reynolds number, trailing distance, ratio of decelerator base diameter to space-vehicle base diameter, cone angle, and size of disk added to the base of a cone.

There are three stability regions for a decelerator in the wake of a vehicle: (a) in close proximity to the vehicle base (for decelerators having diameter larger than the space-vehicle base diameter, portions of decelerator are in supersonic flow) the decelerator may be stable; (b) at slightly longer trailing distances, where the decelerator is entirely in a subsonic wake, it is unstable; and (c) at still longer trailing distances, where the decelerator is essentially fully exposed to supersonic flow, it is stable subject only to geometry limitations. In the flow behind a space vehicle the drag coefficient for a decelerator is closely related to its stability characteristics in that the drag values are greater where a decelerator is stable. The 80° cone with an attached disk whose diameter is 10 percent larger than the base diameter of the cone has the highest drag coefficient values of any of the stable decelerators tested in this series. Considerable increase in drag-coefficient values can be obtained by increasing the ratio of the decelerator base diameter to the space-vehicle base diameter.

INTRODUCTION

The investigation discussed herein is part of an overall program to study possible decelerator configurations capable of providing satisfactory deceleration performance at supersonic speeds. Such decelerators would be employed for the recovery of spacecraft, launch vehicles, and other high-speed vehicles. Parachutes, balloons, retro-rockets, conical rings, and cones are some of the drag devices that are being considered as decelerators. (See refs. 1 to 4.) All of these drag devices have certain advantages and disadvantages, and the

final selection for a particular application will be based upon such factors as weight, drag coefficient, stability, and simplicity of design.

The recovery of space vehicles by the use of trailing decelerators has created a new requirement for a decelerator in that it has to perform satisfactorily at very high altitudes and supersonic speeds. Even though the lift-drag type of configurations may be the most likely choice for many of the recovery operations in the future, their development will take time. In the meantime, trailing decelerators will find many uses, and in addition, trailing drag devices will probably find many continuing applications in the future primarily because of their simplicity. One of the nonlifting-type drag devices which has been used extensively with great success at subsonic speeds is the parachute, but its application at supersonic speeds has been limited because of its instability (ref. 1). Only recently have parachute configurations been developed that show promise of extending parachute operations through the supersonic speed range; however, in tests of parachutes in free flight, limited success has been attained only up to $M_\infty = 2.00$. Thus there is a need for further investigation with parachutes or other drag devices that could fulfill the decelerator requirements in the supersonic speed range.

Wind-tunnel tests indicate considerable promise for both towed balloons (ref. 2) and cones (ref. 3) as decelerators at supersonic speeds. With this in mind a group of decelerators - spheres, conical rings, cones, and modified cones - were tested in the wake of several possible spacecraft configurations through a Mach number range of 1.57 to 4.65 to provide basic drag data and obtain some indication of their stability.

SYMBOLS

a length of decelerator, in.

C_D drag coefficient, $\frac{D}{q_\infty S}$

D decelerator drag, lb

d base diameter of space vehicle, in.

d_c reference (maximum) diameter of decelerator, in.

d_f diameter as indicated in figure 4

$\frac{d_c - d_f}{d_f} \times 100$ percentage increase in base diameter of decelerator due to disk

l tow-cable length, in.

l/d trailing distance in terms of space-vehicle base diameters (for space vehicle C, base diameter was taken to be 7.0 in.)

M_∞ free-stream Mach number

q_∞ free-stream dynamic pressure, lb/sq ft

r radius

S reference area (based on maximum cross-sectional area of decelerator), sq ft

θ decelerator cone angle, deg

δ deflection angle of flap with respect to center line of space vehicle C, deg

WIND TUNNEL

The tests were conducted in the Langley Unitary Plan wind tunnel, which is a variable-pressure return-flow tunnel. The tunnel has two test sections which are 4 feet square and approximately 7 feet in length. The nozzles leading to the test sections are asymmetric sliding-block-type nozzles which allow the Mach number to be varied continuously through a range from 1.5 to 2.8 in one test section and from 2.3 to 4.65 in the other. Further details of the wind tunnel may be found in reference 5.

MODELS

A sketch and photographs of the test setup are shown in figure 1. The space vehicle is supported in the center of the tunnel by two thin struts spanning the tunnel in the horizontal plane.

Shown in figure 2 is a sketch of the three space vehicles used in this investigation. They will be referred to hereafter as space vehicles A, B, and C as indicated in the drawing. Space vehicles A and B are both bodies of revolution with identical forebodies. They differ in length and type of afterbody, one having a cylindrical and the other a flared afterbody. Vehicles A and B contained an internal strain-gage balance to which a motor-driven drum was attached as indicated in figure 3. By means of this motor-driven drum the 1/16-inch steel tow cable could be shortened or lengthened remotely.

The third vehicle is a blunt 30° half-cone reentry configuration with a flat upper surface. At the base it has six flaps, as indicated in figure 2, which can be deflected 60° with respect to the center line of the model.

Spheres, conical rings, cones, and modified cones were used as trailing decelerators in this investigation. Dimensions and variables for these models are given in figure 4. Materials and construction details are shown in figure 5. The trip fence was put on the spheres primarily because it is needed at subsonic speeds to improve stability. However, its contribution to stability or drag at supersonic speeds is insignificant.

A line was attached to the rear of all decelerators as shown in figures 1(b) and 1(c) to stabilize the decelerator during starting and stopping of the tunnel and also to prevent the decelerator from striking the test-section wall if it became unstable.

TESTS AND ACCURACIES

The tests were made over a Mach number range from 1.57 to 4.65 at various Reynolds numbers as indicated in table I. For tests to determine the Reynolds number effect, variation in Reynolds number was achieved by changing the stagnation pressure.

The accuracy of the individual quantities is estimated to be within the following limits:

l, in.	±0.5
M_∞ (1.57 to 3.50)	±0.015
M_∞ (3.96 to 4.65)	±0.050
D, lb	±0.50

RESULTS AND DISCUSSION

Stability

The term "stable" as used herein refers to the dynamic behavior of a particular decelerator; it means that any oscillating motion caused by a disturbance dies out or that the decelerator oscillates with an amplitude of less than approximetaly 10 percent of the trailing distance (based on visual observation). The 10-percent oscillation was arbitrarily set as a limit.

The stability of rigid-type decelerators in the wake of vehicles is dependent primarily on two items: (1) the flow field around the decelerator and (2) the geometry of the decelerator.

A decelerator behind a vehicle at supersonic free-stream velocities has been regarded as having stable characteristics for long trailing distances (decelerator in supersonic flow field) and unstable characteristics for short trailing distances (decelerator in subsonic flow field). (See refs. 3 and 6.) The current tests indicate still another region with stable decelerator characteristics the very short trailing distance, at which a large enough body (decelerator) is

partly in a subsonic and partly in a supersonic flow field. The amount of the decelerator that must be exposed to the supersonic flow in order to produce a stable configuration is not, at present, defined. These three types of flow fields that may exist for a decelerator in the wake of a vehicle are illustrated in figure 6.

The dependence of stability on the geometry of a decelerator is well recognized. For example, towed cones with apex angles up to 80° were found to be stable in a supersonic flow field (ref. 3); however, those having an apex angle of 90° or larger were unstable. Similar results were observed with conical rings in the present investigation. A modified 60° cone (see fig. 4) was very stable when a/d_c was 0.547, but when this ratio was decreased to 0.291 the cone became marginally stable. Also, an 80° cone, which was stable with a disk whose diameter was 10 percent larger than the base diameter of the cone, became unstable when the disk diameter was increased to 15 percent. There were no noticeable effects on the stability of the spheres due to the trip fence.

It should be noted that the bow-shock fluctuations, which present a serious problem for parachute operation at supersonic speeds (ref. 1), also exist with rigid-type bodies having blunt frontal areas such as spheres or 60° modified cones, but the bow shock has little influence on their stability.

Drag Characteristics

The basic drag-coefficient data, and schlieren photographs of the associated flow fields for some of the drag devices, are presented in figures 7 to 20. A comparison of the drag coefficients for the various stable decelerators tested is made in figure 21.

The effects of Reynolds number were determined for the 80° cone towed behind space vehicles A and B. The results, presented in figure 7, show that at $M_\infty = 2.30$ a change in Reynolds number causes a sizable divergence of drag coefficient with decreasing l/d. The Reynolds number has little effect on drag coefficient at other test Mach numbers except for the 80° cone in the wake of space vehicle B at a Mach number of 3.50.

The drag of a decelerator is dependent on the type of flow field it is in, as was previously discussed, which is closely related to the trailing distances. High drag-coefficient values are obtained for long trailing distances and low drag-coefficient values are obtained for short trailing distances. This phenomenon is illustrated in figure 9, where typical schlieren photographs are superimposed on a drag-coefficient plot for a 6-inch sphere in the wake of space vehicle B at a Mach number of 3.96. It may be seen that the lower drag-coefficient values are obtained for the short trailing distances, where the sphere is in the subsonic wake of the vehicle, whereas the higher drag-coefficient values are obtained when a significant portion of the sphere is in a supersonic flow field. A transition region is also illustrated in figure 9 where either high or low drag coefficients may be obtained for the 6-inch sphere at l/d values from about 2.65 to 3.1, depending on the direction from which the decelerator approaches this region as indicated by the arrows. At very short trailing

distances where the decelerator is partially in subsonic and partially in supersonic flow fields it has intermediate drag-coefficient values, as can be seen from figure 8(a). It should be pointed out that drag values were not obtained for some of the configurations at short trailing distances because of violent oscillations of the decelerator.

The data of figure 8(b) show that for a given space vehicle, the larger the sphere the greater the trailing distance at which the transition occurs from one type of flow to the other. Inspection of the schlieren photographs in figure 10 shows that as the sphere approaches the space vehicle, the bow shock wave of the sphere affects the trailing shock wave from the space vehicle. Where the effect of the bow shock becomes strong enough, the trailing shock spreads farther out from the center of the wake, allowing portions of the decelerator to be in subsonic flow. Then, with decreasing trailing distance, at some point there is a sudden change to a completely subsonic wake. Further decrease in trailing distance, for a sphere that is large in comparison with the base area of the space vehicle, leads to a condition in which an appreciable portion of the sphere emerges into the supersonic stream. The effect of the bow wave of a small sphere is not felt by the trailing shock of a vehicle as soon as that of a larger sphere. Thus the transition for the larger spheres occurs at larger trailing distances.

The effect of the relative sizes of the sphere and space vehicle on the drag coefficient is shown in figure 8. For example, in figure 8(b) at $M_\infty = 3.50$, increasing d_c/d from 0.73 to 1.45 increases C_D by as much as 33 percent. This result would be expected because a smaller percentage of a large decelerator is acted upon by the wake from the space vehicle and tow cable. Further indications of the effect of the vehicle wake on the drag coefficient of a decelerator are seen in figure 8(c), since there is an appreciable reduction in decelerator drag when the control surfaces on the space vehicle are deflected. A comparison between the data of figures 8(a) and 8(b), on the other hand, shows that for a given sphere size and tow-cable length the drag coefficients behind space vehicle A are lower at some Mach numbers than those behind vehicle B. This result is opposite to the above trend concerning wake size but an explanation can be obtained from figure 11. This figure shows the decelerator bow wave much farther in front of the sphere for space vehicle A than for space vehicle B. This difference is primarily due to the method of attachment of the spheres to the tow line (see fig. 5). In either case the attachment method was not completely uniform throughout the tests and may have varied somewhat from one decelerator to another; however, the swivel on the tow cable causes a more forward separation of the shock and results in a more oblique shock wave. The more oblique shock structure for the decelerator behind space vehicle A will necessarily lead to lower pressures and, of course, lower drag coefficients for this configuration in comparison with the one behind space vehicle B. Thus the method of attachment is an important factor in obtaining maximum drag for a given decelerator in a supersonic stream.

Up to this point, only spheres have been used to illustrate the drag-coefficient characteristics of decelerators. However, the foregoing discussion is, in general, applicable to all decelerators in this investigation.

The drag-coefficient data of figure 12 indicate that conical rings may be effective drag devices since they have relatively large drag coefficients. In addition, the conical ring may be carried with little or no weight penalty in the form of an interstage fairing. In the case of the conical-ring decelerator with $d_c/d = 2.05$ and $d_f/d = 1.39$, there is little or no drag-coefficient decrement with decrease in two-line length. This result indicates that there is no influence of vehicle wake on the decelerator and little or no effect of decelerator bow wave on the trailing wake of the vehicle. This relatively constant drag-coefficient value with trailing distance is believed to prevail for d_f/d values down to only a little greater than 1.

Tests performed on a series of modified 60° and 80° cones with and without base disks (figs. 14 and 15) show that the largest drag coefficients of a stable configuration were obtained for an 80° cone with a disk whose diameter was 10 percent larger than the cone base diameter. Although larger drag-coefficient values could be obtained with a disk having a diameter 15 percent larger than the cone base diameter, as indicated in figure 15(b) at $M_\infty = 2.00$, this configuration was very unstable. It should be noted that at some Mach numbers the drag coefficient of an 80° cone was increased by as much as 45 percent by addition of a disk having a diameter 10 percent larger than the base diameter of the cone.

The variation of drag coefficient with Mach number for various l/d values is cross plotted in figures 17 to 20 for the convenience of the reader. In general higher drag-coefficient values were obtained at lower supersonic speeds.

Shown in figure 17(c) are supersonic data along with some previously unpublished subsonic data (obtained from tests in the Langley 8-foot transonic pressure tunnel) for spheres in the wake of space vehicle C. This figure shows considerably lower drag-coefficient values for spheres at subsonic Mach numbers.

A comparison between the drag-coefficient values for the various stable decelerators investigated is made in figure 21. The 80° cone with a disk whose diameter is 10 percent larger than the cone base diameter has the highest drag coefficients throughout the test Mach number range. Even though drag is not the only consideration in choosing a decelerator for a specific mission, large drag does represent a wider margin in trade-off with such factors as reduction in size of decelerator, which essentially means reduction in weight.

CONCLUSIONS

A wind-tunnel investigation to determine the drag and dynamic behavior of spheres, conical rings, cones, and modified cones towed as decelerators in the wake of space vehicles at supersonic speeds leads to the following conclusions:

1. The stability of rigid-type decelerators in the wake of vehicles is dependent primarily on two items: the flow field around the decelerator and the geometry of the decelerator.

2. From visual observations in the course of this investigation it was established that in general there are three stability regions for a decelerator in the wake of a vehicle: (a) in close proximity to the vehicle base (for decelerators having diameter larger than the space-vehicle base diameter, portions of decelerator are in supersonic flow) the decelerator may be stable; (b) at slightly longer trailing distances, where the decelerator is entirely in a subsonic wake, it is unstable; and (c) at still longer trailing distances, where the decelerator is essentially fully exposed to supersonic flow, it is again stable subject only to geometry limitations.

3. In the flow behind a space vehicle the drag coefficient for a decelerator is closely related to its stability characteristics in that the drag values are greater where a decelerator is stable.

4. The 80° cone with an attached disk whose diameter is 10 percent greater than the base diameter of the cone has the highest drag-coefficient values of any of the stable decelerators tested in this series.

5. Considerable increase in drag-coefficient values can be obtained by increasing the ratio of the decelerator base diameter to the space-vehicle base diameter.

Langley Research Center,
National Aeronautics and Space Administration,
Langley Station, Hampton, Va., February 14, 1963.

REFERENCES

1. Maynard, Julian D.: Aerodynamic Characteristics of Parachutes at Mach Numbers From 1.6 to 3. NASA TN D-752, 1961.

2. McShera, John T., and Keyes, J. Wayne: Wind-Tunnel Investigation of a Balloon as a Towed Decelerator at Mach Numbers From 1.47 to 2.50. NASA TN D-919, 1961.

3. Charczenko, Nickolai, and McShera, John T.: Aerodynamic Characteristics of Towed Cones Used as Decelerators at Mach Numbers From 1.57 to 4.65. NASA TN D-994, 1961.

4. Charczenko, Nickolai, and Hennessey, Katherine W.: Investigation of a Retrorocket Exhausting From the Nose of a Blunt Body Into a Supersonic Free Stream. NASA TN D-751, 1961.

5. Anon.: Manual for Users of the Unitary Plan Wind Tunnel Facilities of the National Advisory Committee for Aeronautics. NACA, 1956.

6. Coats, Jack D.: Static and Dynamic Testing of Conical Trailing Decelerators for the Pershing Re-Entry Vehicle. AEDC-TN-60-188 (Contract No. AF 40(600)-800 S/A 11(60-110)), Arnold Eng. Dev. Center, Oct. 1960.

TABLE I.- TEST CONDITIONS

Decelerator	Mach number	Space vehicle A			Space vehicle B			Space vehicle C		
		Dynamic pressure, lb/sq ft	Reynolds number per foot	l/d range	Dynamic pressure, lb/sq ft	Reynolds number per foot	l/d range	Dynamic pressure, lb/sq ft	Reynolds number per foot	l/d range
4-inch sphere	2.00	257	1.16×10^6	2.0-12.0	260	1.17×10^6	2.0-6.0	260	1.17×10^6	2.0-5.0
	2.50	185	.85	2.0-12.0	185	.85	2.0-6.0	185	.85	2.0-5.0
	2.87	137	.70	2.0-12.0	138	.70	2.0-6.0	138	.70	2.0-5.0
	3.00	149	.78	2.0-12.0	149	.78	3.3-6.3	---	---	---
	3.50	162	1.00	2.0-12.0	162	1.00	1.5-6.3	---	---	---
	3.96	154	1.05	2.0-13.0	154	1.05	1.5-6.3	---	---	---
	4.65	126	1.09	2.0-13.0	126	1.09	1.5-6.3	---	---	---
6-inch sphere	2.00	258	1.16×10^6	2.0-12.0	260	1.17×10^6	2.0-6.0	260	1.17×10^6	2.0-4.0
	2.50	185	.85	2.0-12.0	185	.85	2.0-6.0	185	.85	2.0-5.0
	2.87	137	.70	2.0-12.0	139	.70	2.0-6.0	138	.70	3.0-5.0
	3.00	148	.78	2.0-12.0	147	.78	1.0-6.0	---	---	---
	3.50	162	1.00	2.0-12.0	161	1.00	1.0-6.0	---	---	---
	3.96	154	1.05	2.0-12.0	154	1.05	1.0-6.0	---	---	---
	4.65	126	1.09	2.0-12.0	126	1.09	1.0-6.0	---	---	---
8-inch sphere	2.00	259	1.17×10^6	2.0-10.0	258	1.16×10^6	3.0-4.0	259	1.17×10^6	3.0-4.0
	2.30	---	---	---	213	.94	4.0	---	---	---
	2.50	185	.85	2.0-12.0	185	.85	2.0-6.0	185	.85	3.0-5.0
	2.70	---	---	---	157	.76	4.0	---	---	---
	2.87	138	.70	2.0-12.0	137	.70	2.0-6.0	138	.70	3.0-5.0
	2.90	---	---	---	158	.81	4.0	---	---	---
	3.00	148	.78	4.0-12.0	148	.78	1.0-6.0	---	---	---
	3.20	---	---	---	146	.82	4.0	---	---	---
	3.40	---	---	---	159	.95	4.0	---	---	---
	3.50	162	1.00	4.0-12.0	162	1.00	1.0-6.0	---	---	---
	3.70	---	---	---	150	1.00	4.0	---	---	---
	3.96	154	1.05	6.0-12.0	154	1.05	1.0-6.0	---	---	---
	4.20	---	---	---	153	1.14	4.0	---	---	---
	4.40	---	---	---	145	1.16	4.0	---	---	---
	4.65	126	1.09	2.0-12.0	126	1.09	1.0-6.0	---	---	---
60° conical ring	1.57	306	1.18×10^6	2.0-6.0	---	---	---	---	---	---
	2.00	255	1.16	2.0-12.0	262	1.18×10^6	1.7-6.0	258	1.17×10^6	2.0-5.0
	2.50	185	.85	2.0-12.0	185	.85	1.7-6.0	185	.85	2.0-5.0
	2.87	137	.70	2.0-12.0	139	.70	2.0-6.0	138	.70	2.0-4.0
70° conical ring	1.57	306	1.18×10^6	2.0-6.0	---	---	---	---	---	---
	2.00	256	1.16	2.0-12.0	259	1.17×10^6	3.0-6.0	259	1.17×10^6	3.0-5.0
	2.50	185	.85	2.0-12.0	185	.85	2.0-6.0	185	.85	3.0-5.0
	2.87	138	.70	2.0-12.0	139	.70	2.0-6.0	138	.70	3.0-5.0
80° conical ring	2.00	260	1.17×10^6	2.0-12.0	---	---	---	260	1.17×10^6	3.0-5.0
	2.30	---	---	---	214	0.95	4.0	---	---	---
	2.50	185	.85	2.0-12.0	185	.85	3.0-6.0	185	.85	3.0-5.0
	2.70	---	---	---	159	.77	4.0	---	---	---
	2.87	138	.70	2.0-12.0	139	.70	2.0-6.0	138	.70	3.0-5.0
	2.90	---	---	---	161	.77	4.0	---	---	---
	3.00	149	.78	2.0-12.0	149	.78	2.0-6.0	---	---	---
	3.20	---	---	---	146	.82	4.0	---	---	---
	3.40	---	---	---	159	.95	4.0	---	---	---
	3.50	162	1.00	2.0-12.0	162	1.00	2.5-6.0	---	---	---
	3.70	---	---	---	150	.99	4.0	---	---	---
	3.96	154	1.05	2.0-12.0	154	1.05	2.0-6.0	---	---	---
	4.20	---	---	---	153	1.14	4.0	---	---	---
	4.40	---	---	---	145	1.16	4.0	---	---	---
	4.65	126	1.09	2.0-12.0	126	1.09	2.0-6.0	---	---	---
90° conical ring	2.00	260	1.17×10^6	2.0-12.0	259	1.17×10^6	3.0-6.0	---	---	---
	2.50	185	.85	2.0-12.0	186	.85	4.0-6.0	---	---	---
	2.87	---	---	---	138	.70	2.0-6.0	---	---	---

TABLE I.- TEST CONDITIONS - Concluded

Decelerator	Mach number	Space vehicle A			Space vehicle B			Space vehicle C		
		Dynamic pressure, lb/sq ft	Reynolds number per foot	l/d range	Dynamic pressure, lb/sq ft	Reynolds number per foot	l/d range	Dynamic pressure, lb/sq ft	Reynolds number per foot	l/d range
80° cone	2.00	258	1.16×10^6	4.0-12.0	---	---	---	---	---	---
	2.30	215	.95	4.0-12.0	213	0.94×10^6	3.0-6.0	---	---	---
	2.30	440	1.95	4.0-12.0	440	1.95	3.0-6.0	---	---	---
	2.50	---	1.95	---	185	.85	3.0-6.0	---	---	---
	2.50	---	---	---	468	2.16	3.0-6.0	---	---	---
	3.00	245	1.30	4.0-13.0	148	.78	1.0-6.0	---	---	---
	3.00	469	2.47	2.0-13.0	469	2.47	1.0-6.0	---	---	---
	3.50	161	1.00	4.0-13.0	162	1.00	2.0-6.0	---	---	---
	3.50	534	3.30	4.0-13.0	534	3.30	2.7-6.0	---	---	---
	3.96	154	1.05	4.0-14.8	154	1.05	1.0-6.0	---	---	---
	3.96	476	3.24	6.0-13.0	276	1.87	1.0-6.0	---	---	---
	4.65	126	1.09	2.0-15.9	126	1.09	1.0-6.0	---	---	---
	4.65	460	3.99	4.0-13.0	297	2.57	1.0-6.0	---	---	---
80° cone with 5-percent disk	2.00	260	1.17×10^6	6.0-12.0	258	1.16×10^6	3.2-6.7	---	---	---
	2.30	256	1.14	6.0-14.8	213	.95	4.0	---	---	---
	2.50	---	---	---	184	.85	4.0	---	---	---
	2.70	---	---	---	158	.78	4.0	---	---	---
	2.90	---	---	---	160	.78	4.0	---	---	---
	3.00	148	.78	2.0-12.0	149	.78	2.0-6.0	---	---	---
	3.20	---	---	---	146	.82	4.0	---	---	---
	3.40	---	---	---	159	.95	4.0	---	---	---
	3.50	162	1.00	4.0-12.0	162	1.00	2.0-6.0	---	---	---
	3.70	---	---	---	149	.93	4.0	---	---	---
	3.96	154	1.05	4.0-12.0	154	1.05	2.0-6.0	---	---	---
	4.20	---	---	---	153	1.07	4.0	---	---	---
	4.40	---	---	---	145	1.16	4.0	---	---	---
	4.65	126	1.09	2.0-12.0	126	1.09	2.0-6.0	---	---	---
80° cone with 10-percent disk	2.00	260	1.17×10^6	6.0-12.0	260	1.17×10^6	3.2-6.8	---	---	---
	2.30	228	1.01	6.0-12.0	214	.95	3.0-6.0	---	---	---
	2.50	---	---	---	185	.85	3.0-6.0	---	---	---
	3.00	145	.85	4.0-14.0	148	.78	2.0-6.0	---	---	---
	3.50	---	---	---	162	1.00	3.0-6.0	---	---	---
	3.96	154	1.05	6.0-13.0	154	1.05	4.0-6.0	---	---	---
	4.65	126	1.09	6.0-13.0	126	1.09	4.0-6.0	---	---	---
80° cone with 15-percent disk	2.00	---	---	---	165	0.74	4.0-4.9	---	---	---
60° modified cone (a = 2.67)	2.00	257	1.16×10^6	2.0-12.0	258	1.16×10^6	2.0-6.0	260	1.17×10^6	2.0-6.0
	2.50	185	.85	2.0-12.0	185	.85	2.0-6.0	185	.85	2.0-5.0
	2.87	137	.70	2.0-12.0	138	.70	2.0-6.0	137	.70	2.0-5.0
60° modified cone (a = 2.05)	2.00	260	1.17×10^6	2.0-12.0	260	1.17×10^6	2.0-6.0	260	1.17×10^6	3.0-5.0
	2.50	186	.85	2.0-12.0	186	.85	2.0-6.0	185	.85	3.0-5.0
	2.87	137	.70	2.4-12.2	139	.70	2.0-6.0	137	.70	3.0-5.0
60° modified cone (a = 1.42)	2.00	260	1.17×10^6	5.0-12.5	---	---	---	---	---	---
	2.50	186	.85	5.0-10.5	---	---	---	---	---	---
	2.87	137	.70	2.7-10.5	---	---	---	---	---	---
60° modified cone (a = 2.67) with 10-percent disk	2.00	258	1.16×10^6	4.0-12.0	---	---	---	---	---	---

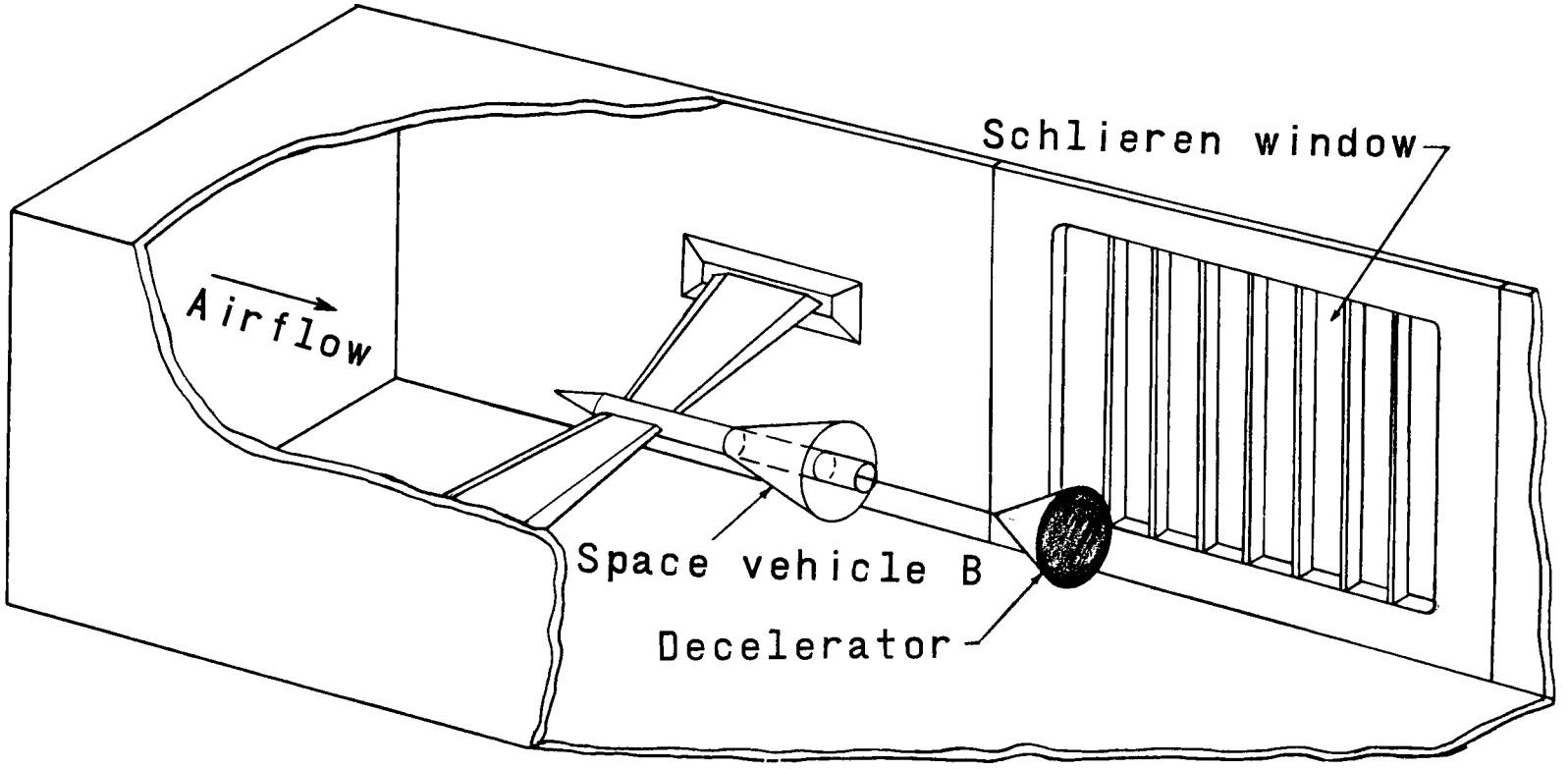

(a) Sketch of space vehicle B mounted on a strut.

Figure 1.- Test section with space-vehicle support system.

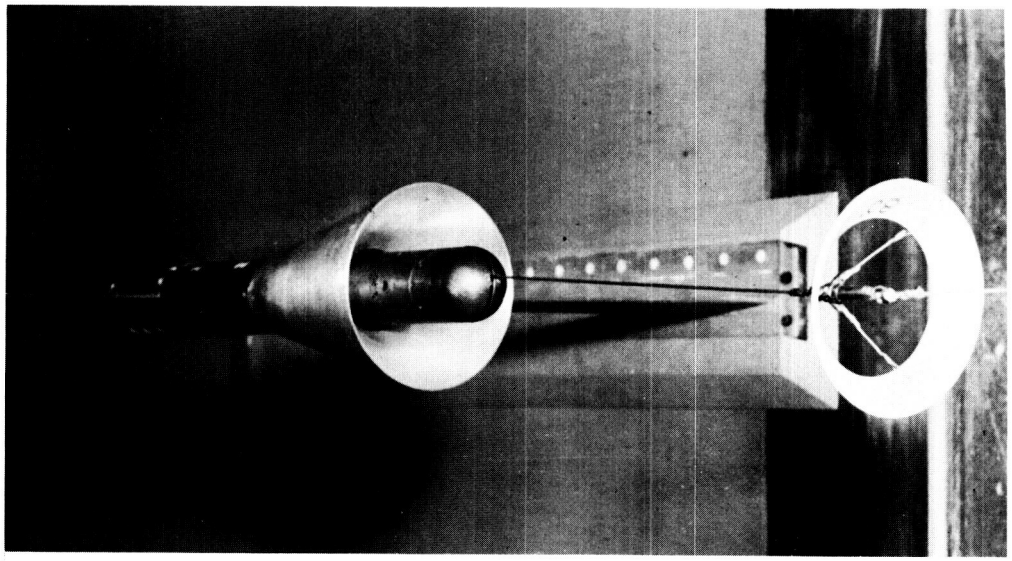

L-61-6188

(b) Space vehicle B mounted on a strut with 80° conical ring attached.

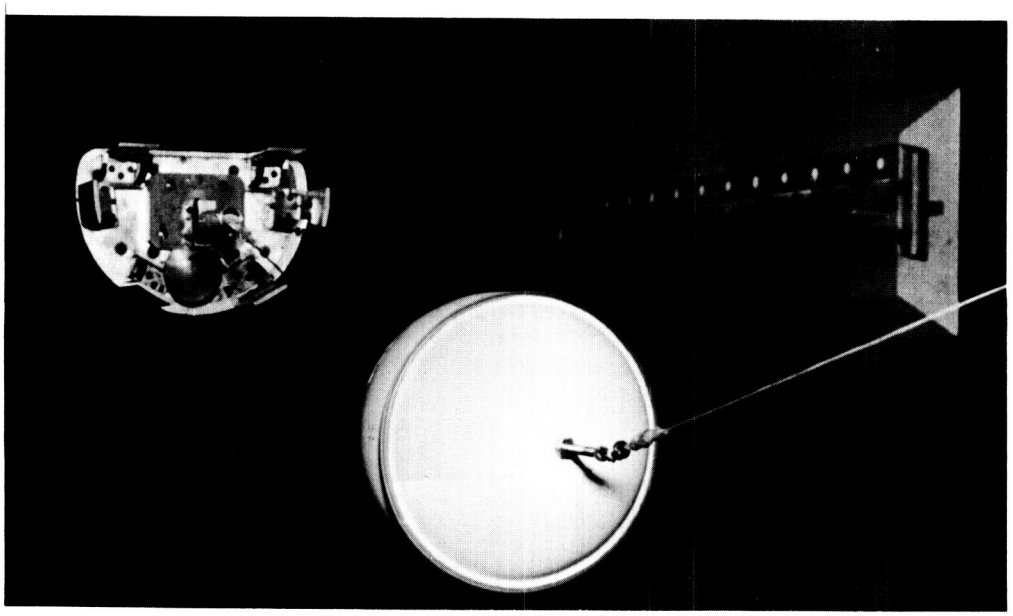

L-61-6186

(c) Space vehicle C mounted on a strut with 8-inch sphere attached.

Figure 1.- Concluded.

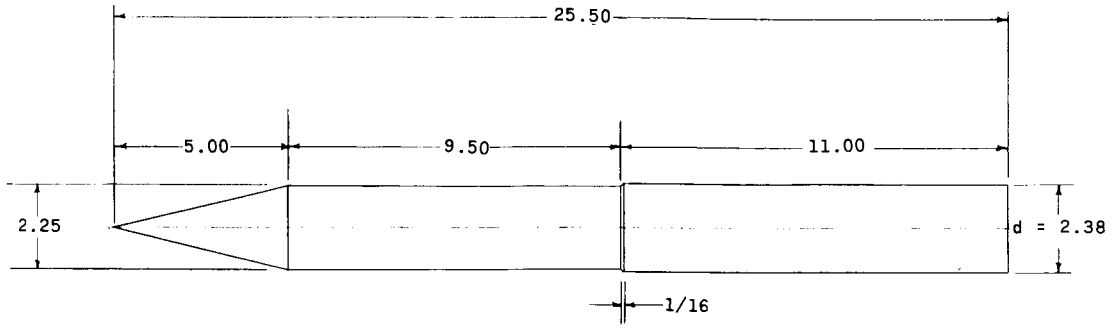

Space Vehicle A

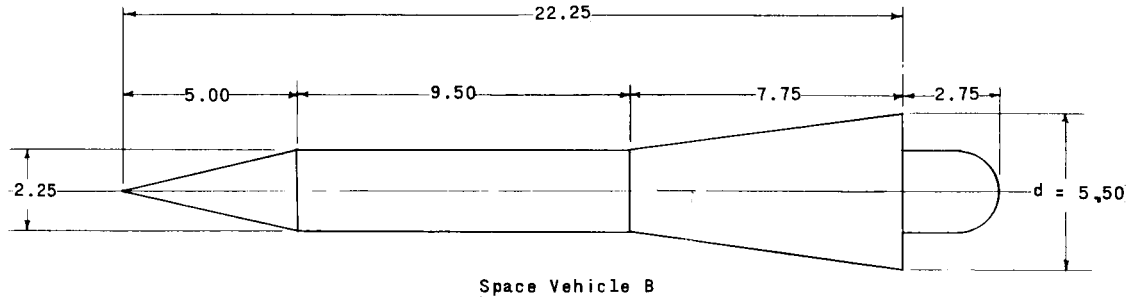

Space Vehicle B

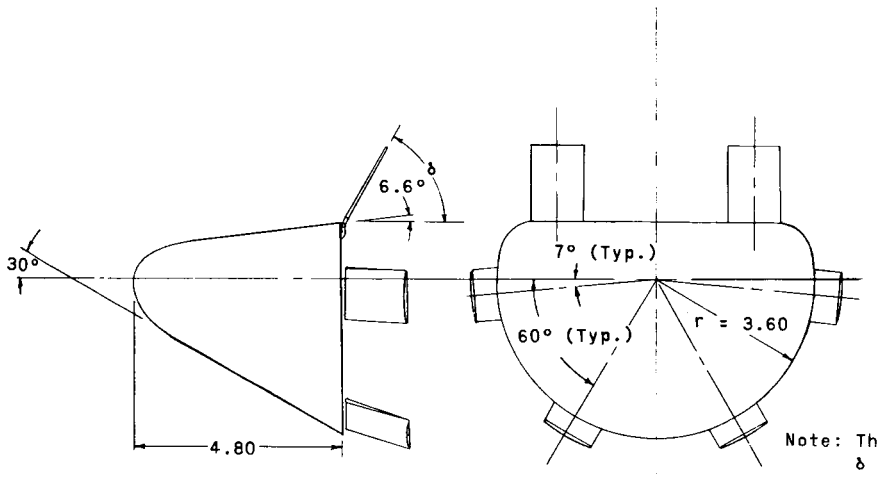

Space Vehicle C

Note: The deflection angle δ for all flaps was either 0° or 60° with respect to the model ℄.

Figure 2.- Drawing of the three space vehicles used in the investigation. All linear dimensions are in inches.

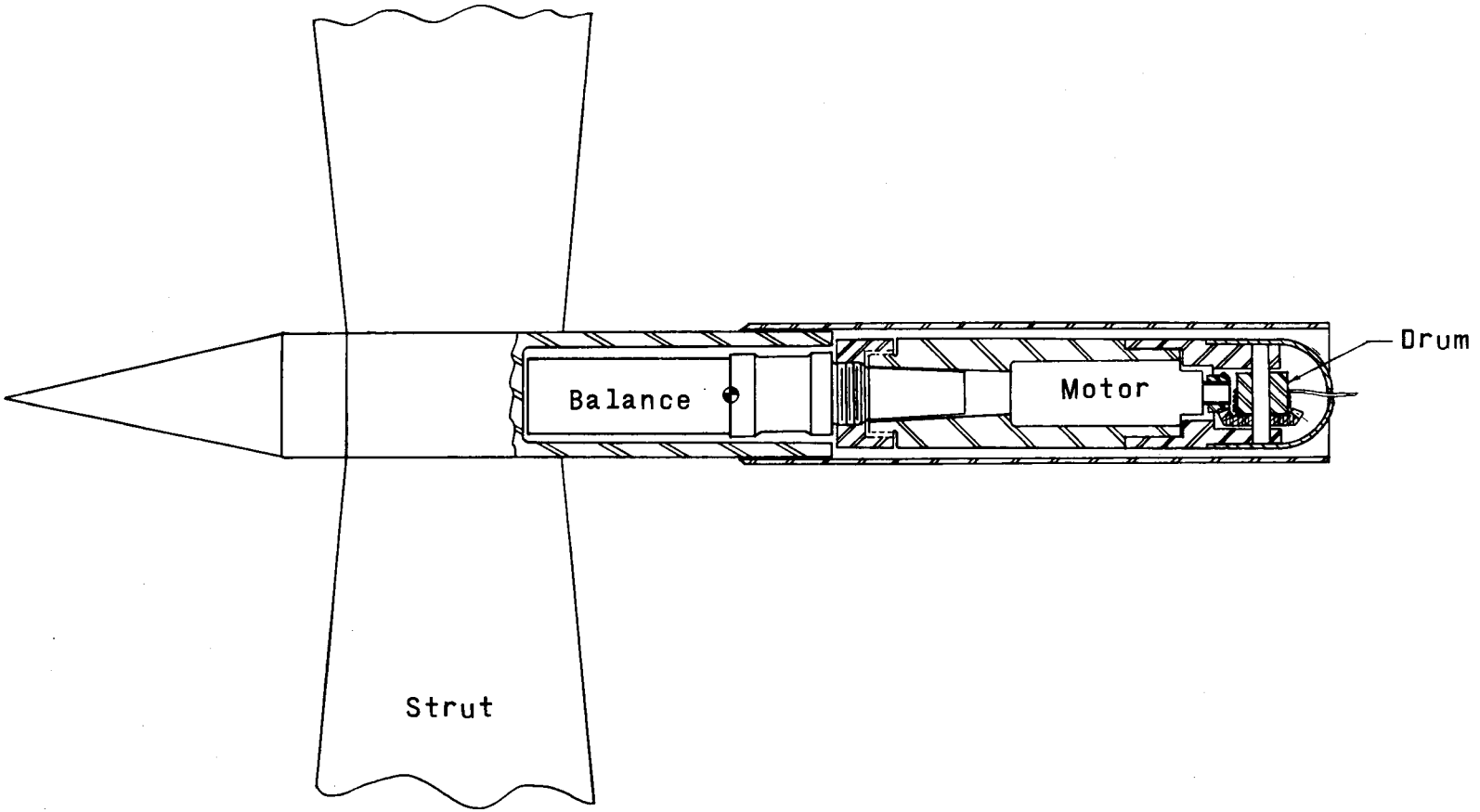

Figure 3.- Balance and motor-driven drum arrangement for space vehicles A and B.

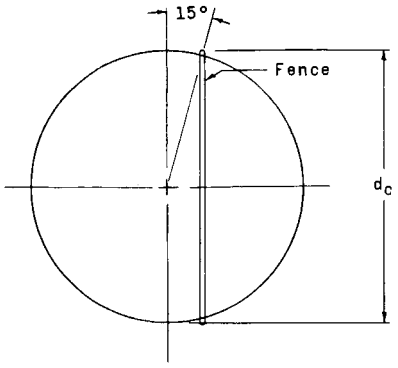

Spheres

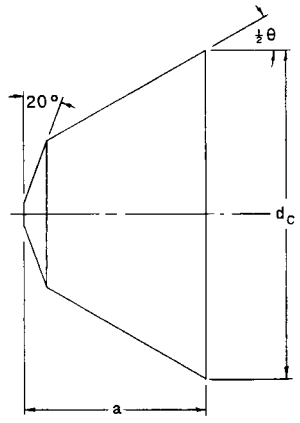

60° modified cones

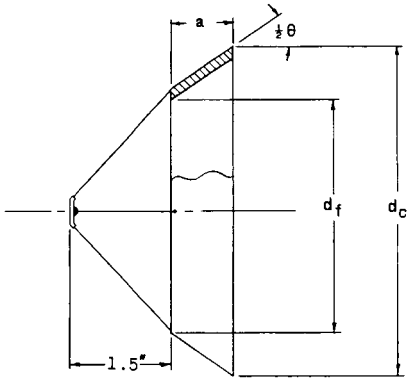

Conical rings

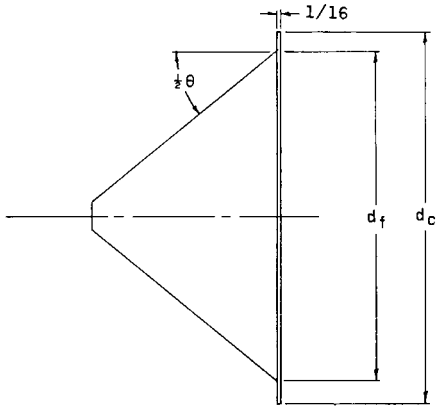

80° modified cones

	Spheres			Conical rings				60° modified cones				80° modified cones			
Reference diameter, d_c, in.	4.00	6.00	8.00	4.88	4.88	4.88	4.88	4.88	4.88	4.88	5.36	4.88	5.12	5.36	5.61
Diameter, d_f, in.	—	—	—	3.30	3.30	3.30	3.30	—	—	—	4.88	4.88	4.88	4.88	4.88
$\frac{d_c - d_f}{d_f} \times 100$	—	—	—	—	—	—	—	—	—	—	10	0	5	10	15
Reference area, S, sq. in.	0.0872	0.196	0.349	0.130	0.130	0.130	0.130	0.130	0.130	0.130	0.157	0.130	0.143	0.157	0.172
Cone angle, θ, deg.	—	—	—	60	70	80	90	60	60	60	60	80	80	80	80
a, in.	—	—	—	1.11	0.91	0.74	0.61	2.67	2.05	1.42	2.67	—	—	—	—

Figure 4.- Drawing of rigid-decelerator shapes investigated.

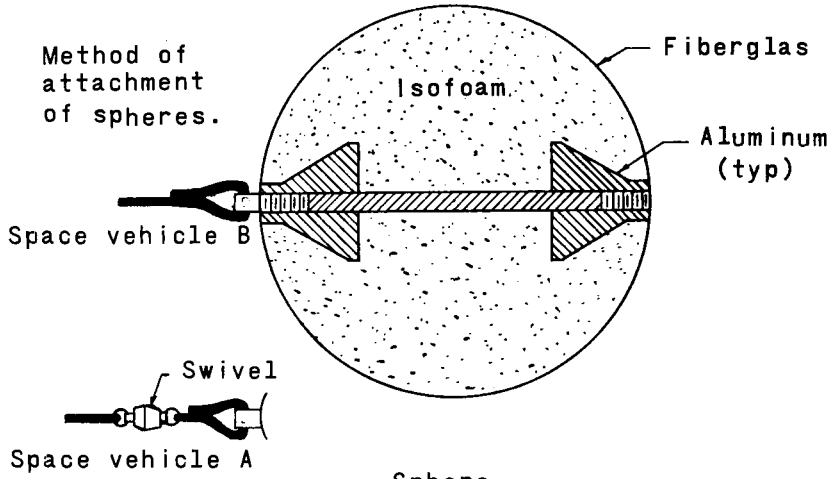

Sphere

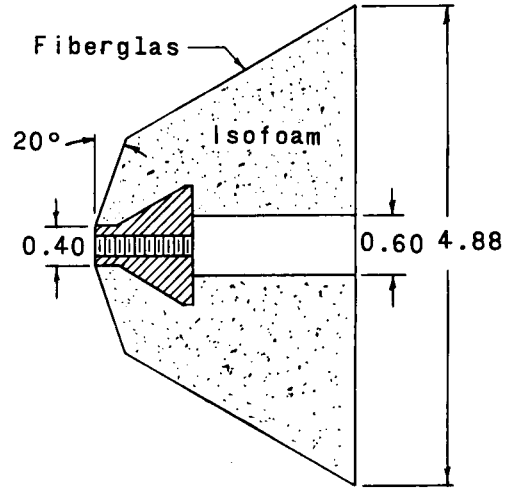

60° modified cone

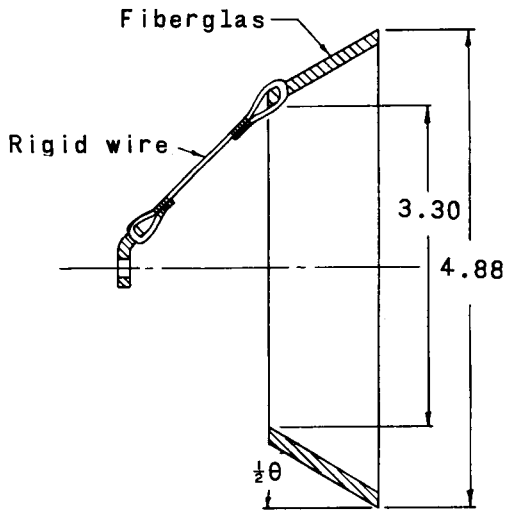

Conical ring

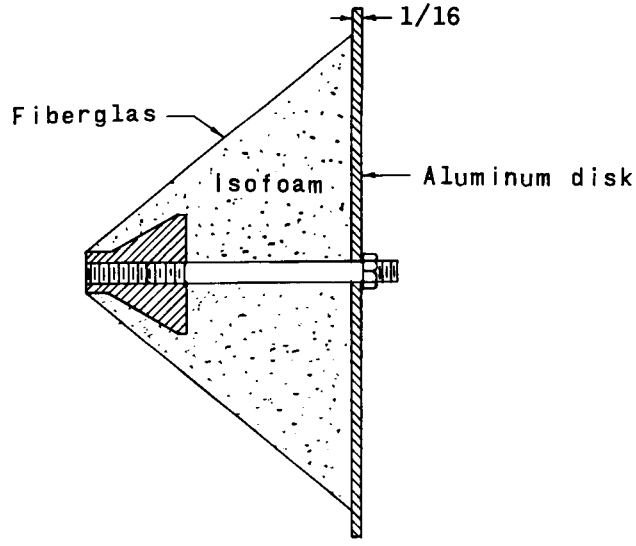

80° modified cone

Figure 5.- Detail drawing of the decelerator models. All linear dimensions are in inches.

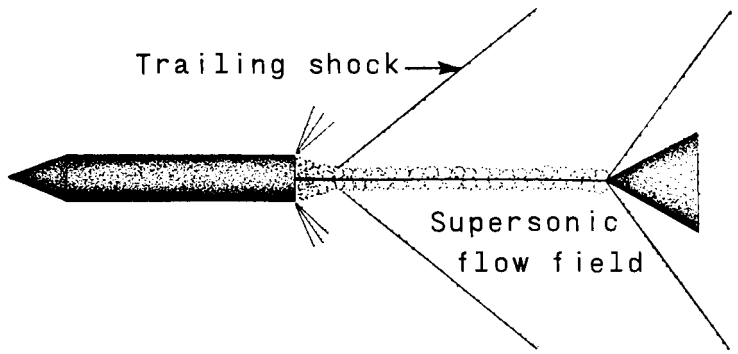

Long trailing distance

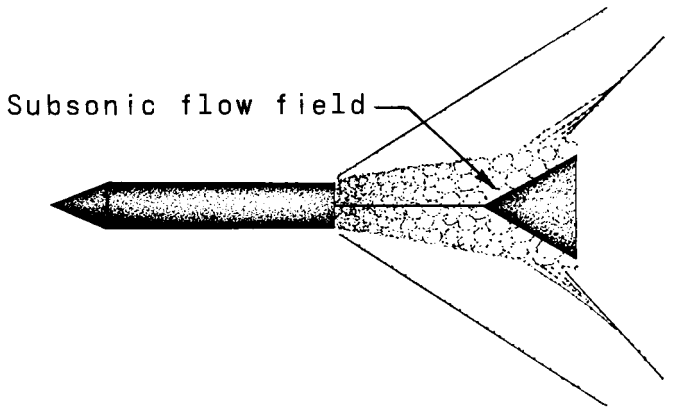

Short trailing distance

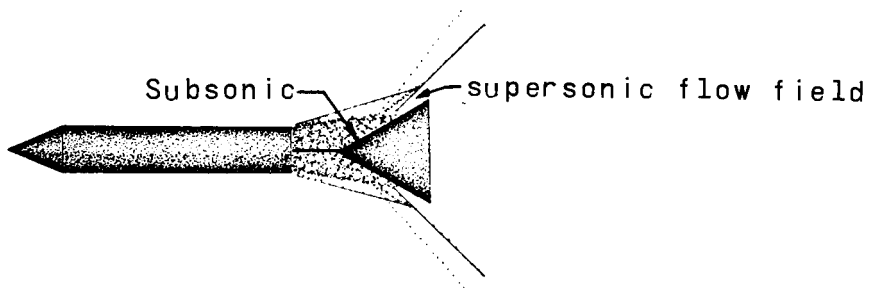

Very short trailing distance

Figure 6.- Schematic representation of various flow fields at supersonic free-stream velocities.

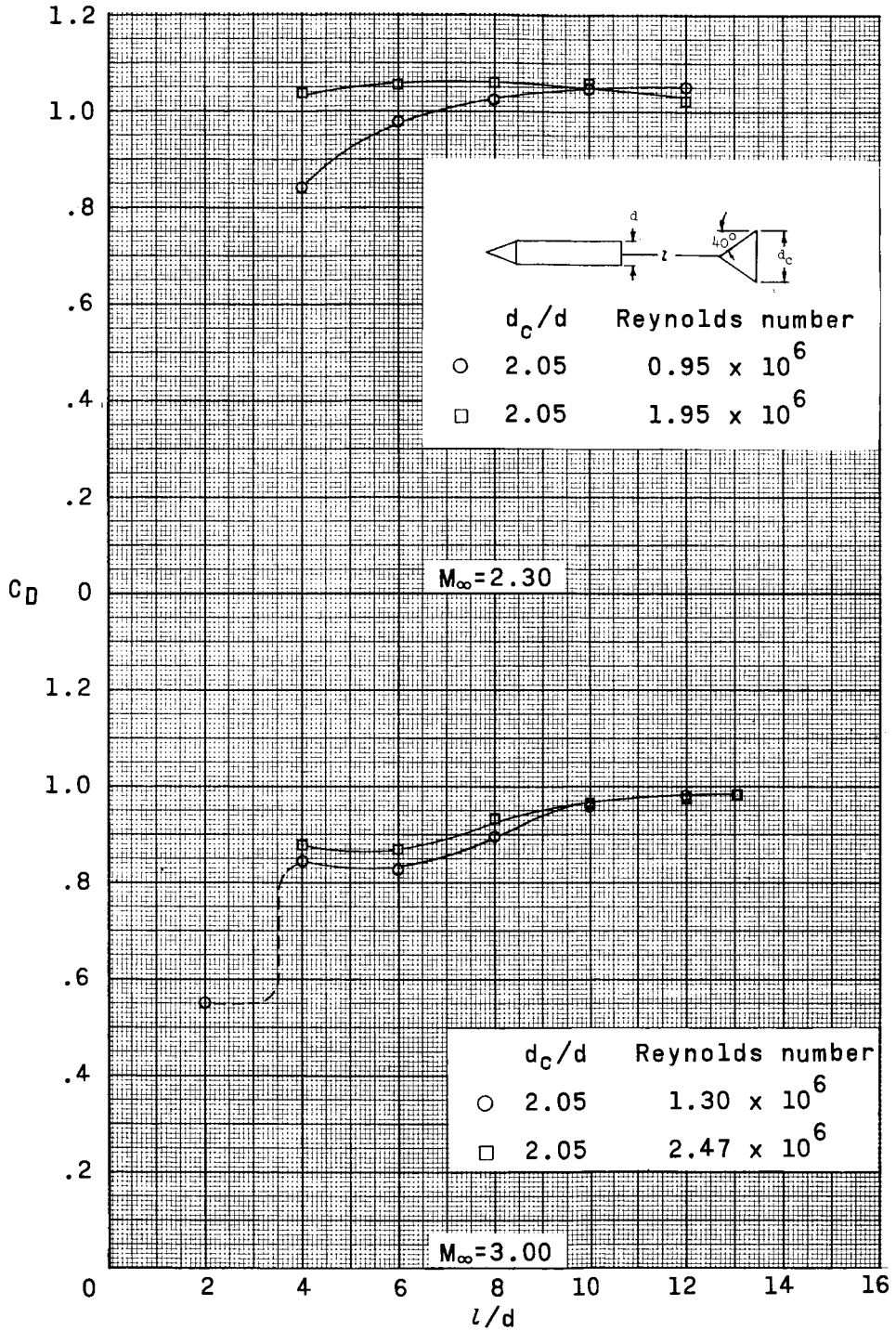

(a) Space vehicle A.

Figure 7.- Reynolds number effect on the drag coefficient of an 80° cone at various Mach numbers.

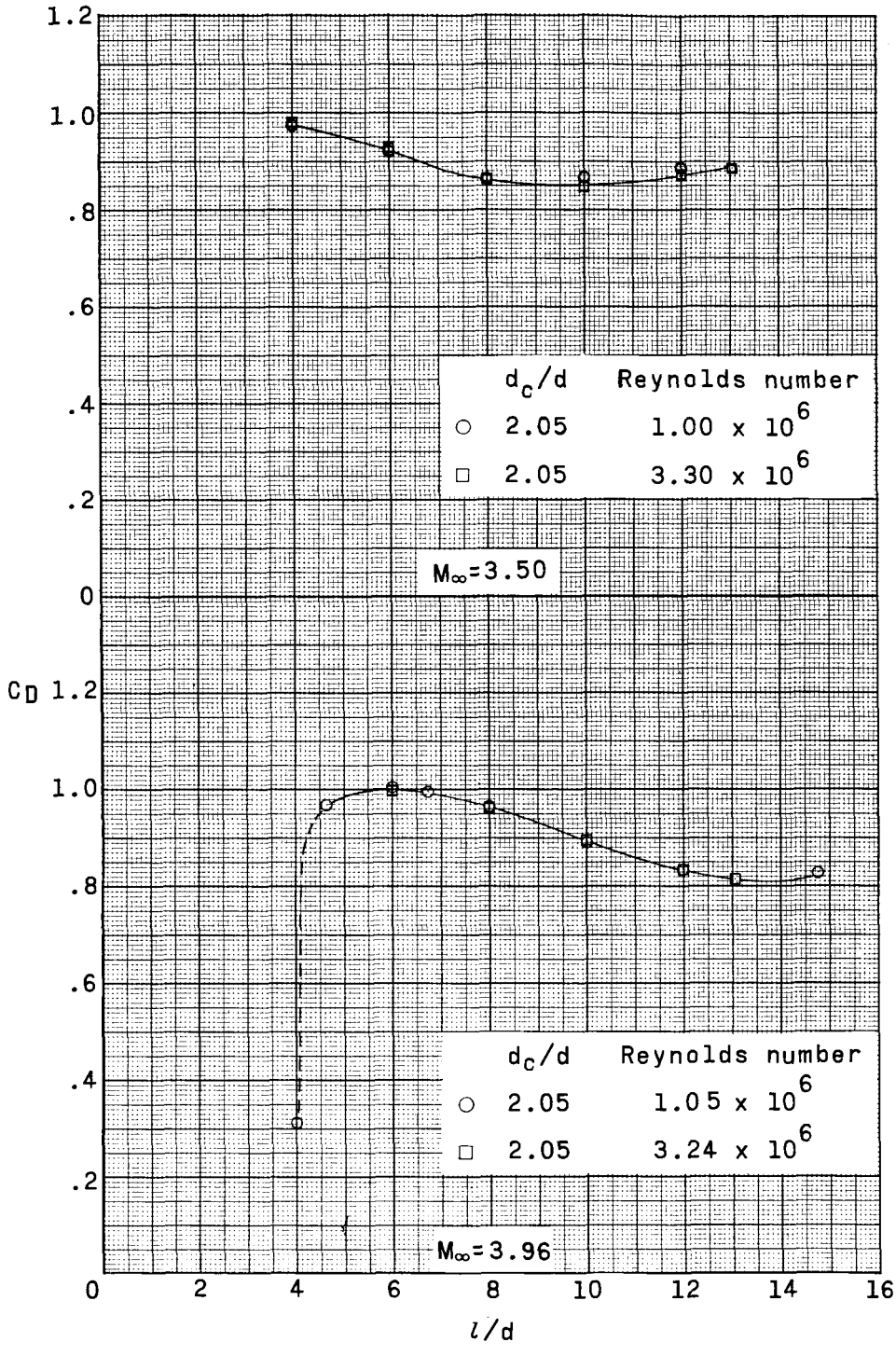

(a) Continued.

Figure 7.- Continued.

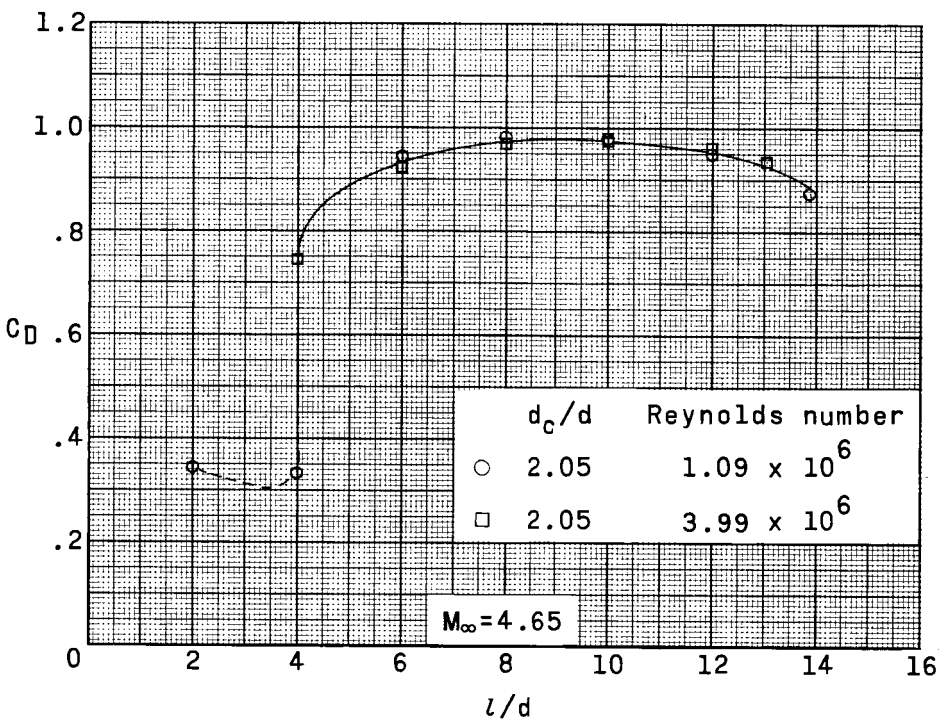

(a) Concluded.

Figure 7.- Continued.

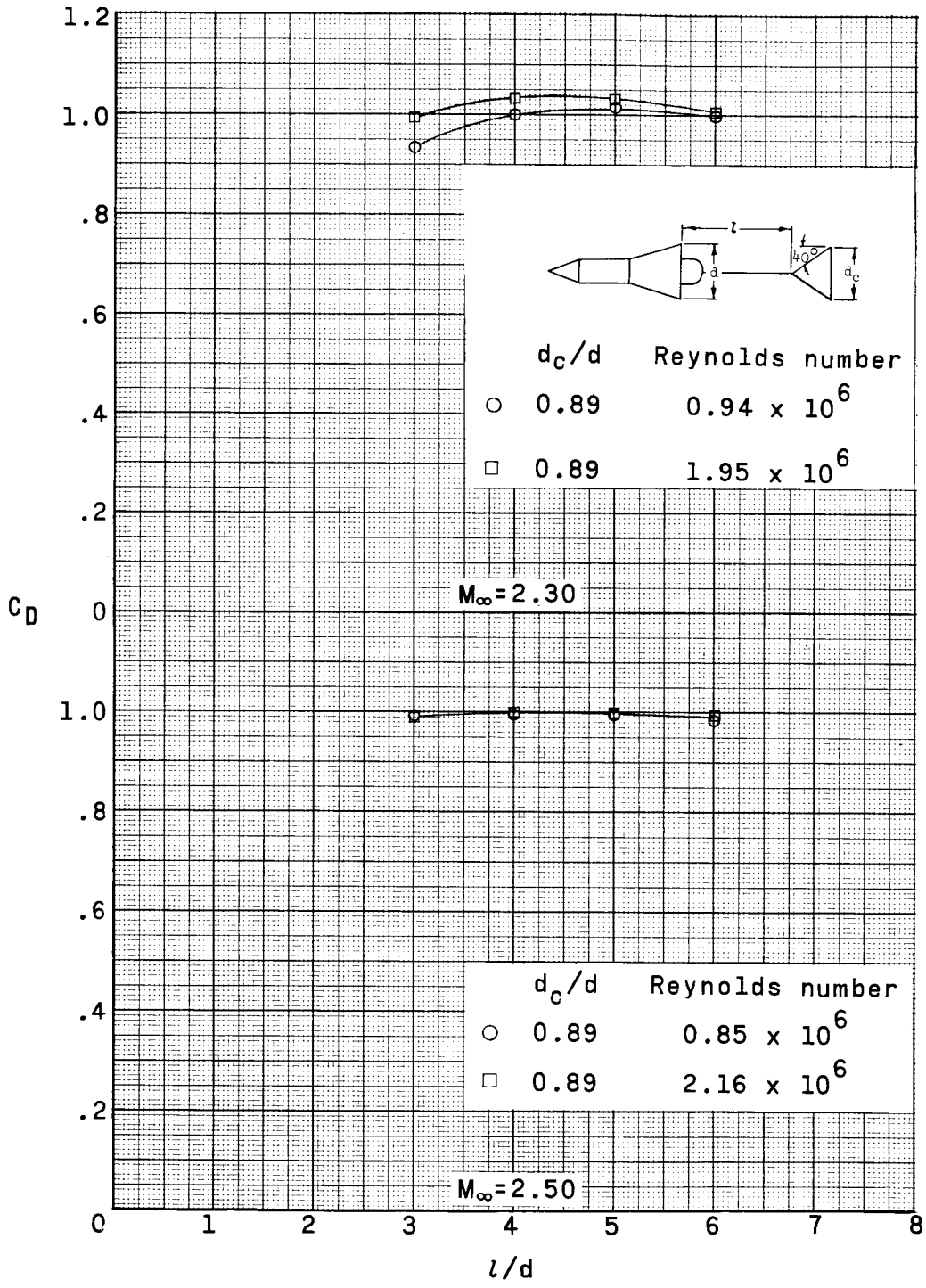

(b) Space vehicle B.

Figure 7.- Continued.

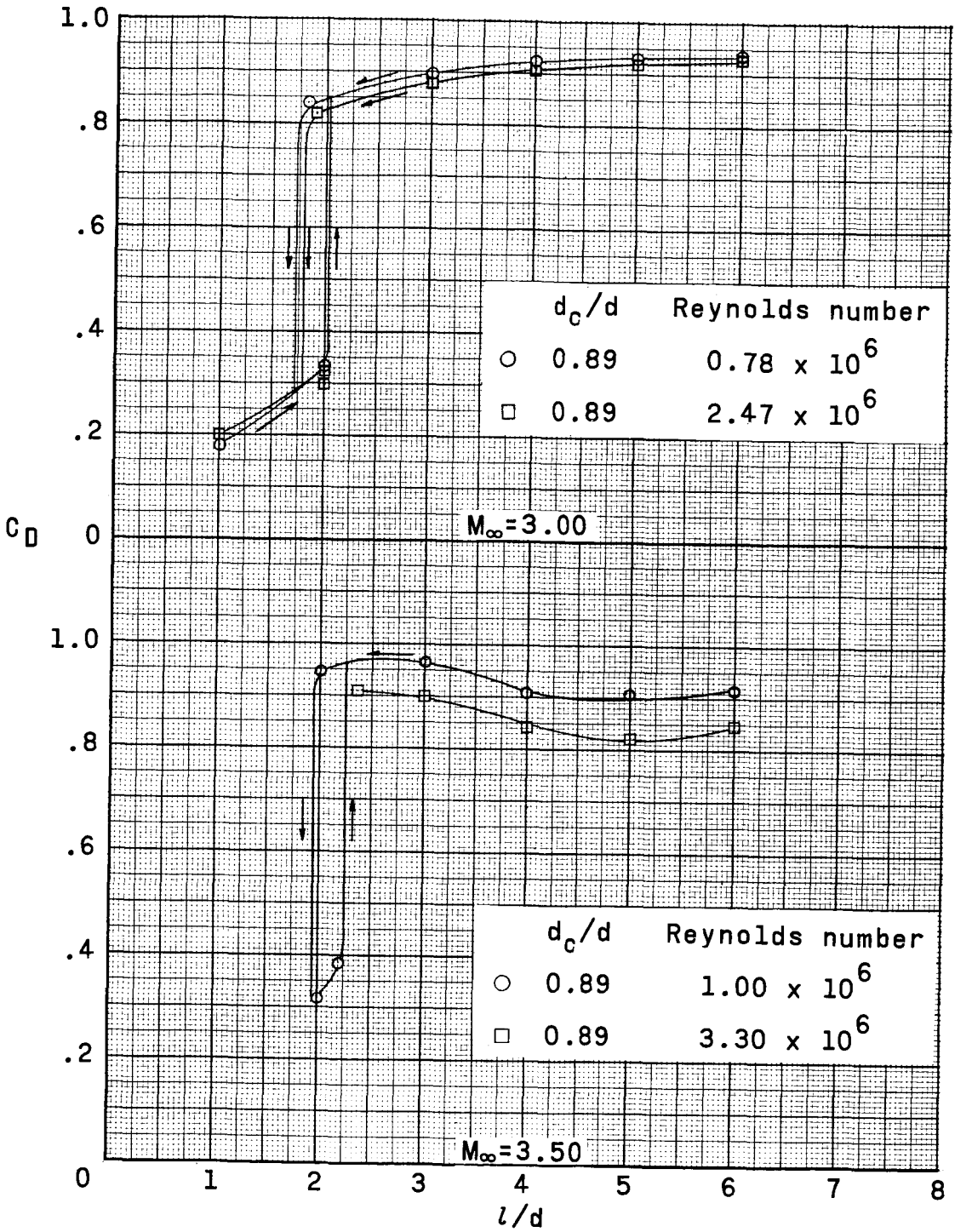

(b) Continued.

Figure 7.- Continued.

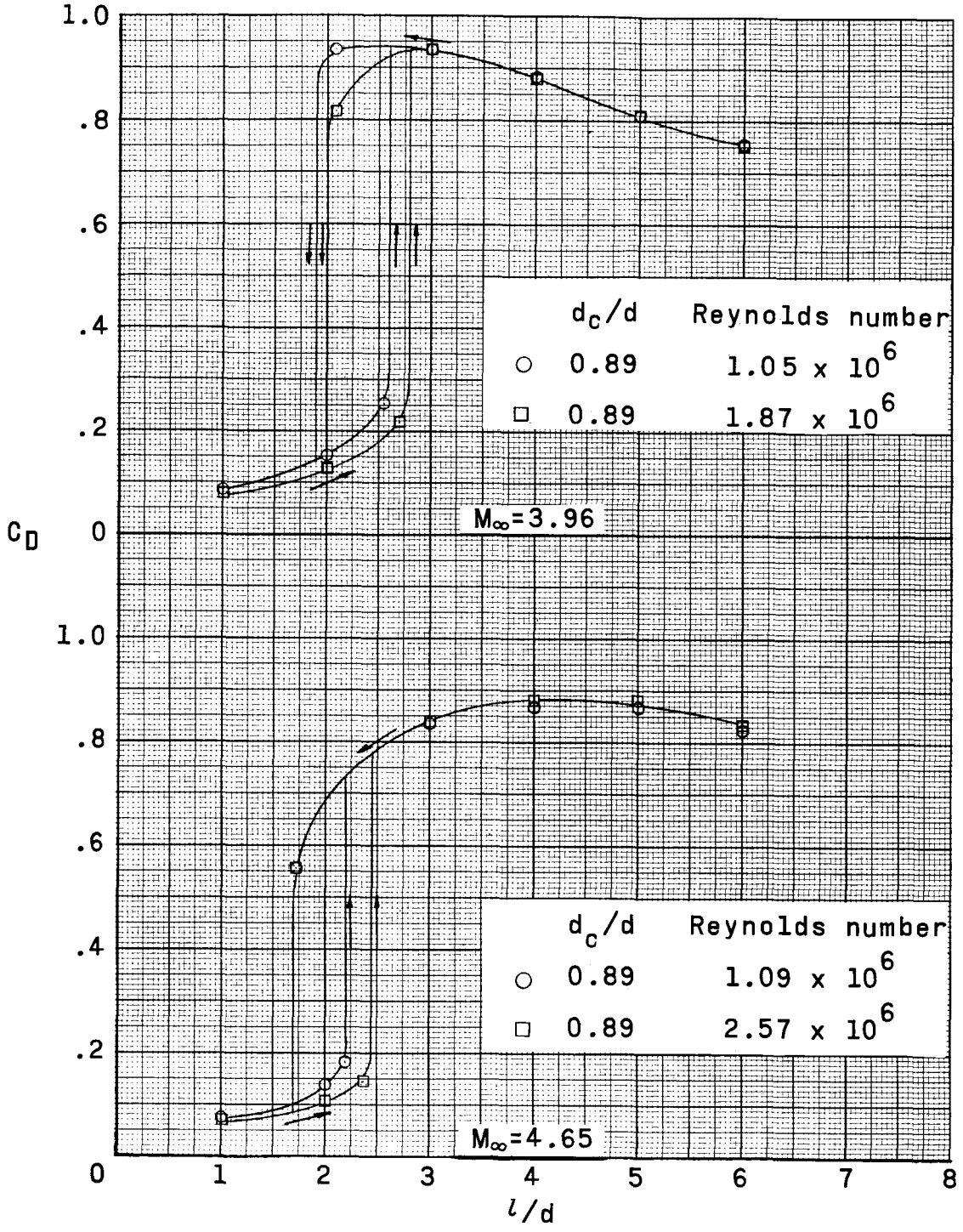

(b) Concluded.

Figure 7.- Concluded.

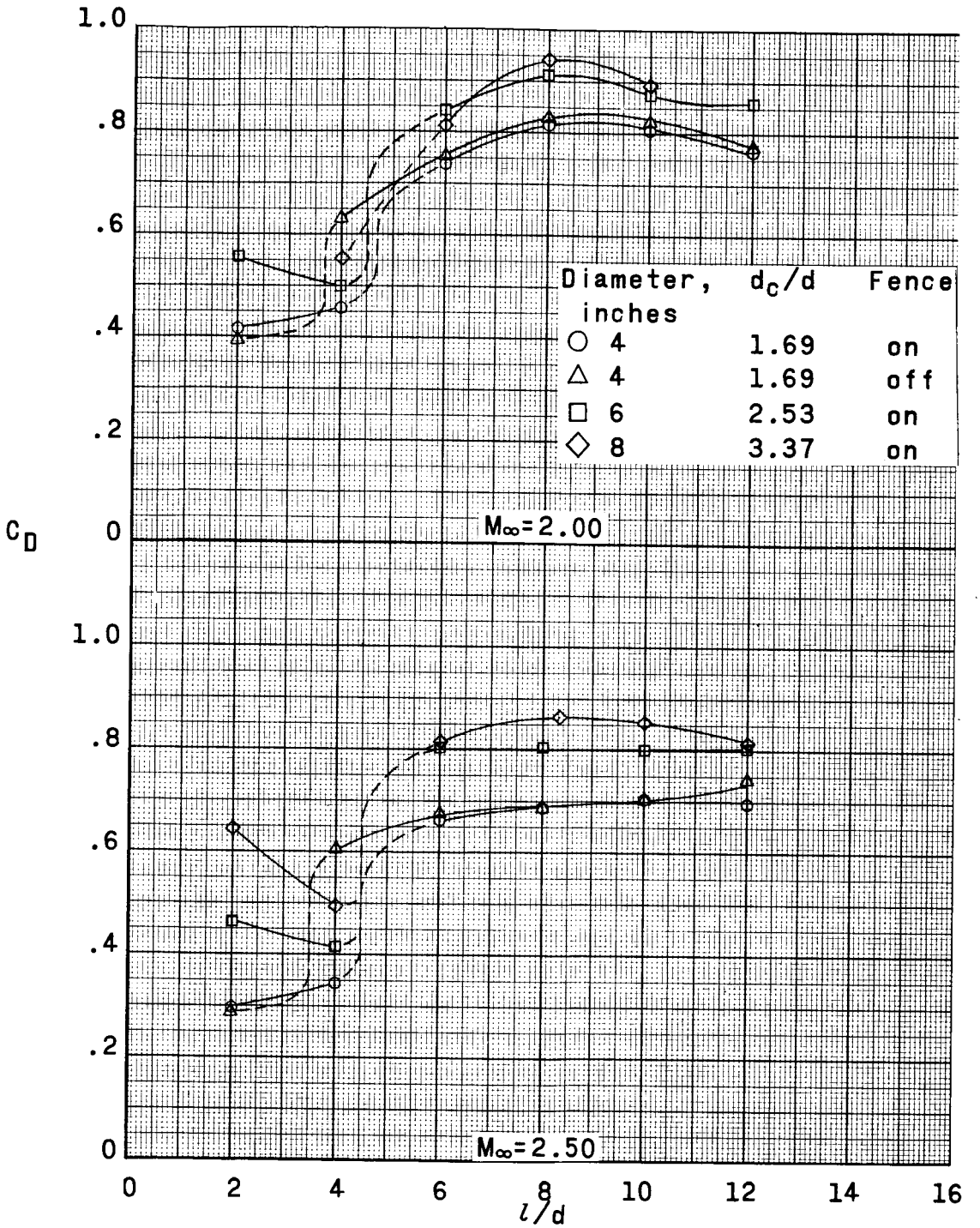

(a) Space vehicle A.

Figure 8.- Variation of drag coefficient with tow-cable length for 4-, 6-, and 8-inch spheres at various Mach numbers.

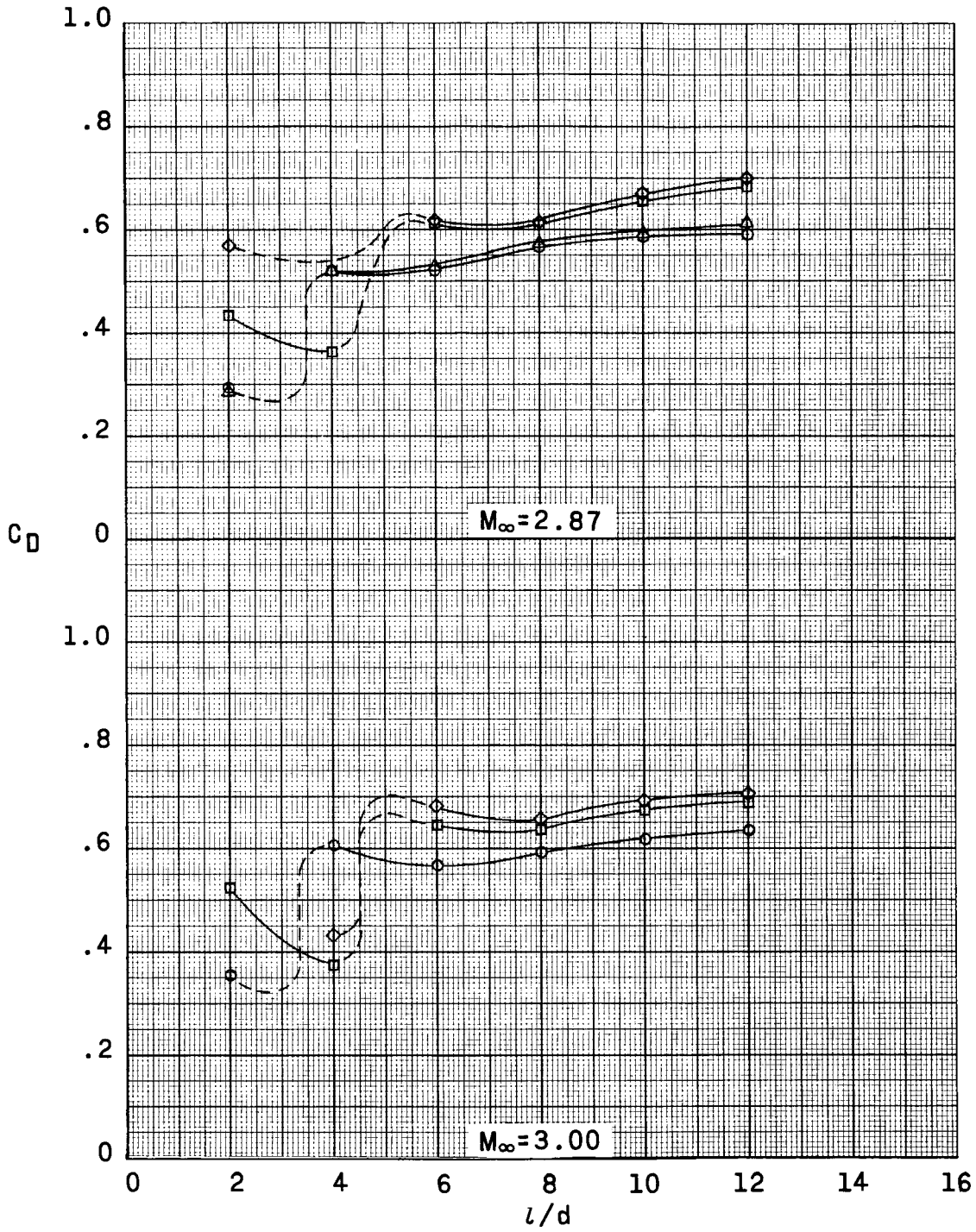

(a) Continued.

Figure 8.- Continued.

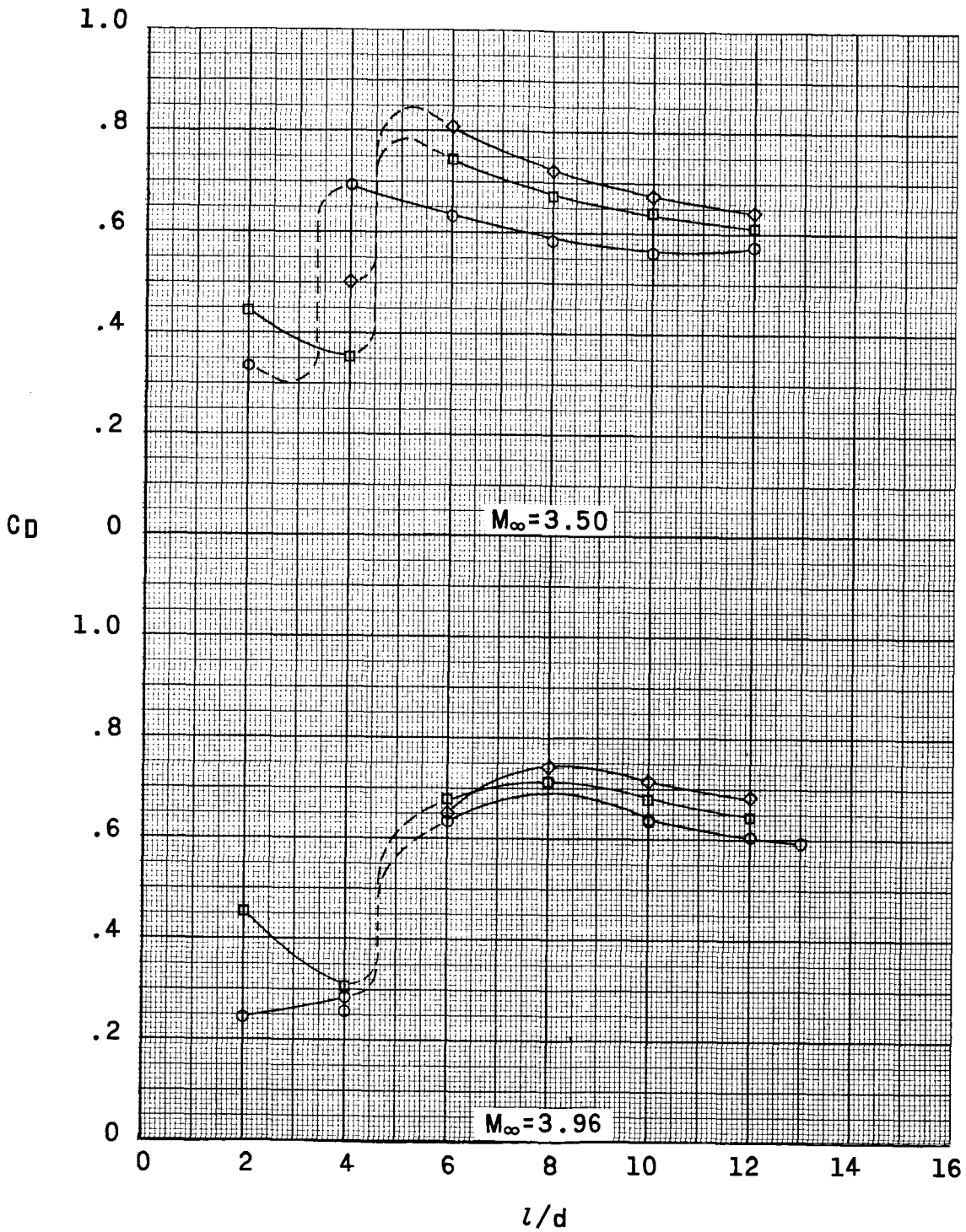

(a) Continued.

Figure 8.- Continued.

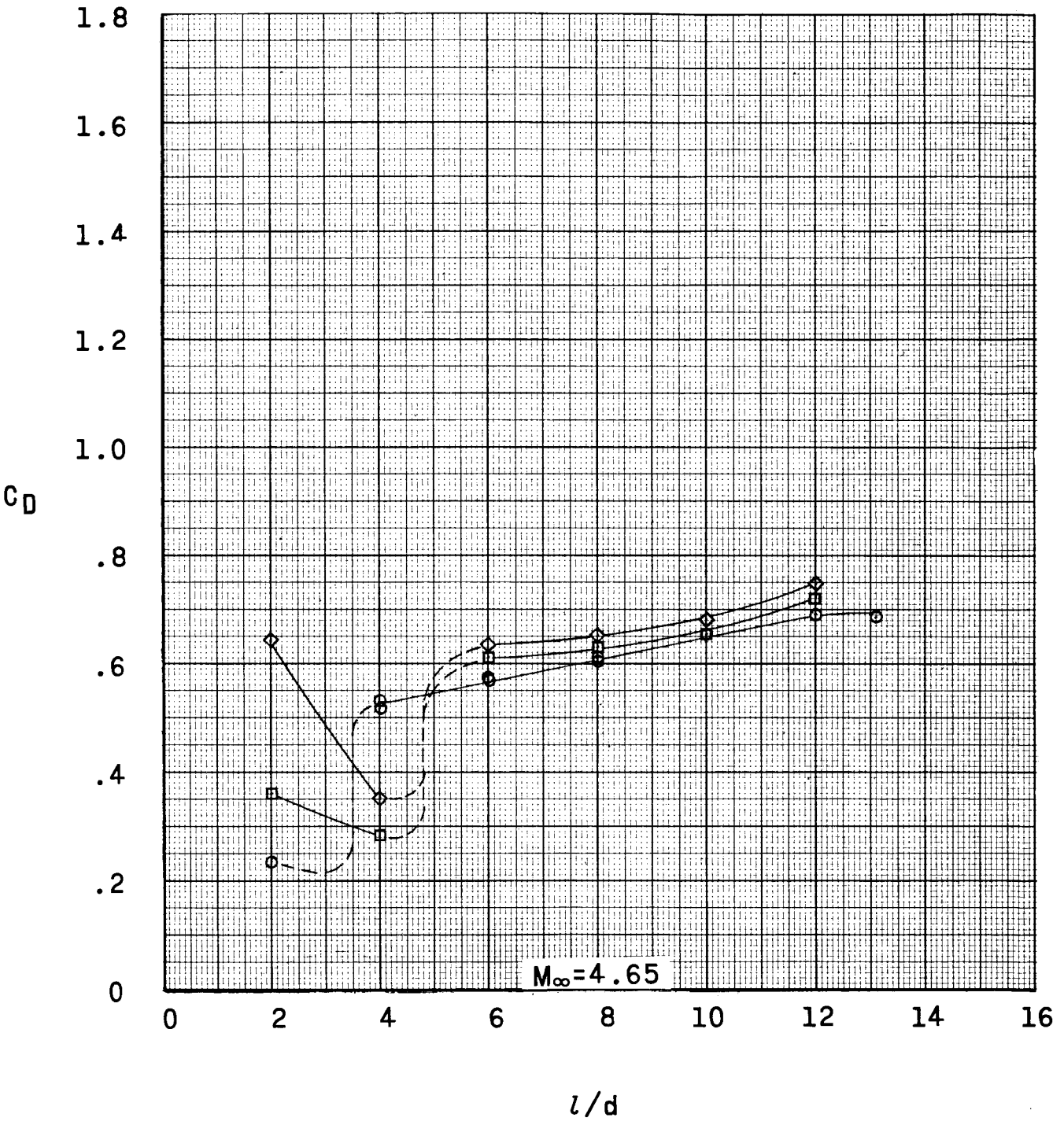

(a) Concluded.

Figure 8.- Continued.

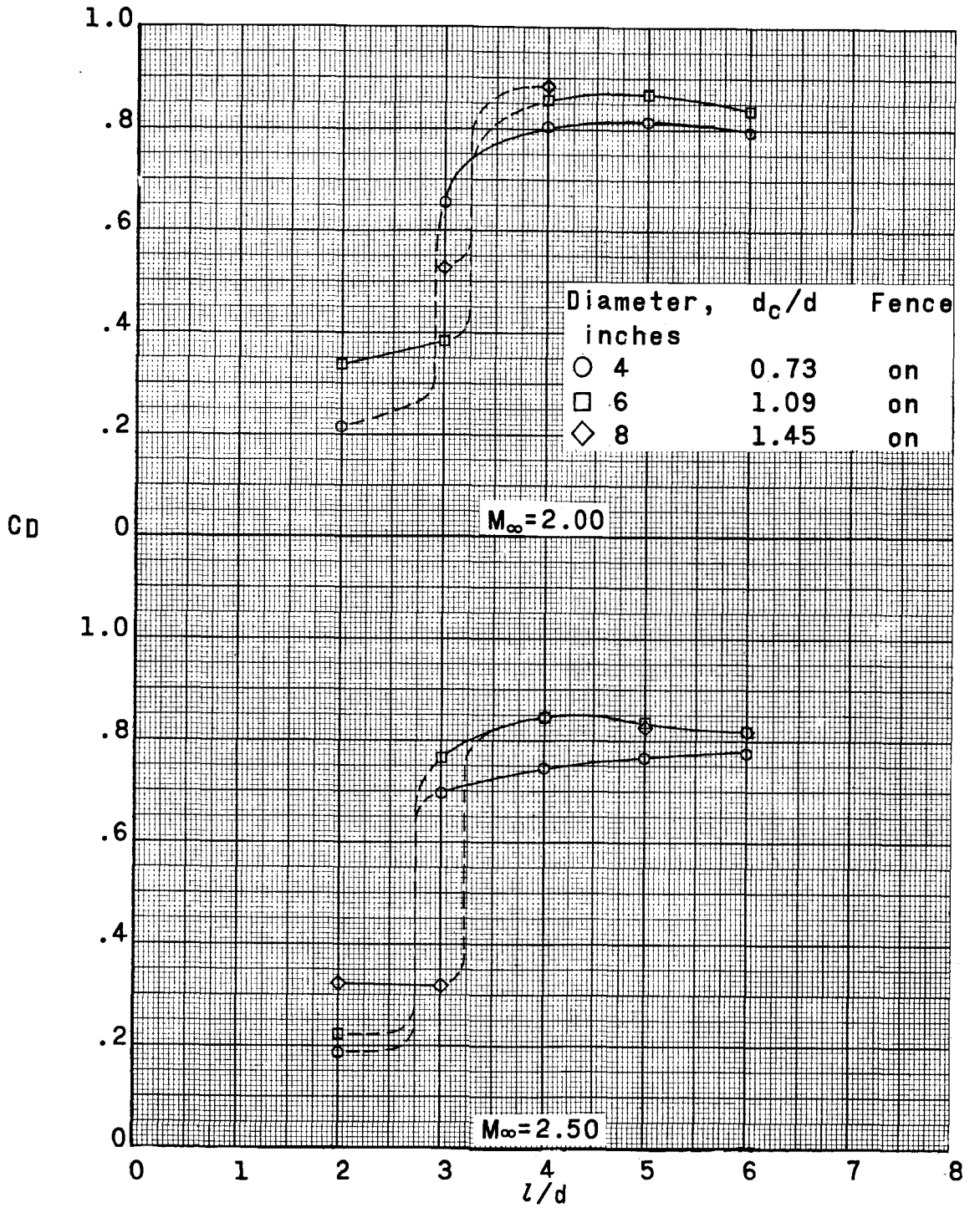

(b) Space vehicle B.

Figure 8.- Continued.

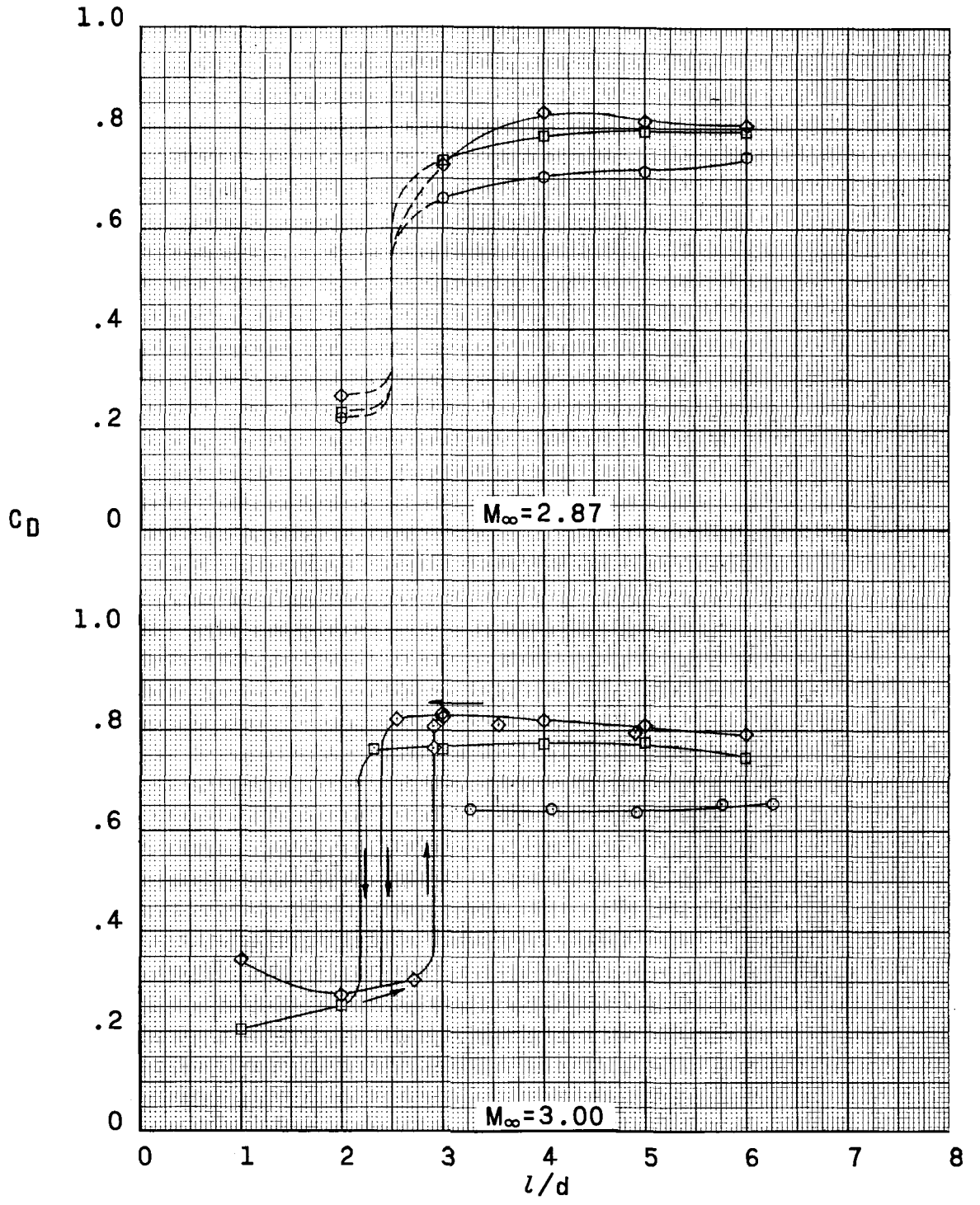

(b) Continued.

Figure 8.- Continued.

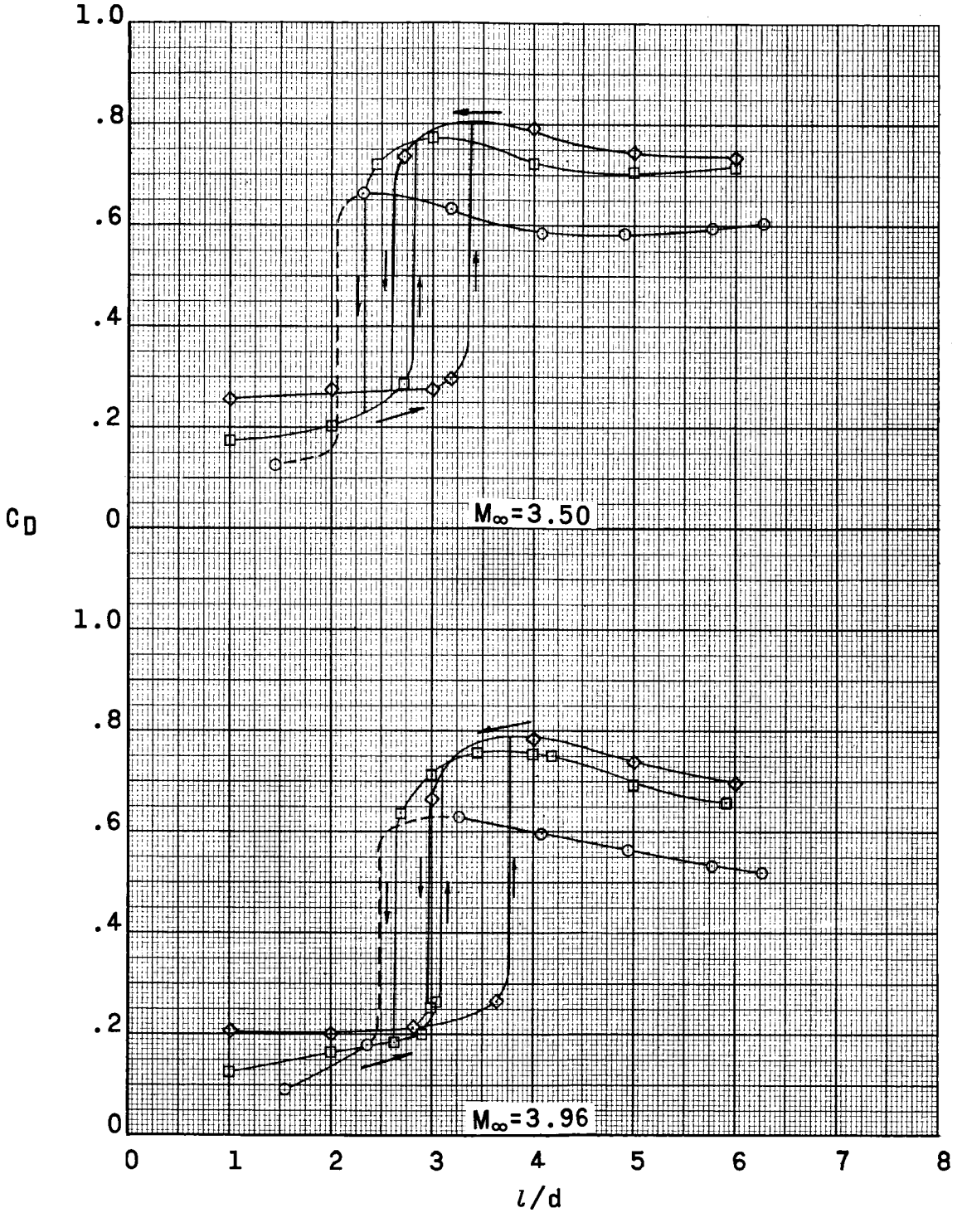

(b) Continued.

Figure 8.- Continued.

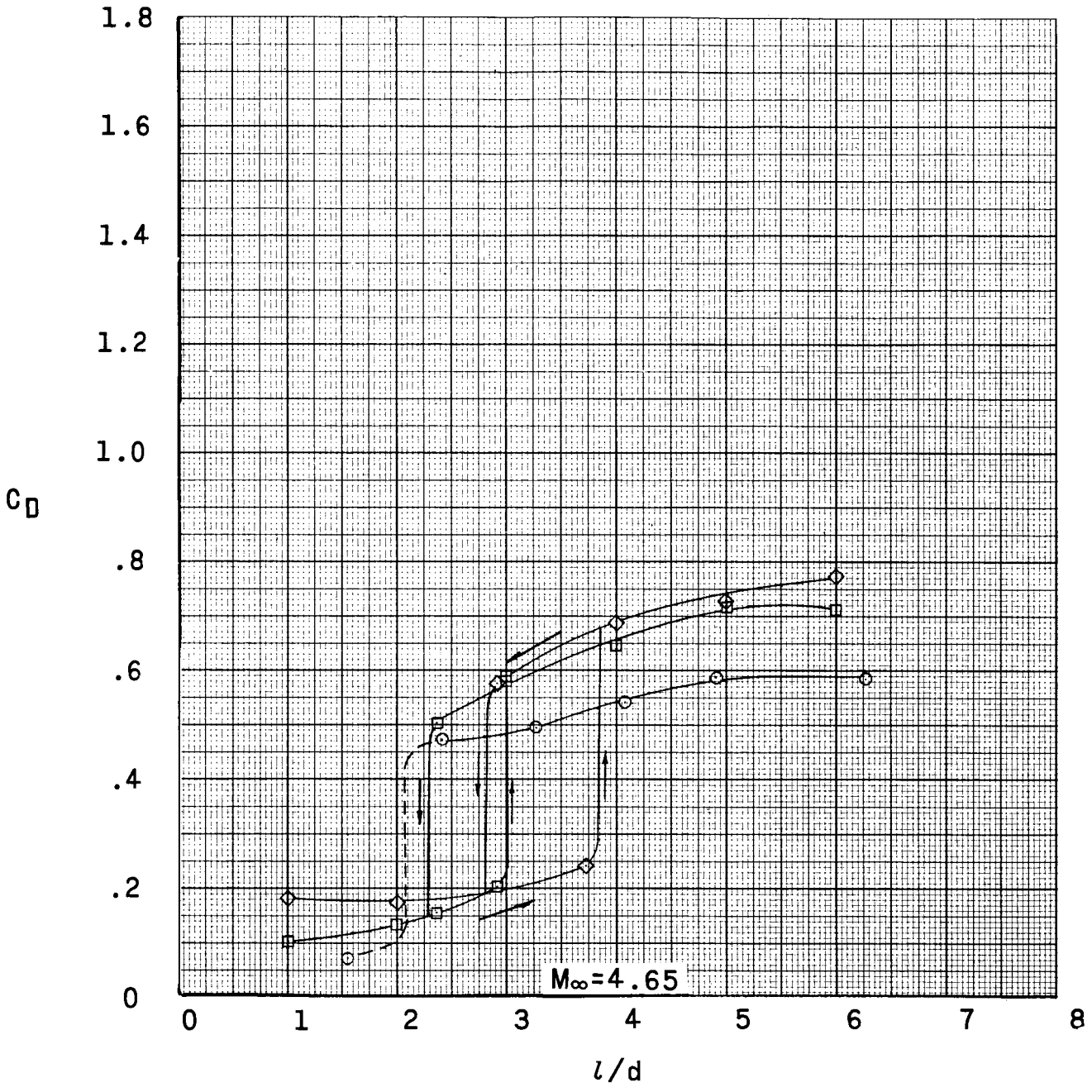

(b) Concluded.

Figure 8.- Continued.

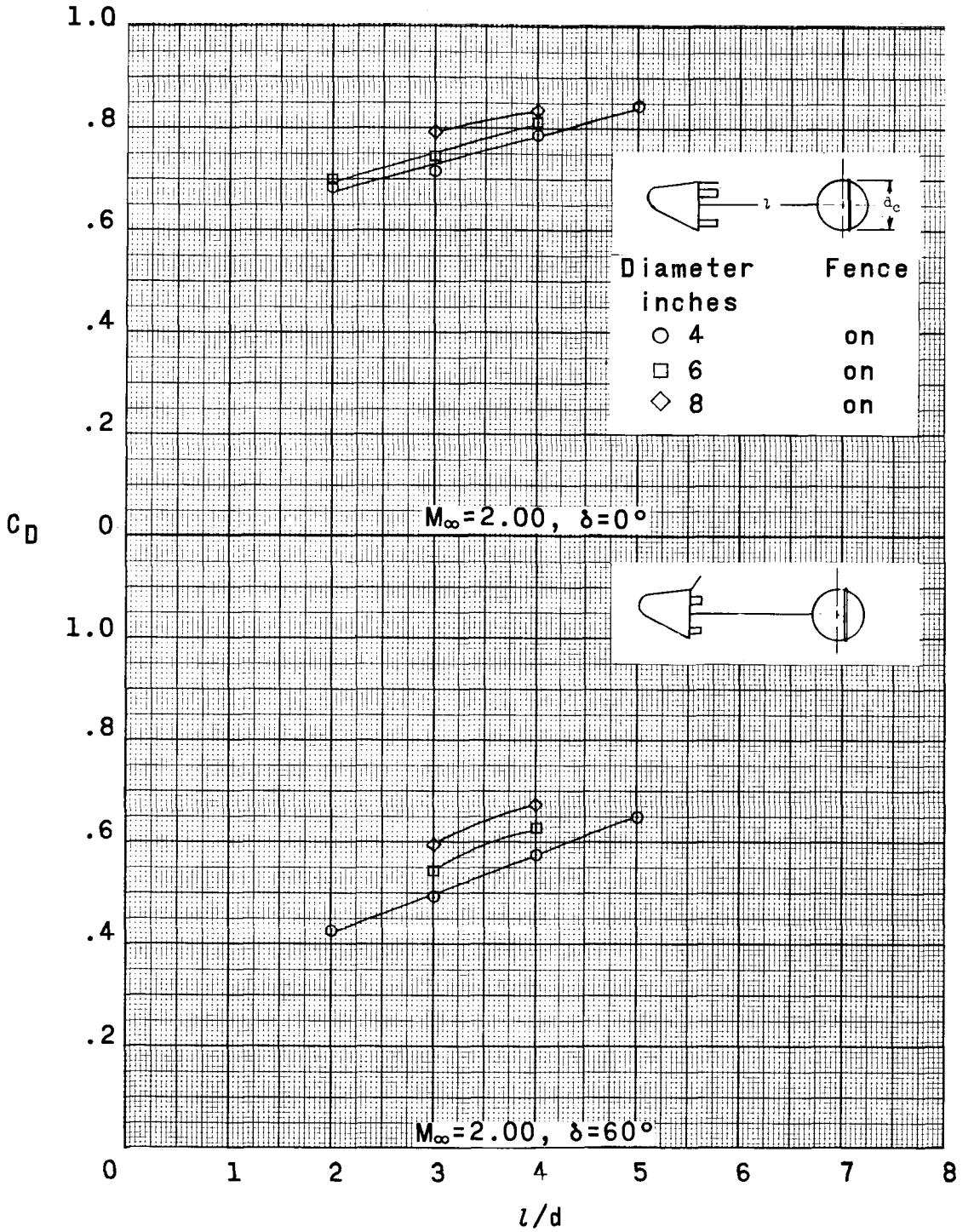

(c) Space vehicle C.

Figure 8.- Continued.

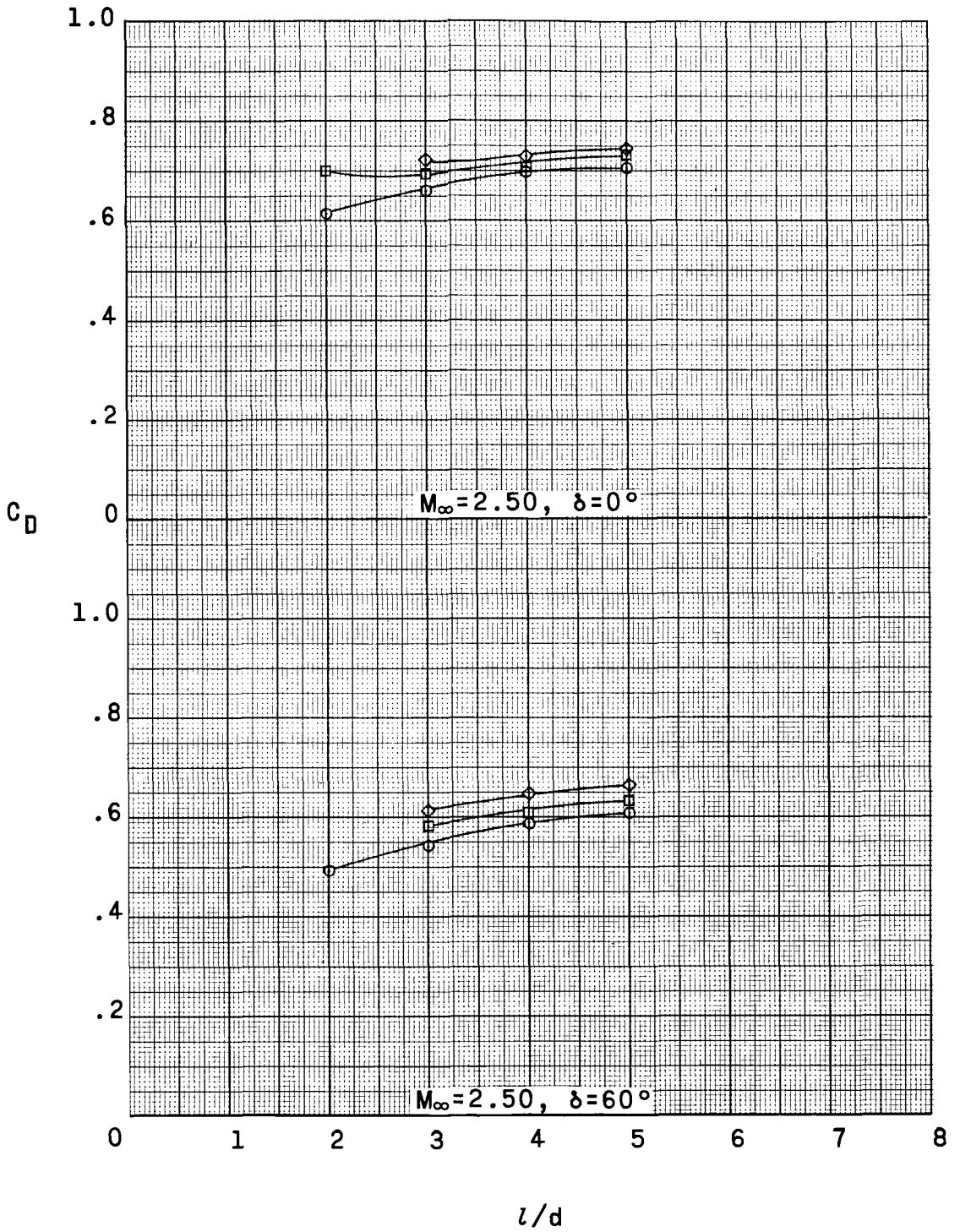

(c) Continued.

Figure 8.- Continued.

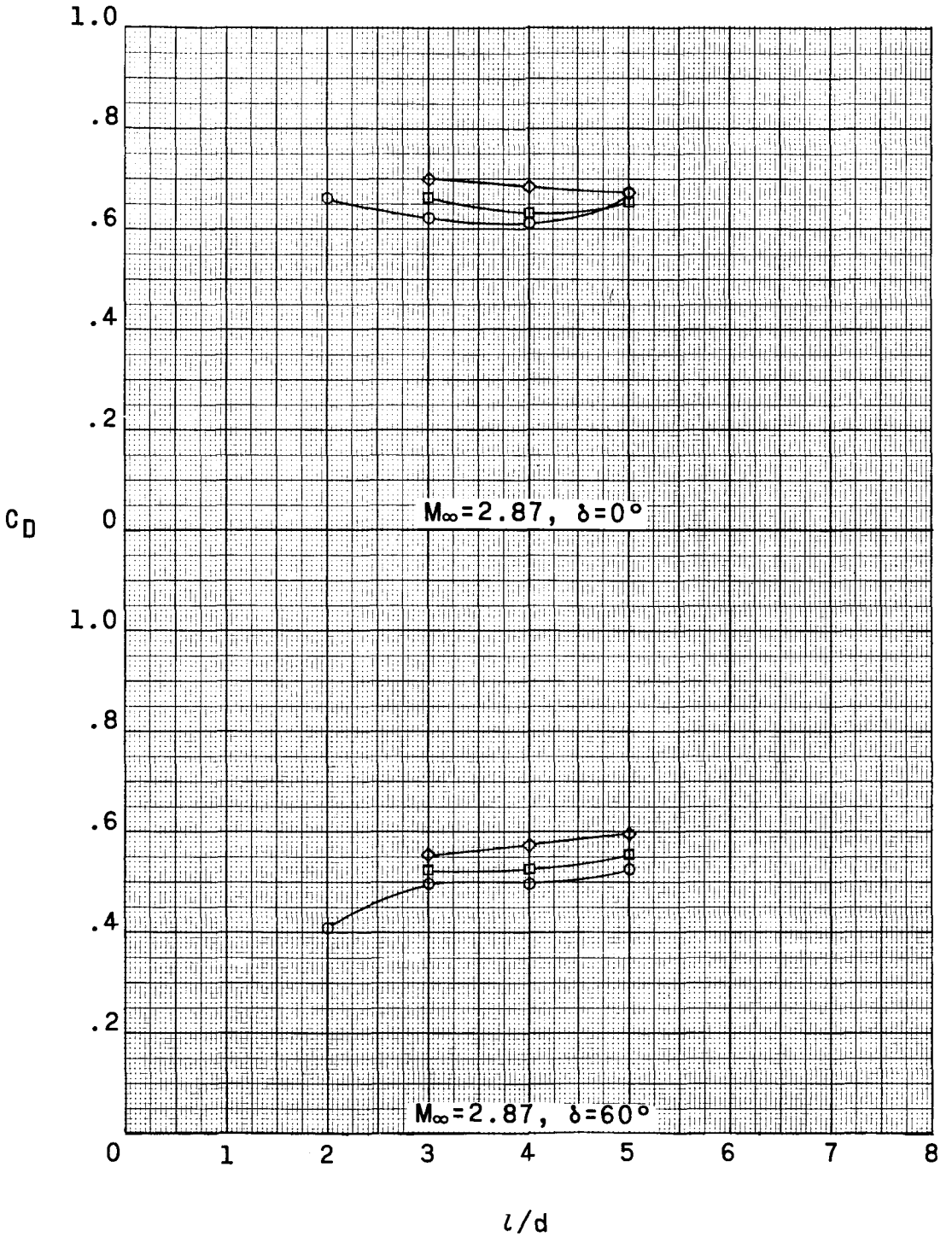

(c) Concluded.

Figure 8.- Concluded.

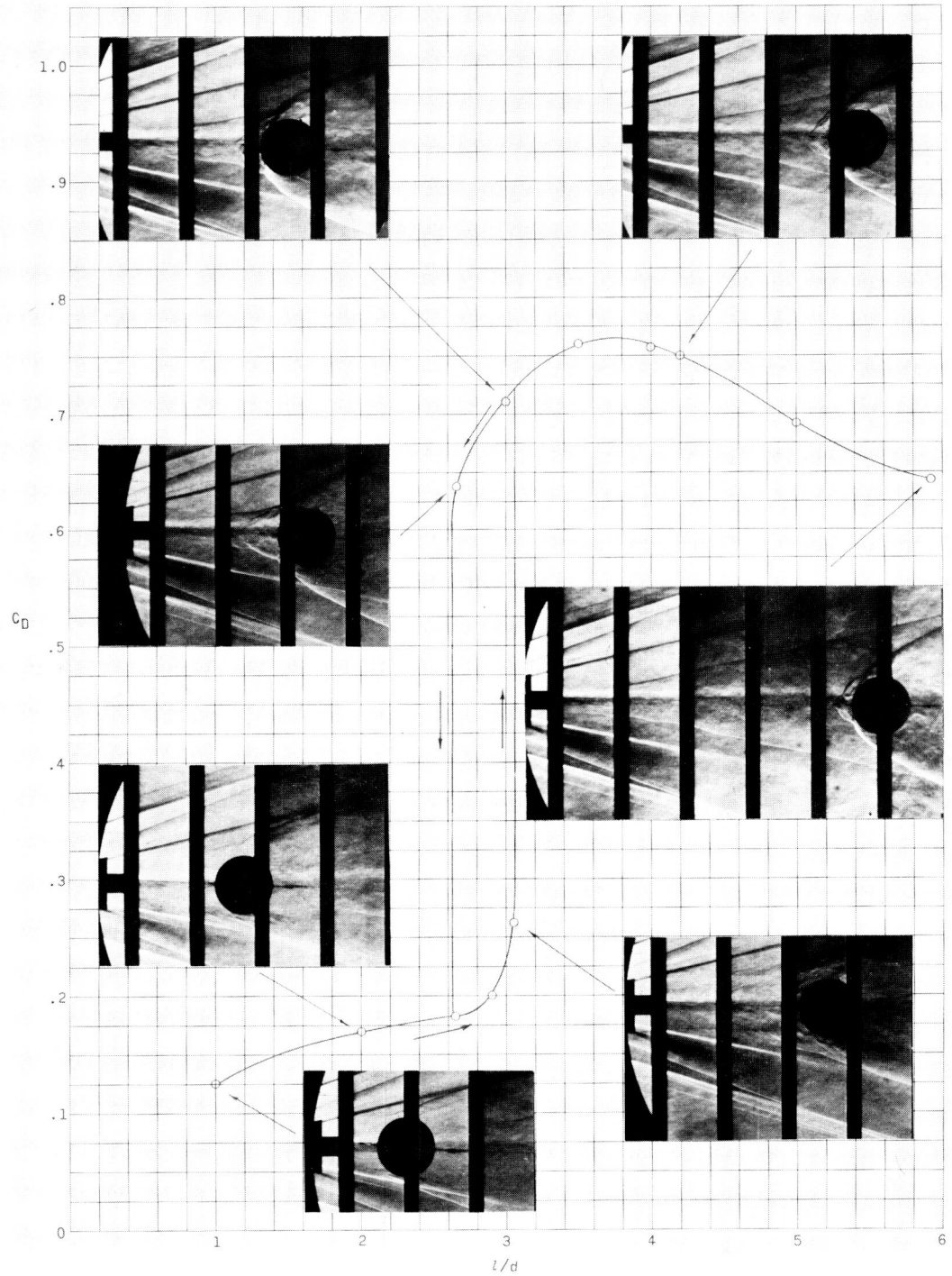

L-63-54

Figure 9.- Variation of drag coefficient and associated flow field with l/d for a 6-inch sphere in the wake of space vehicle B at a Mach number of 3.96.

$l/d = 4.0$, $M_\infty = 2.00$

$l/d = 6.0$, $M_\infty = 2.00$

$l/d = 2.0$, $M_\infty = 2.50$

$l/d = 6.0$, $M_\infty = 2.50$

$l/d = 4.0$, $M_\infty = 2.87$

$l/d = 8.0$, $M_\infty = 2.87$

L-63-46

Figure 10.- Typical flow fields of spheres in the wake of space vehicle A at various Mach numbers. (8-inch sphere.)

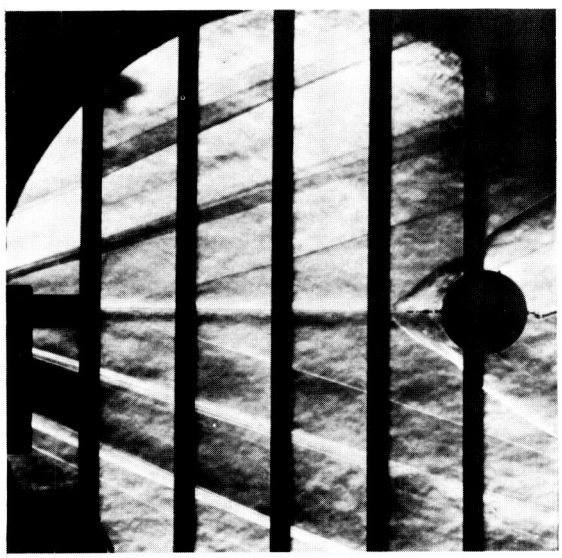

Space vehicle A, l=24 in.

Space vehicle B, l=33 in.

6-inch sphere

Space vehicle A, l=19 in.

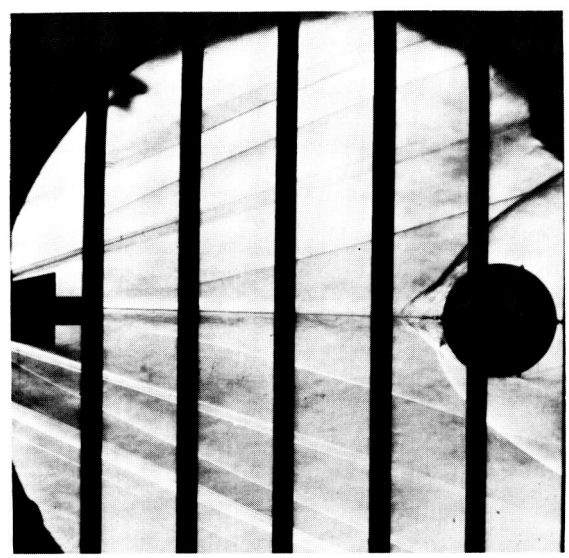

Space vehicle B, l=27 in.

8-inch sphere

L-63-47

Figure 11.- Typical flow fields of spheres in the wake of space vehicles A and B at a Mach number of 2.87.

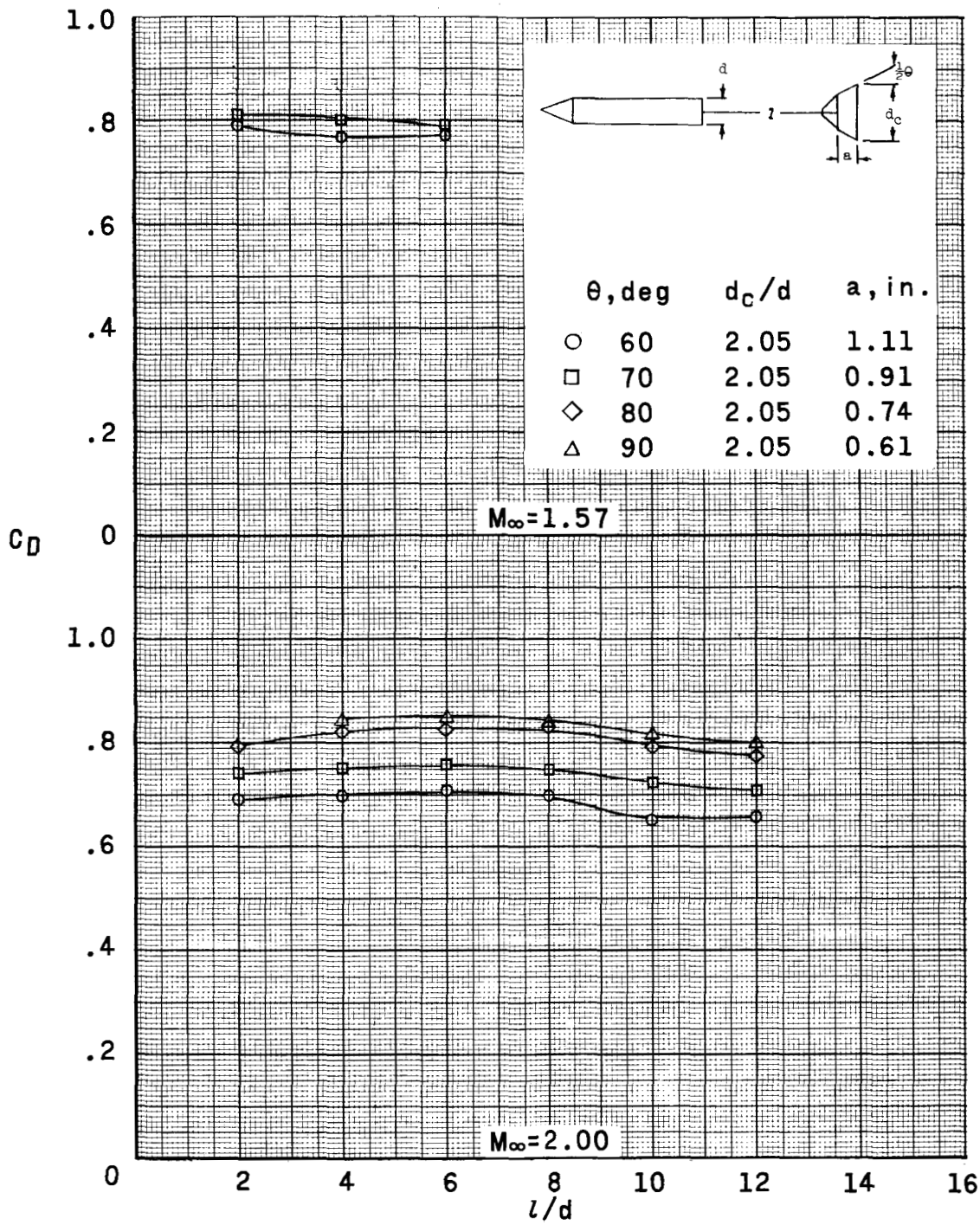

(a) Space vehicle A; d_f/d = 1.39.

Figure 12.- Variation of drag coefficient with tow-cable length for 60°, 70°, 80°, and 90° conical rings at various Mach numbers.

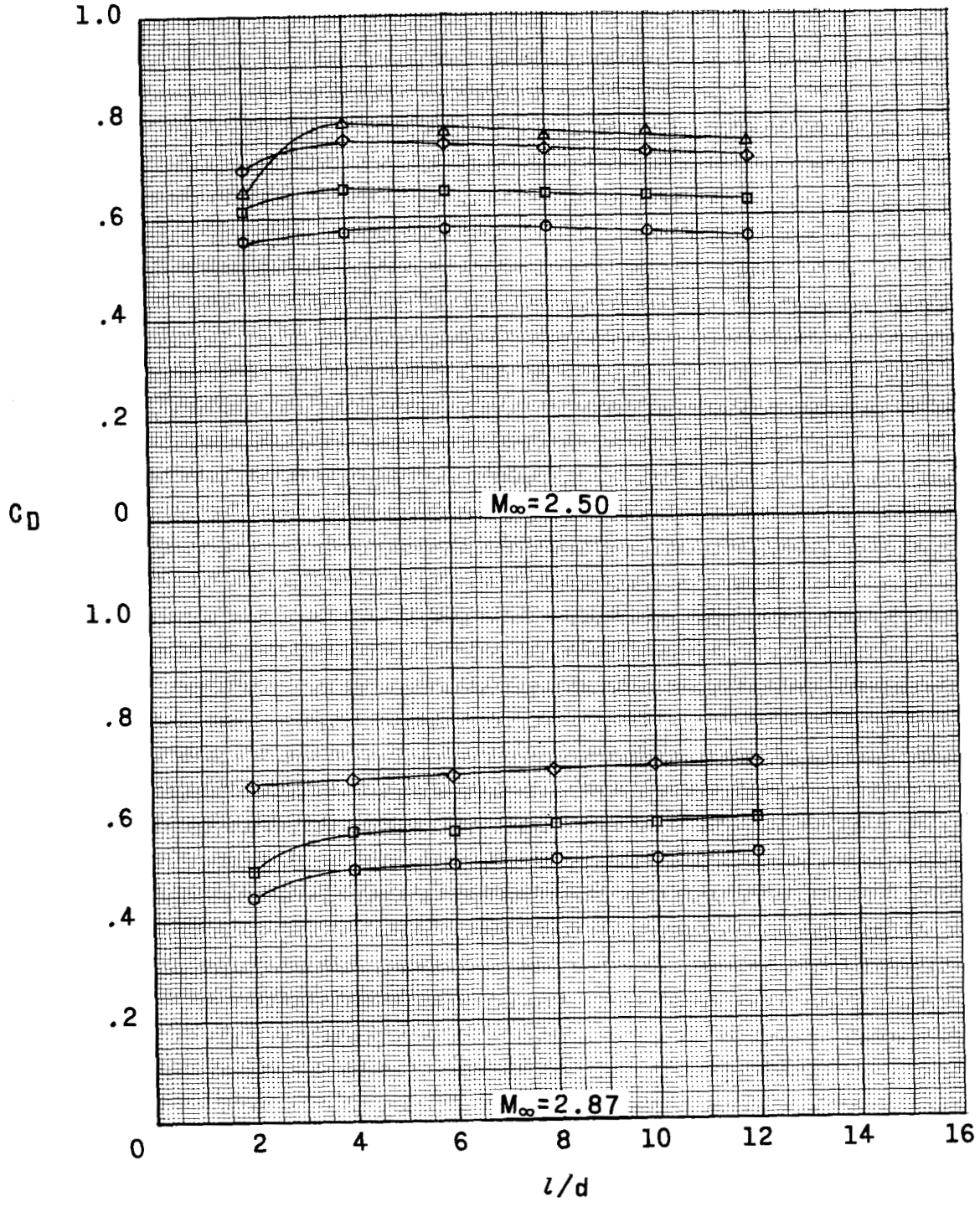

(a) Continued.

Figure 12.- Continued.

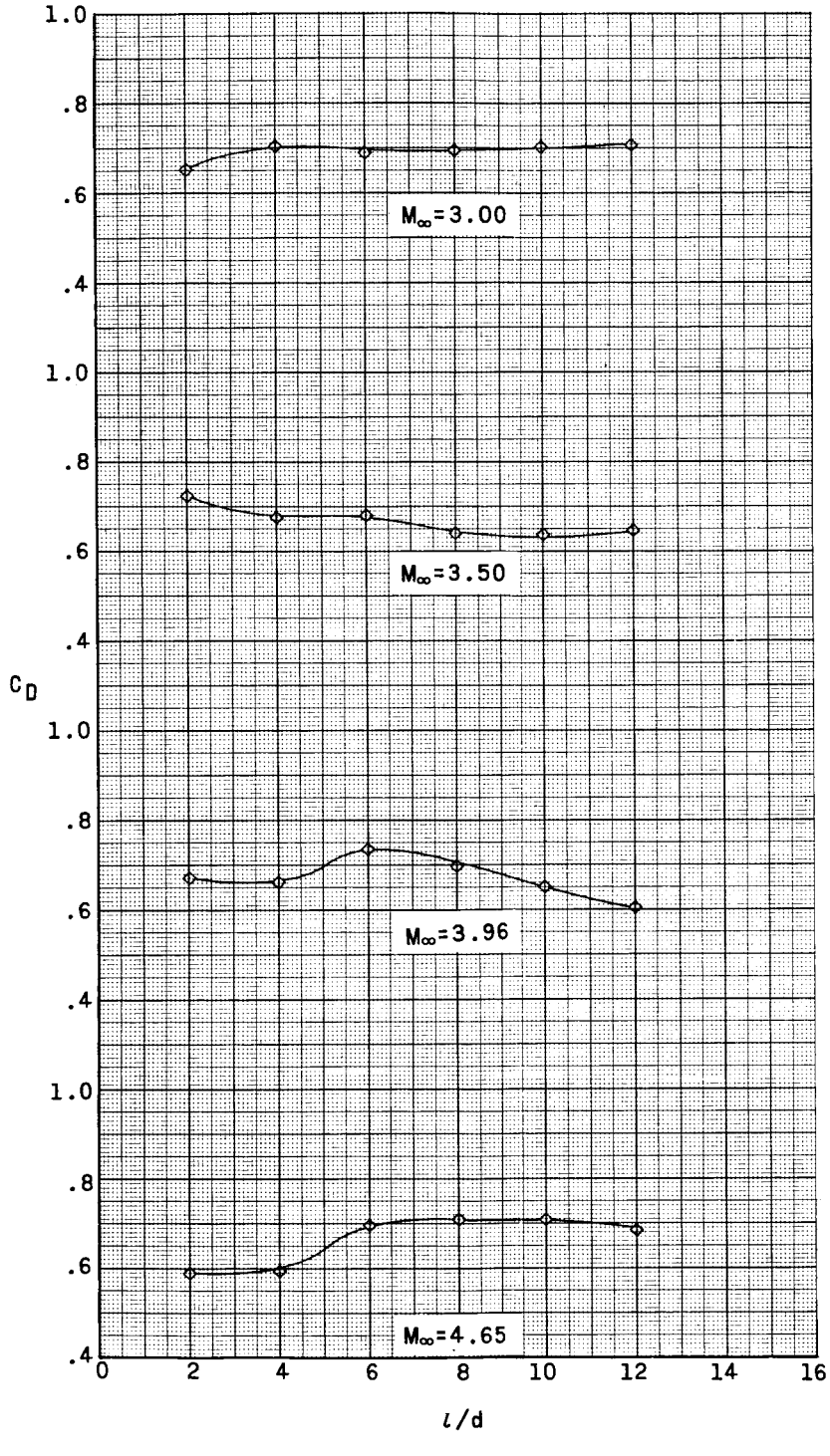

(a) Concluded.

Figure 12.- Continued.

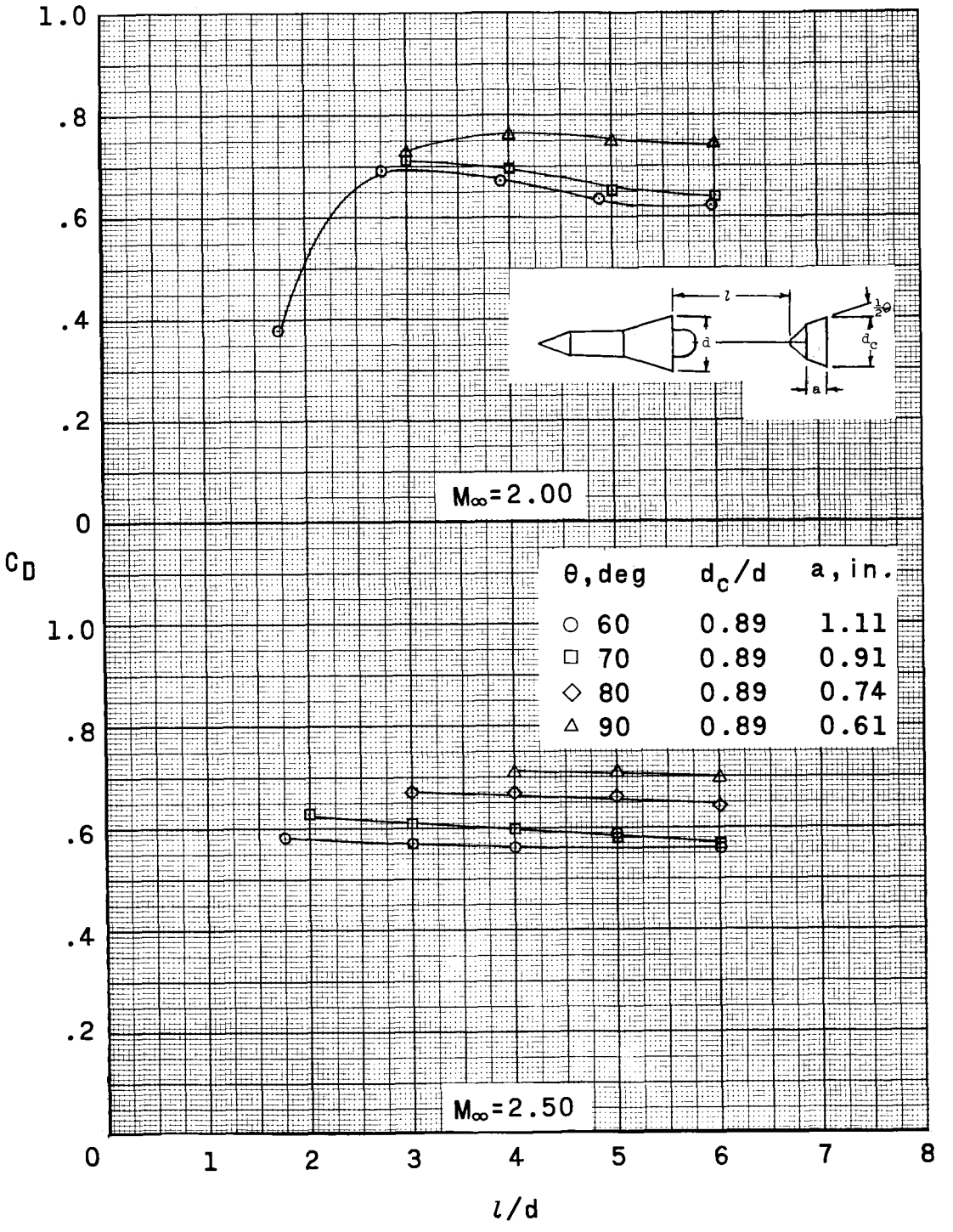

(b) Space vehicle B; $d_f/d = 0.60$.

Figure 12.- Continued.

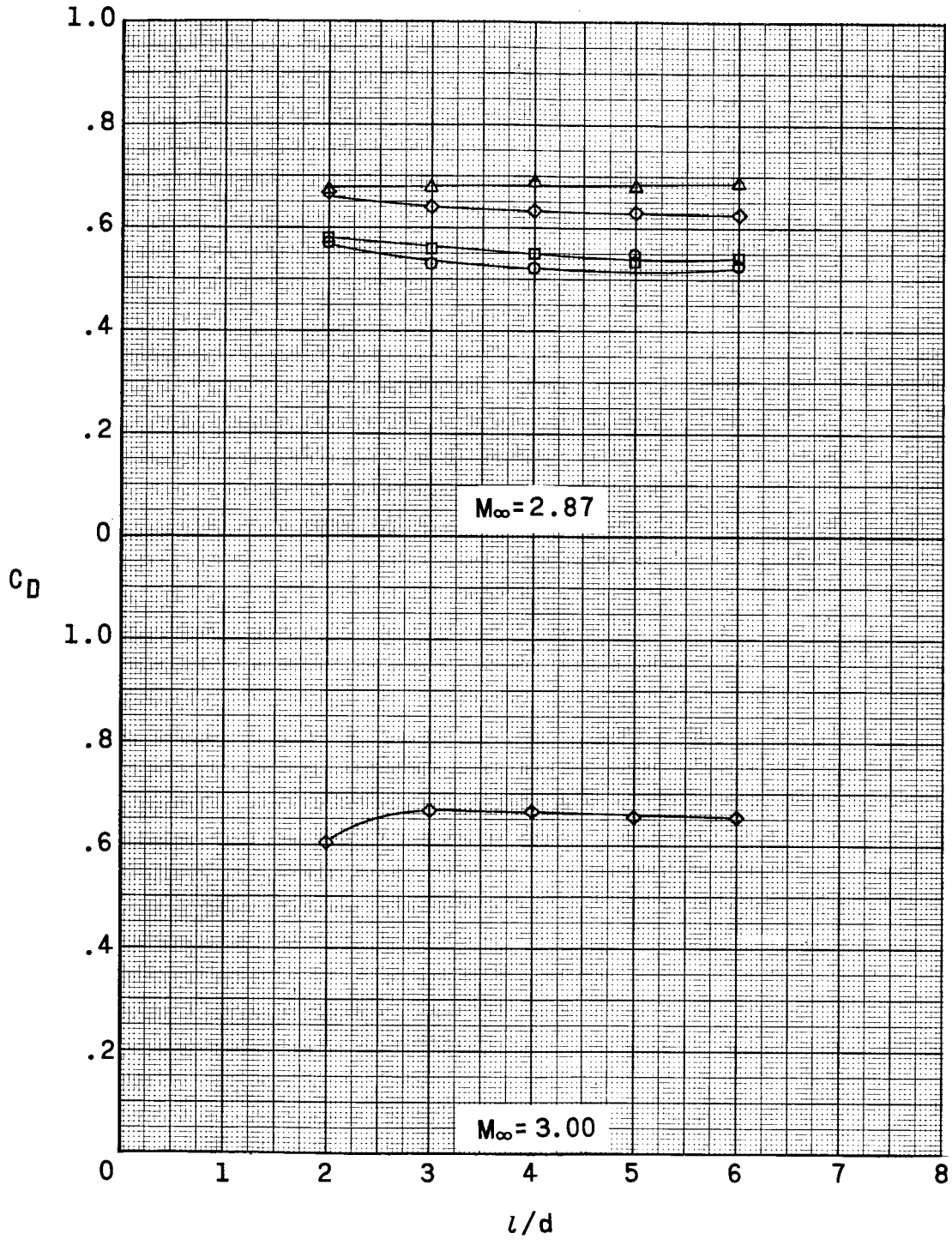

(b) Continued.

Figure 12.- Continued.

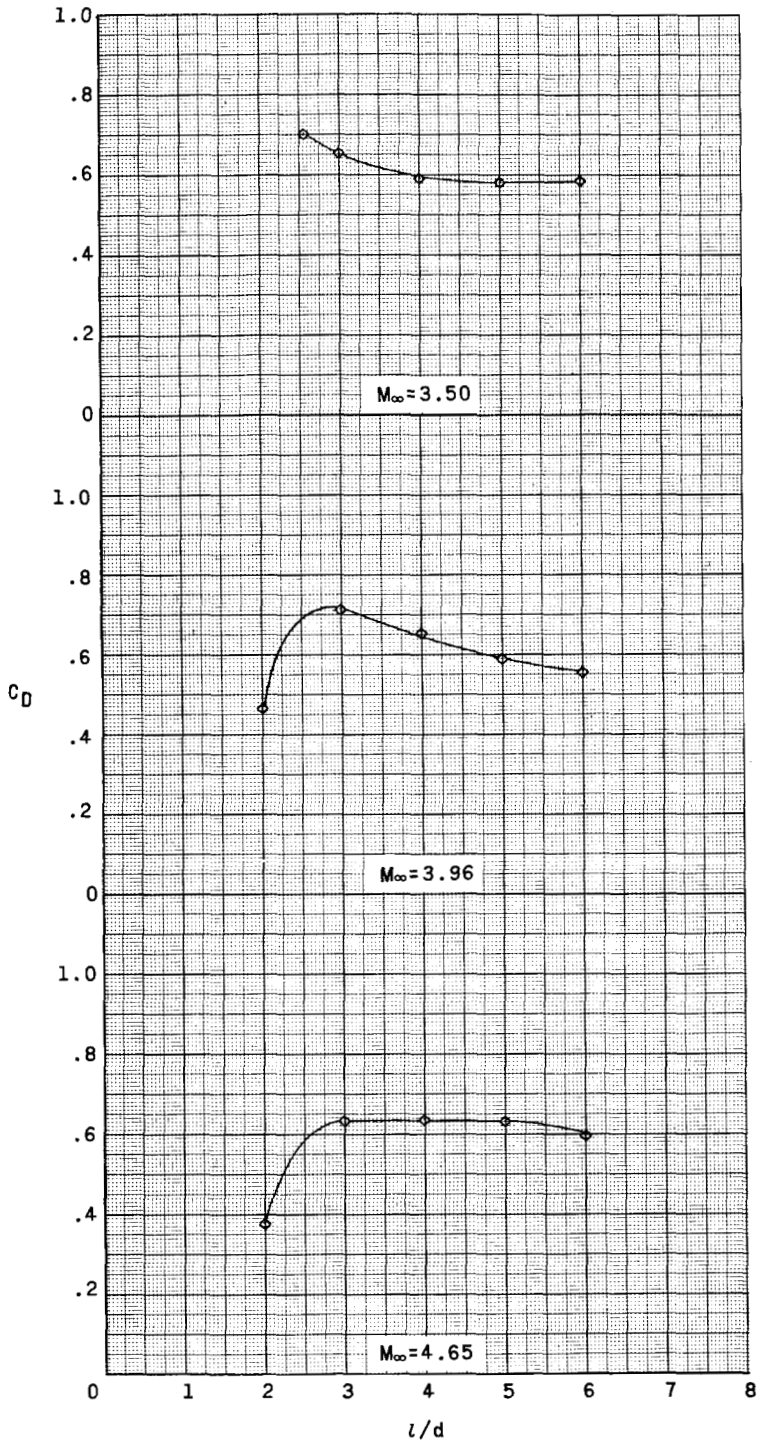

(b) Concluded.

Figure 12.- Continued.

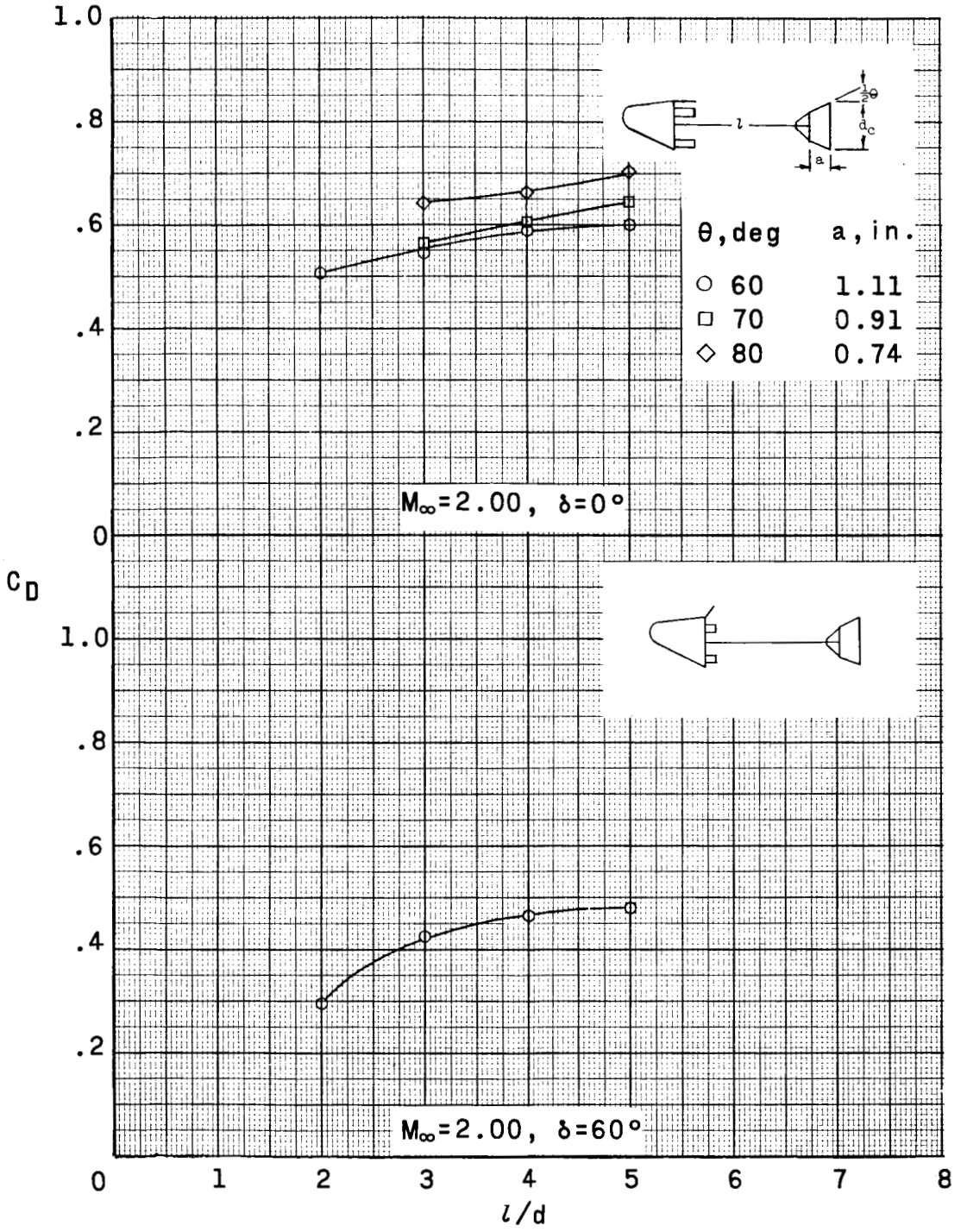

(c) Space vehicle C.

Figure 12.- Continued.

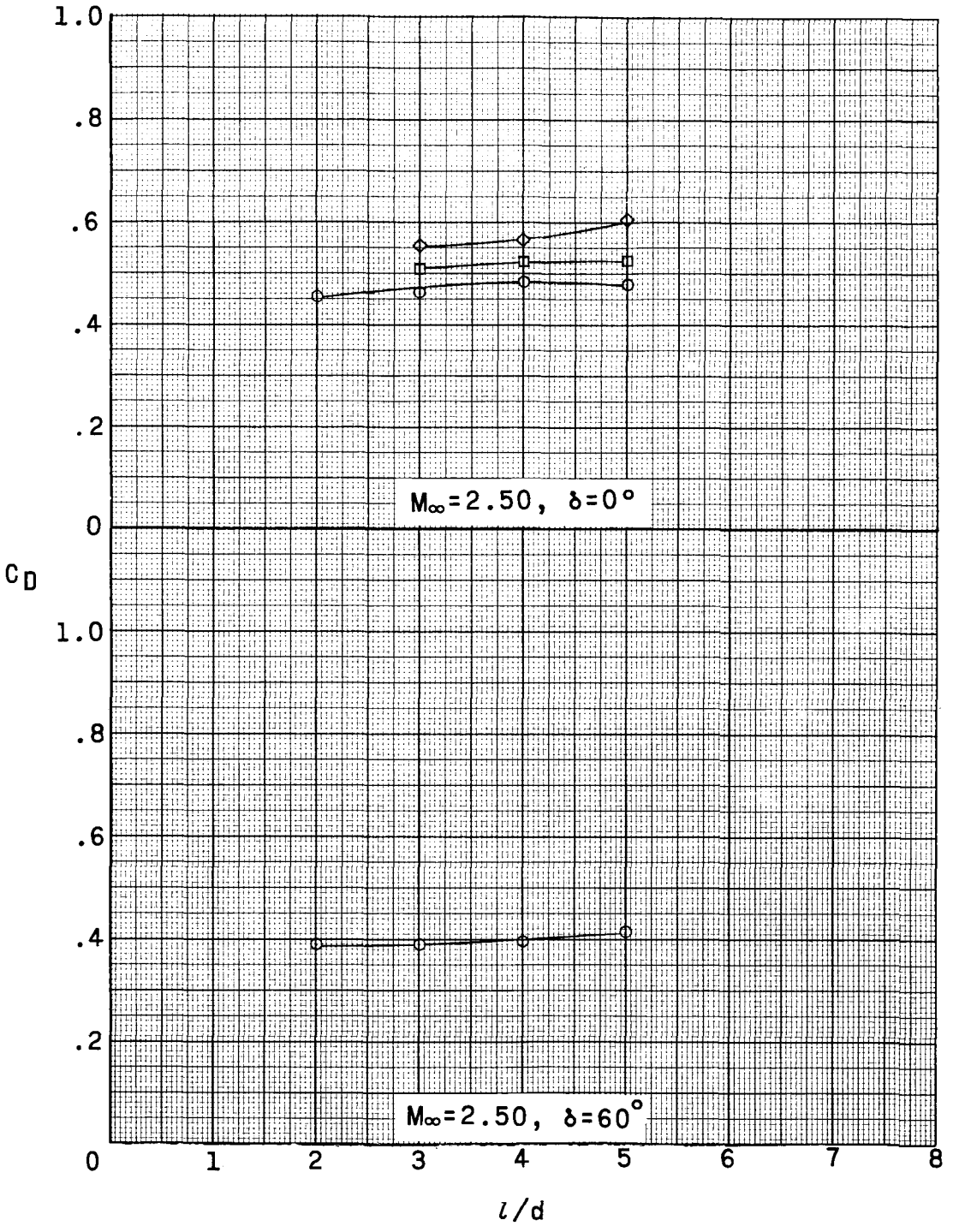

(c) Continued.

Figure 12.- Continued.

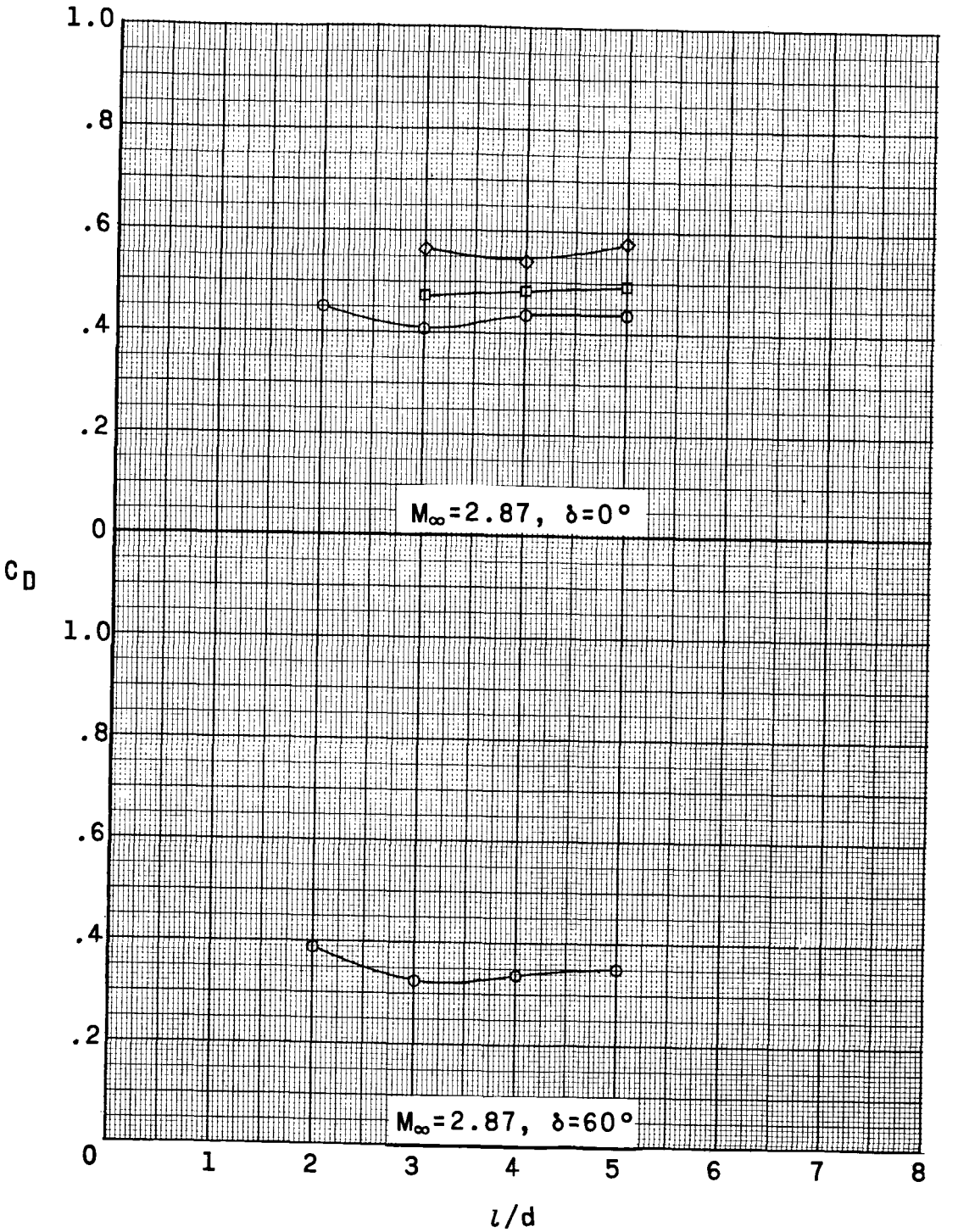

(c) Concluded.

Figure 12.- Concluded.

$\theta = 60°$, $l/d = 2.0$, $M_\infty = 2.00$

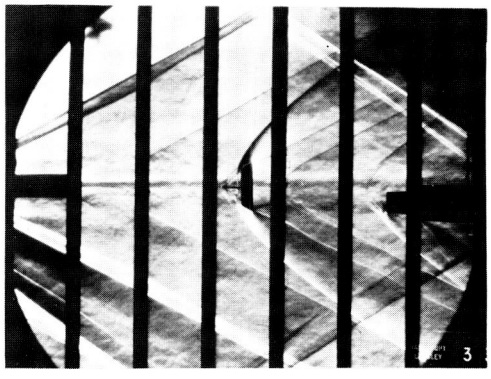

$\theta = 60°$, $l/d = 6.0$, $M_\infty = 2.00$

$\theta = 70°$, $l/d = 4.0$, $M_\infty = 2.50$

$\theta = 70°$, $l/d = 12.0$, $M_\infty = 2.50$

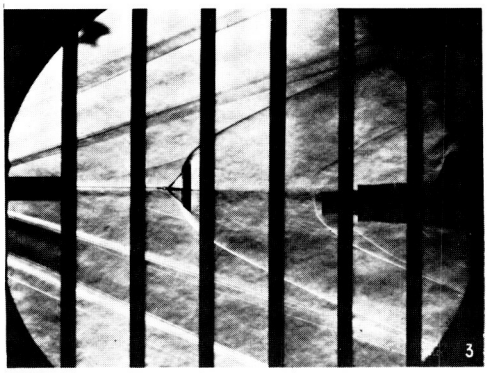

$\theta = 80°$, $l/d = 4.0$, $M_\infty = 2.87$

$\theta = 80°$, $l/d = 10$, $M_\infty = 2.87$

(a) Space vehicle A.

L-63-48

Figure 13.- Typical flow fields about conical rings in the wake of space vehicles A and B at various Mach numbers.

$\theta = 60°$, $l/d = 1.8$, $M_\infty = 2.50$

$\theta = 60°$, $l/d = 3.0$, $M_\infty = 2.50$

$\theta = 80°$, $l/d = 2.0$, $M_\infty = 2.87$

$\theta = 80°$, $l/d = 6.0$, $M_\infty = 2.87$

(b) Space vehicle B.

L-63-49

Figure 13.- Concluded.

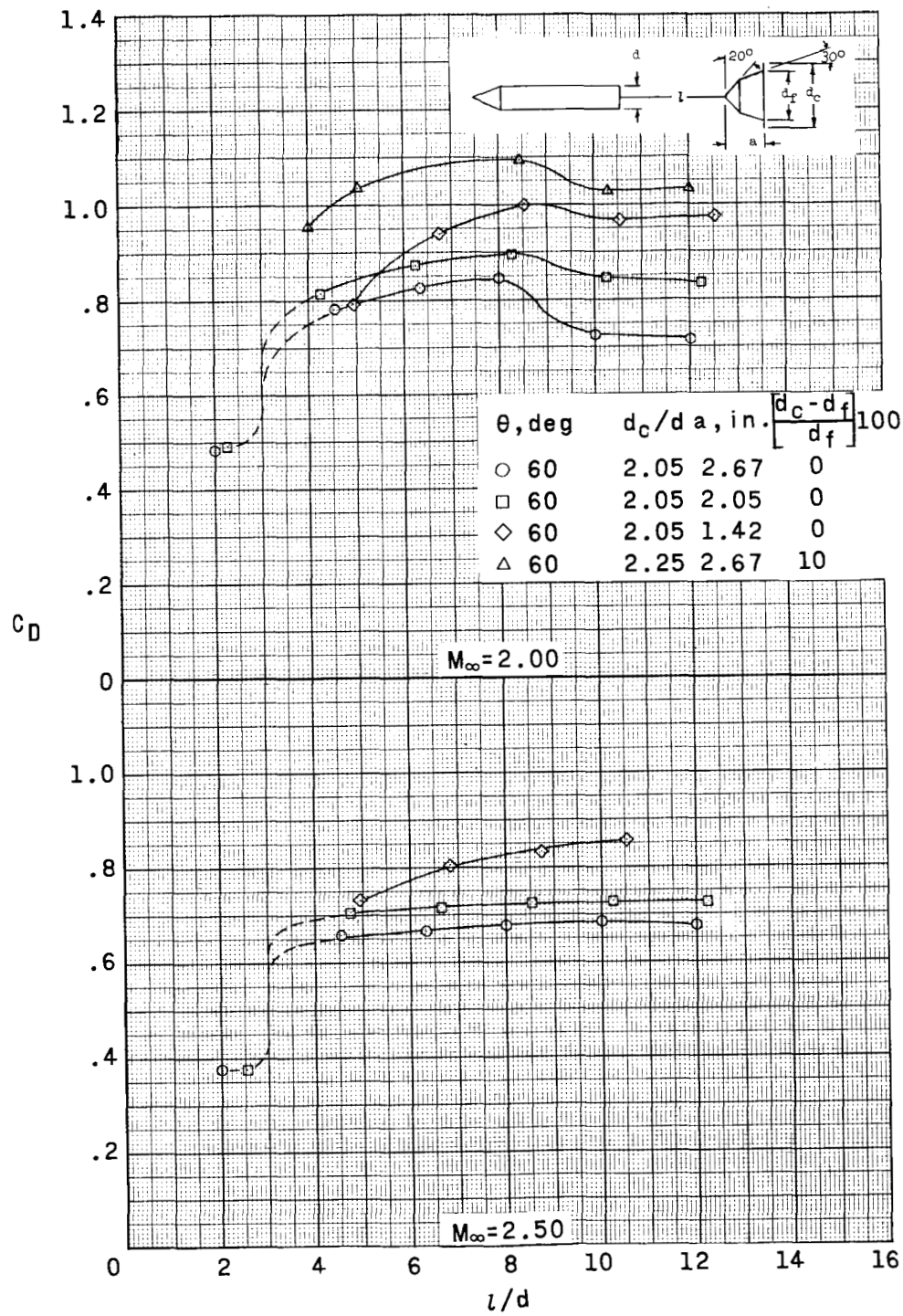

(a) Space vehicle A.

Figure 14.- Variation of drag coefficient with tow-cable length for 60° modified cones at various Mach numbers.

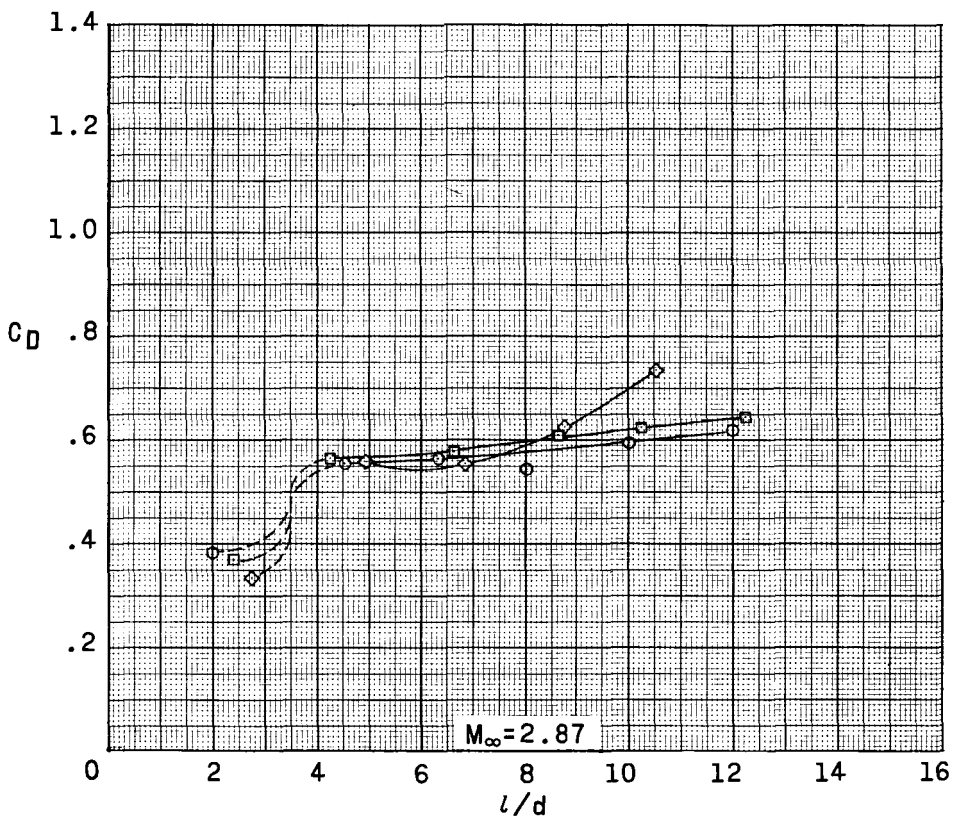

(a) Concluded.

Figure 14.- Continued.

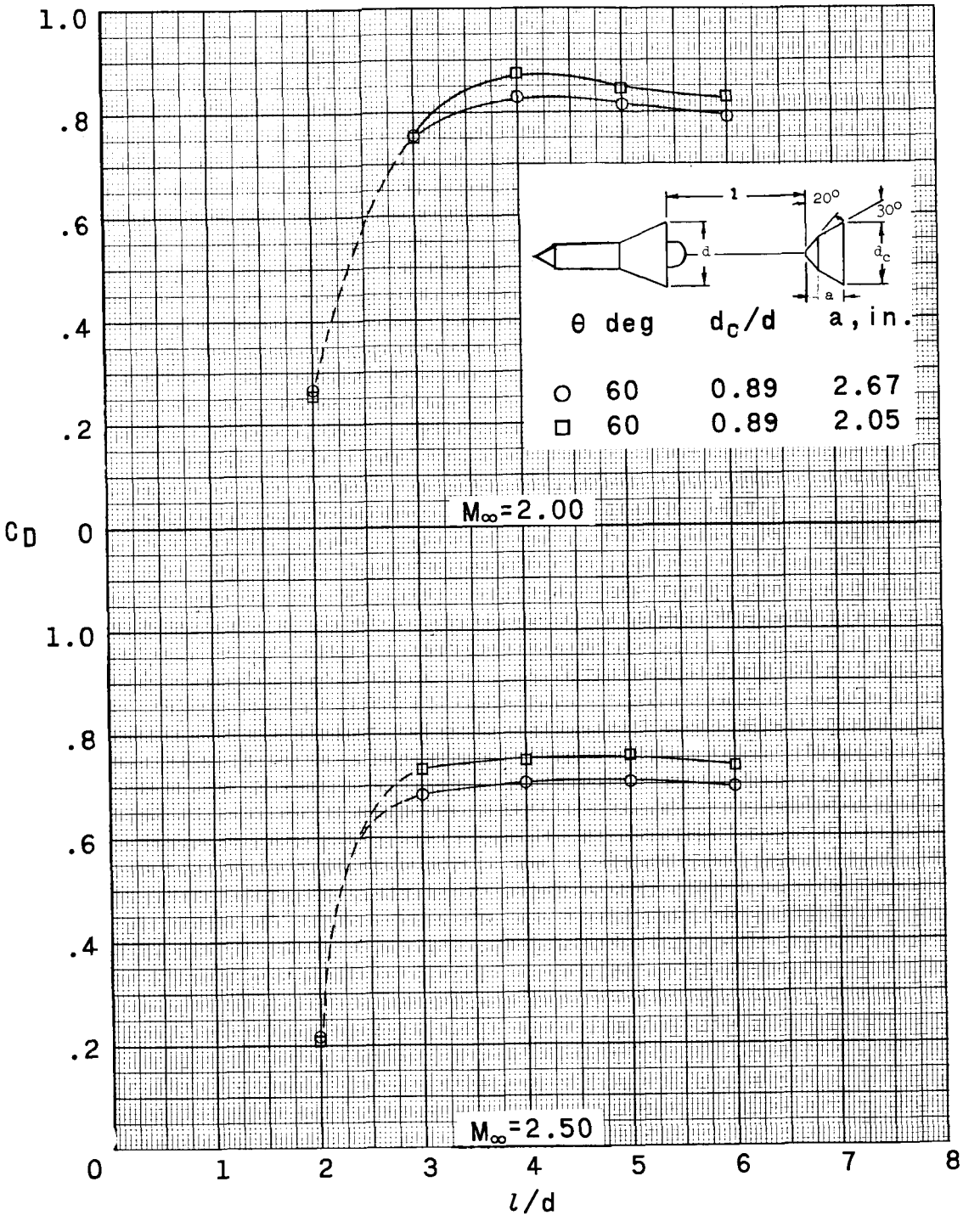

(b) Space vehicle B.

Figure 14.- Continued.

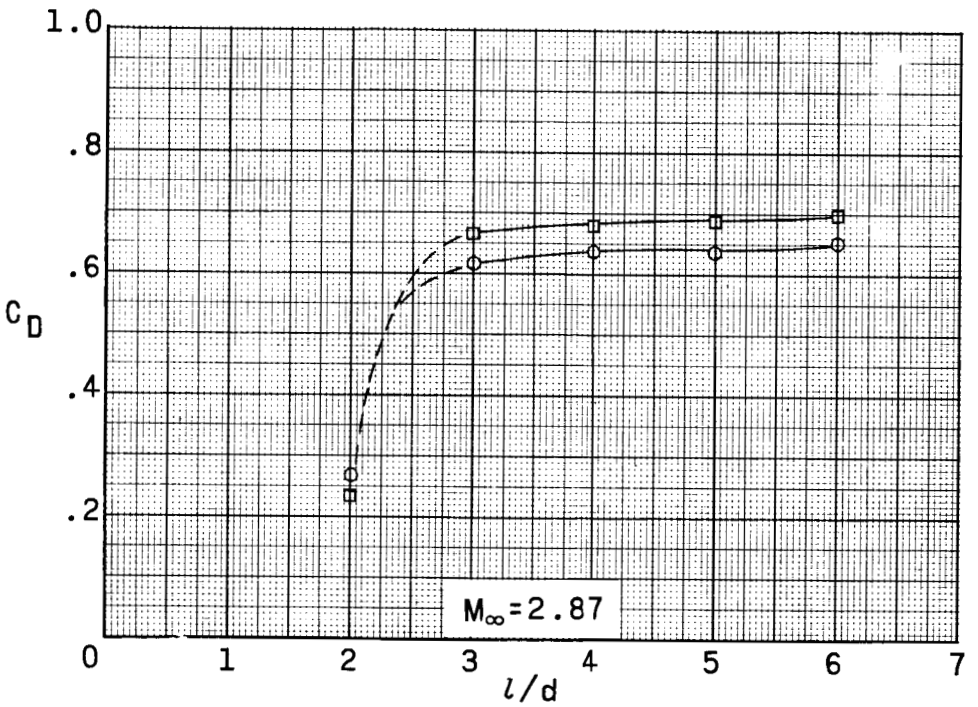

(b) Concluded.

Figure 14.- Continued.

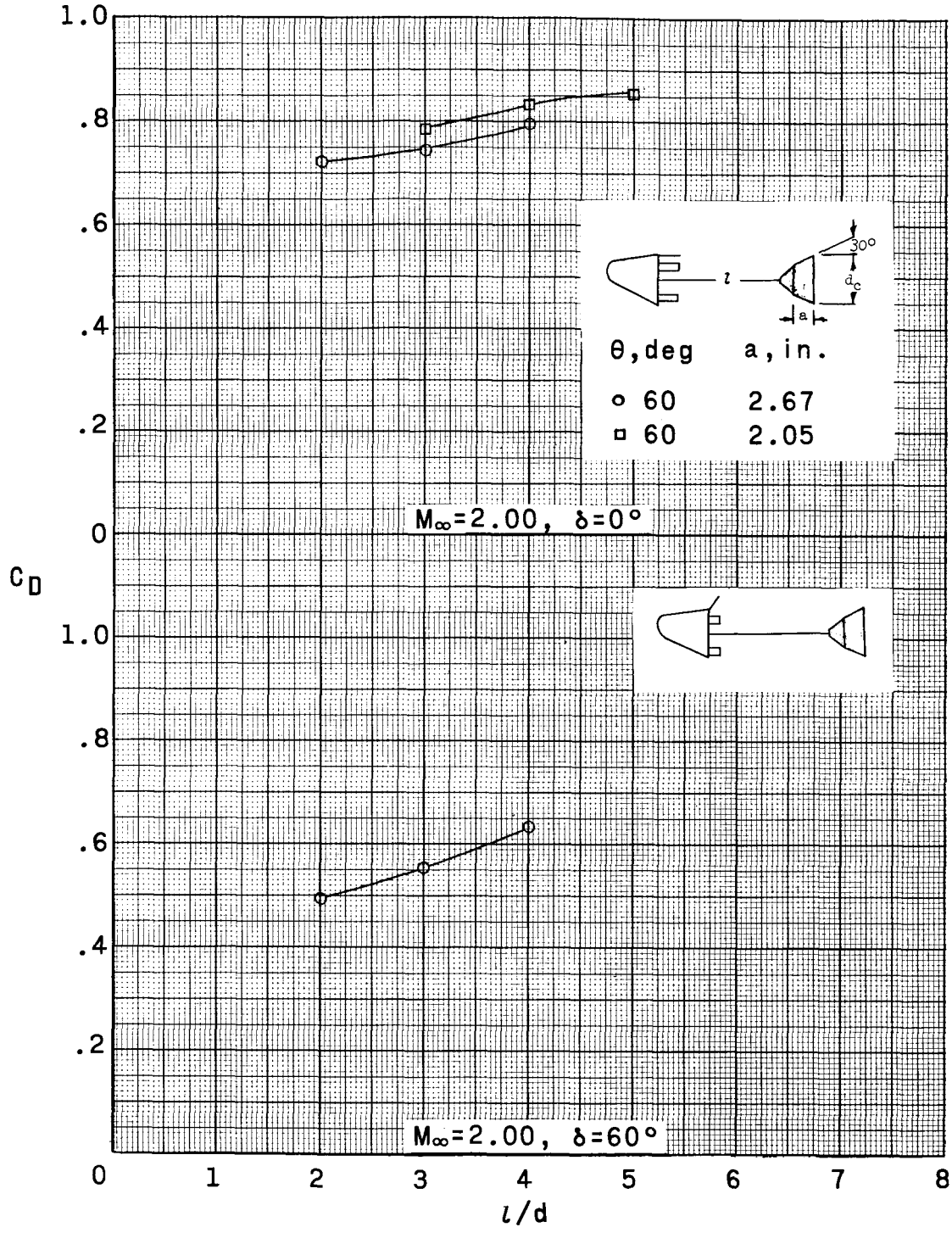

(c) Space vehicle C.

Figure 14.- Continued.

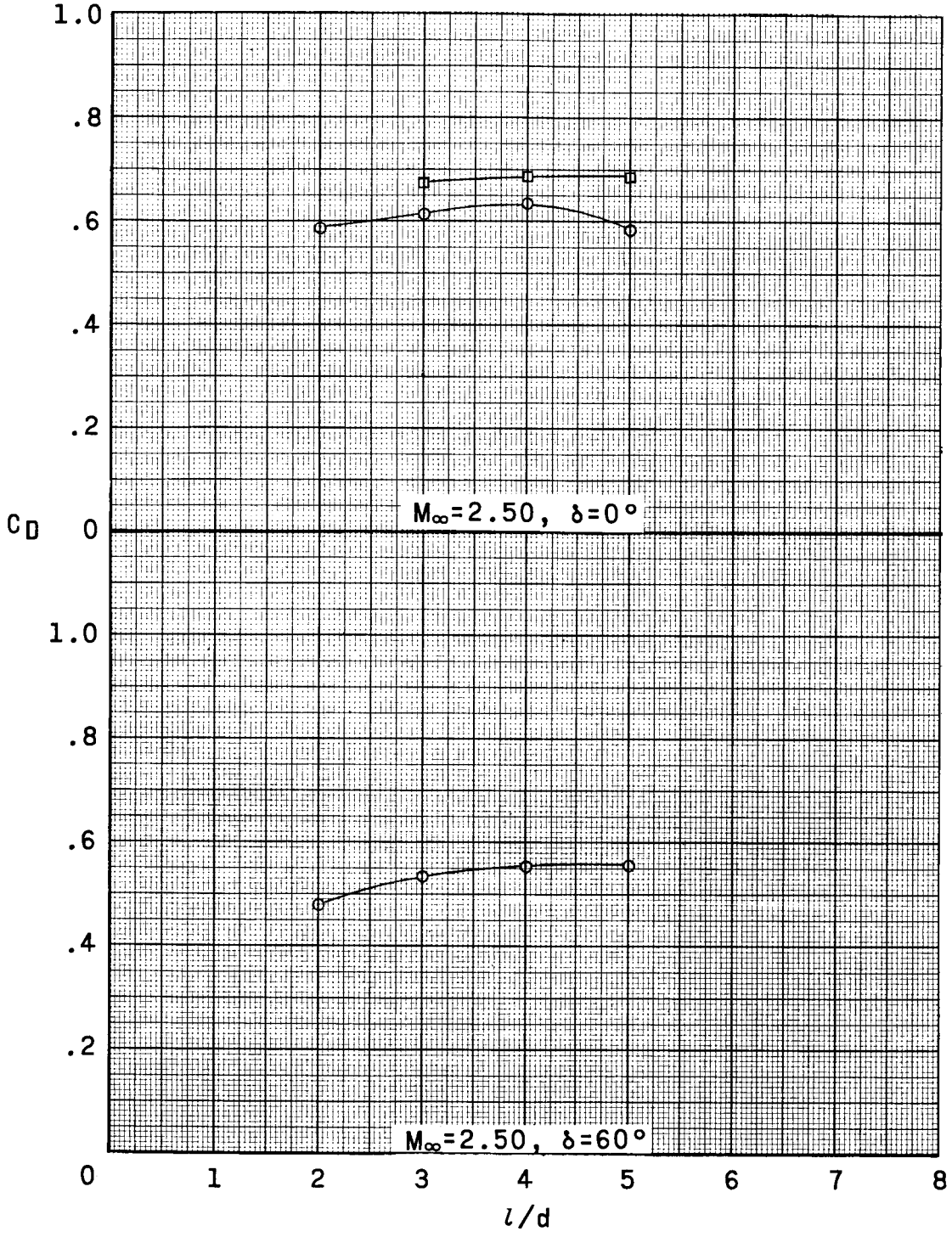

(c) Continued.

Figure 14.- Continued.

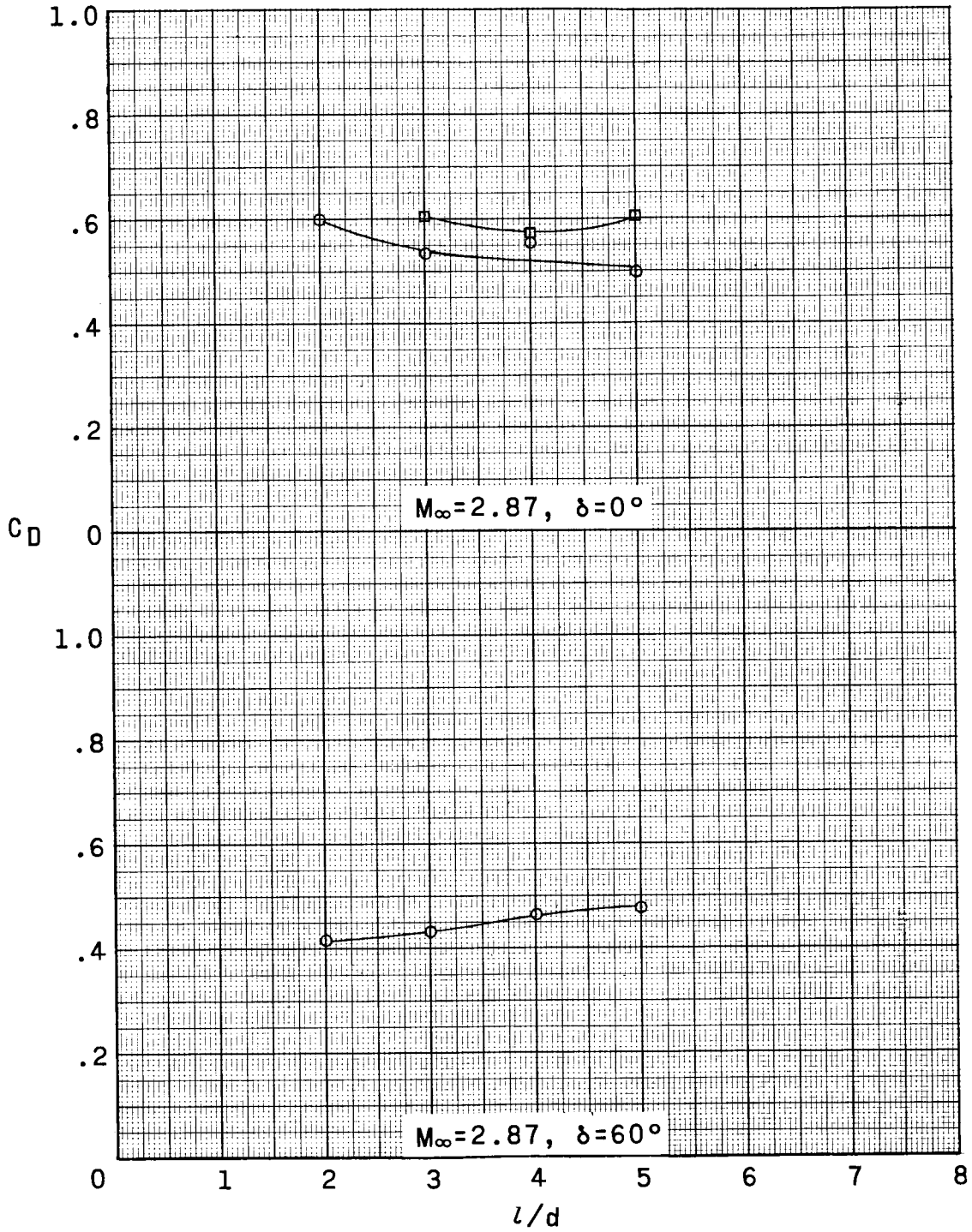

(c) Concluded.

Figure 14.- Concluded.

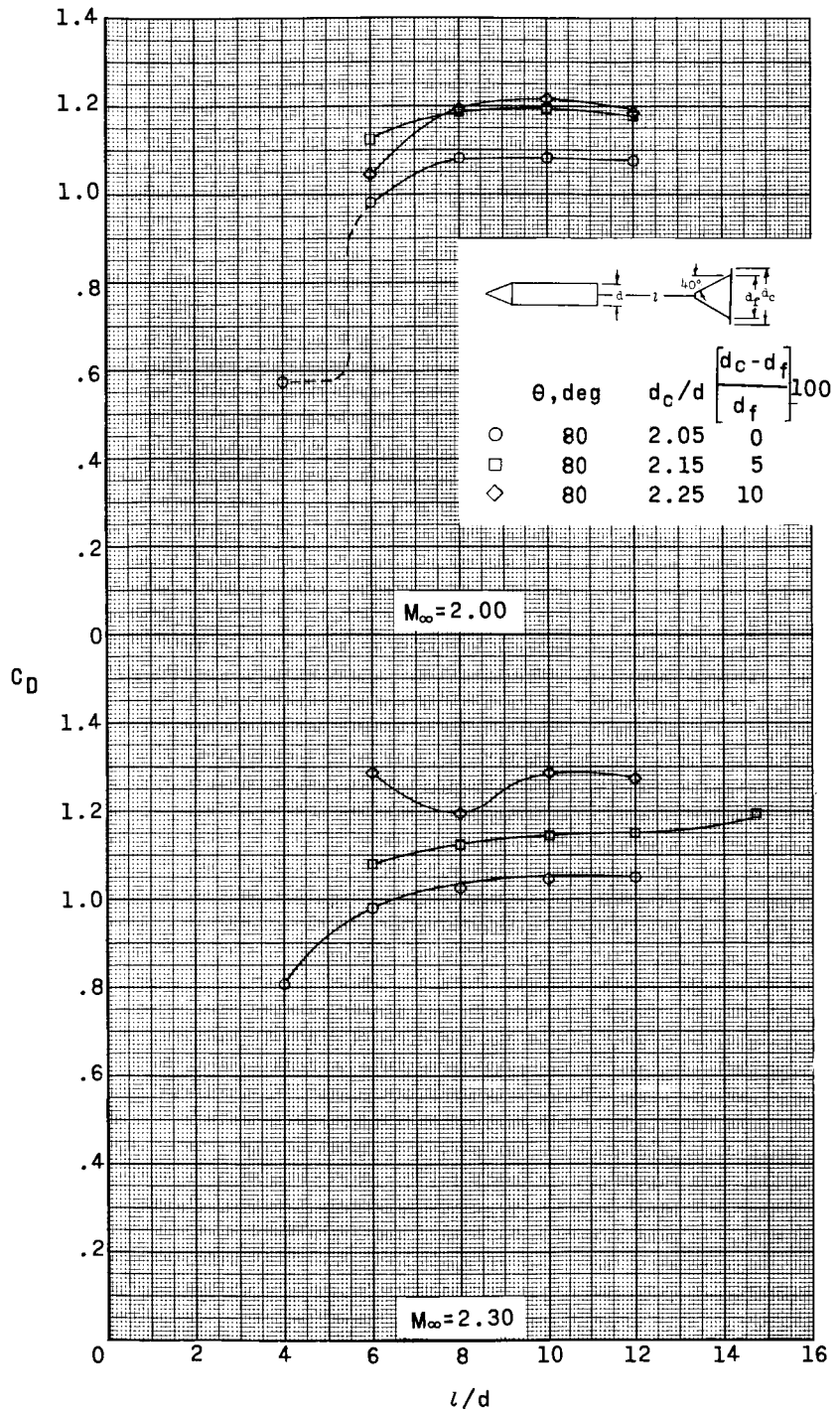

(a) Space vehicle A.

Figure 15.- Variation of drag coefficient with tow-cable length for 80° modified cone at various Mach numbers.

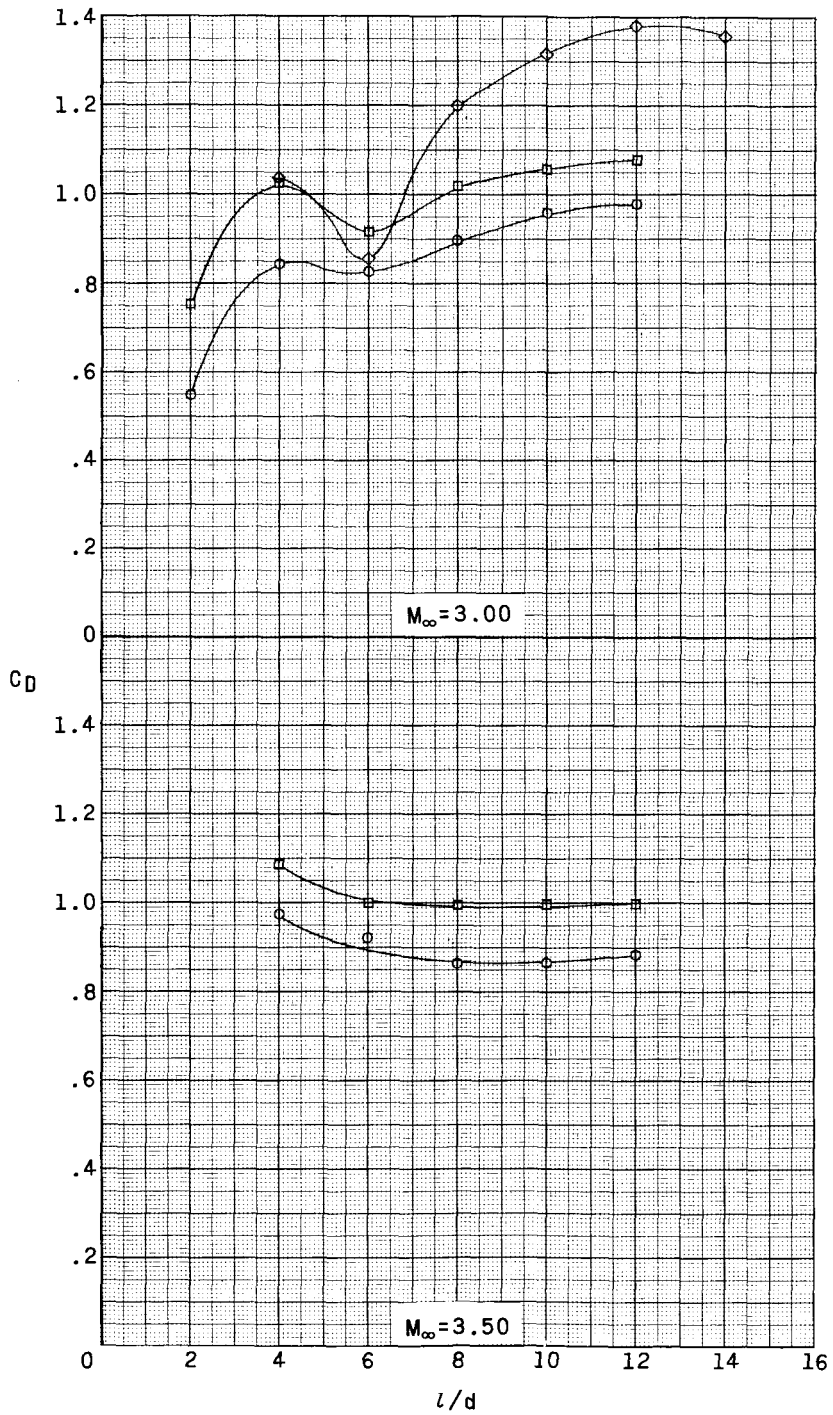

(a) Continued.

Figure 15.- Continued.

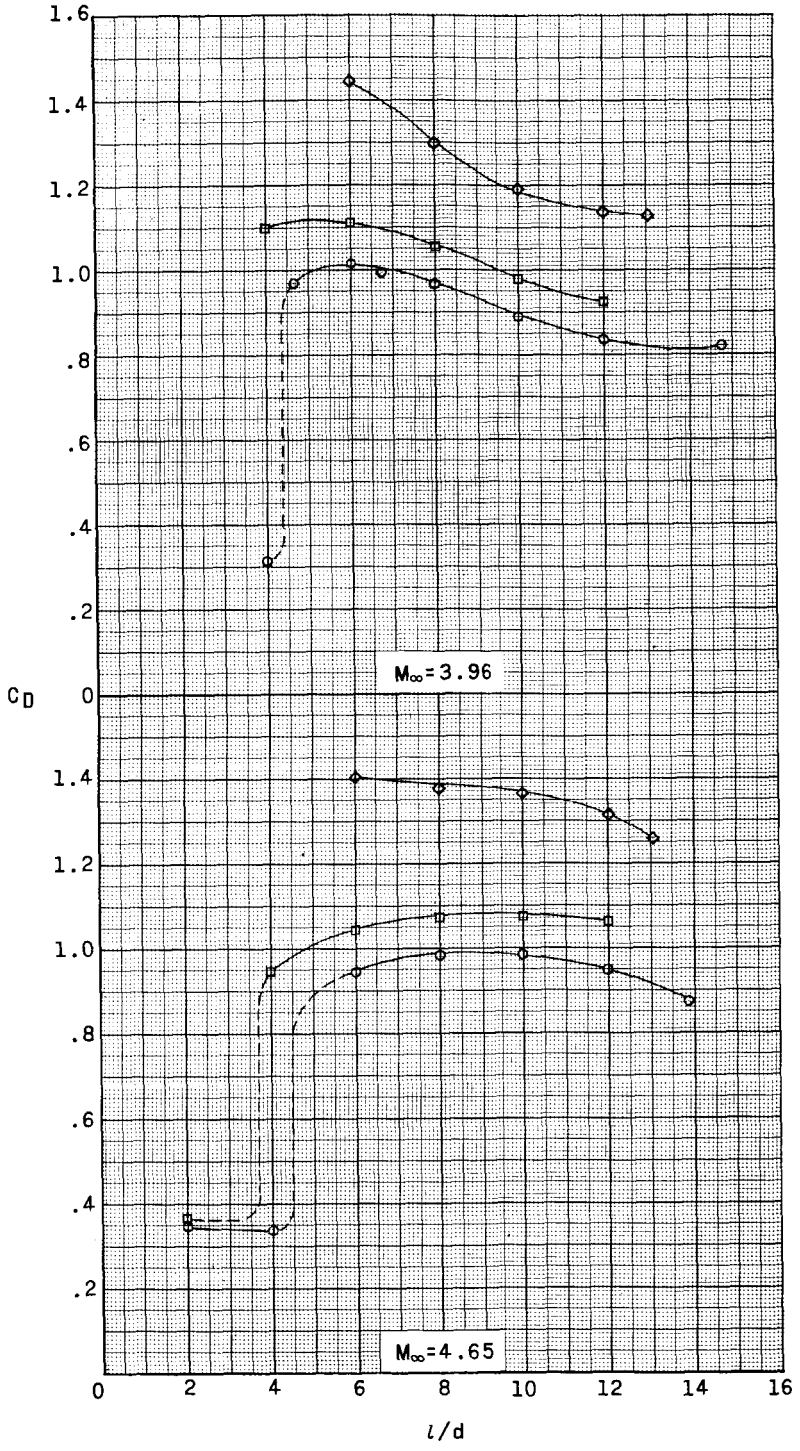

(a) Concluded.

Figure 15.- Continued.

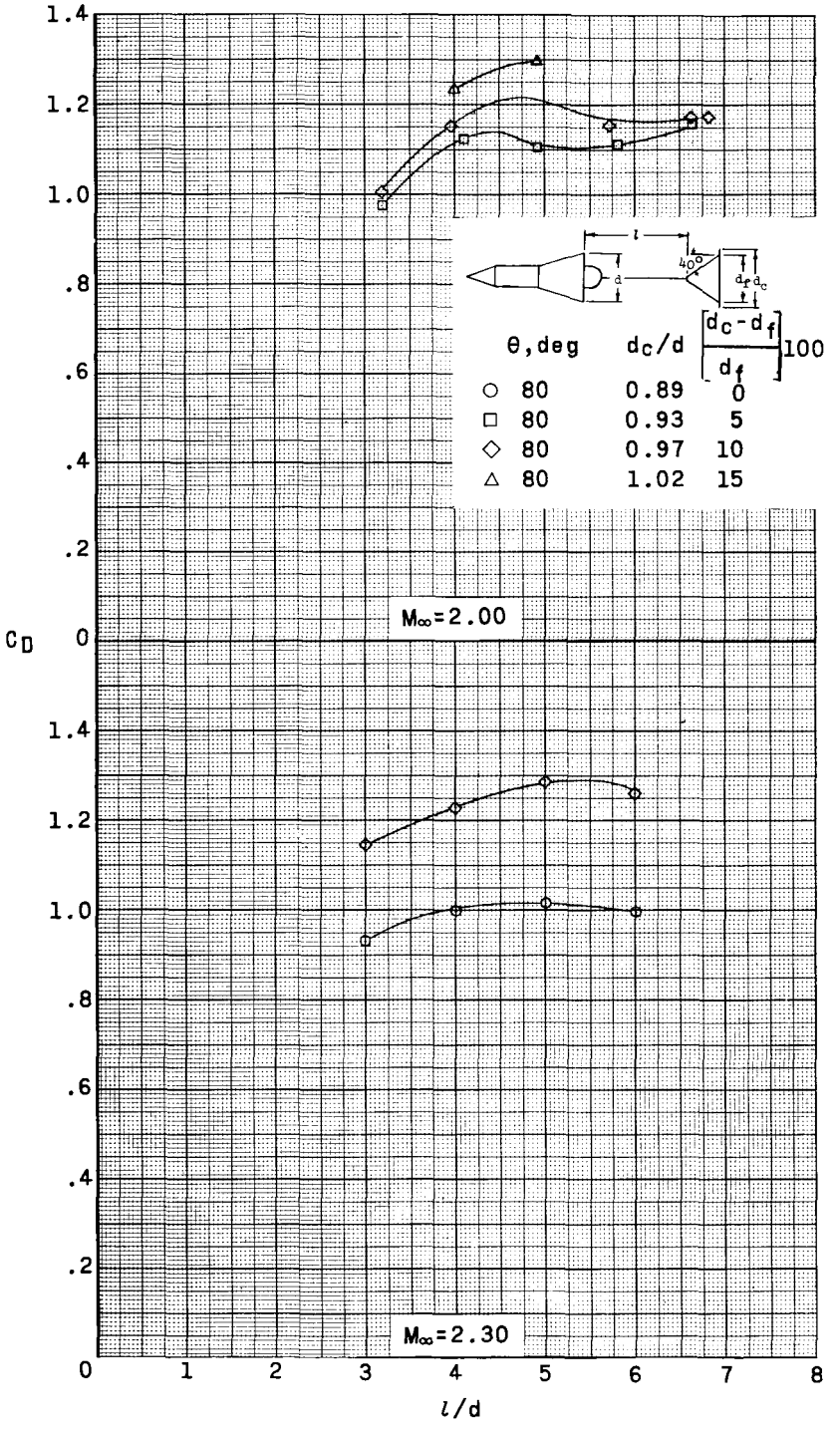

(b) Space vehicle B.

Figure 15.- Continued.

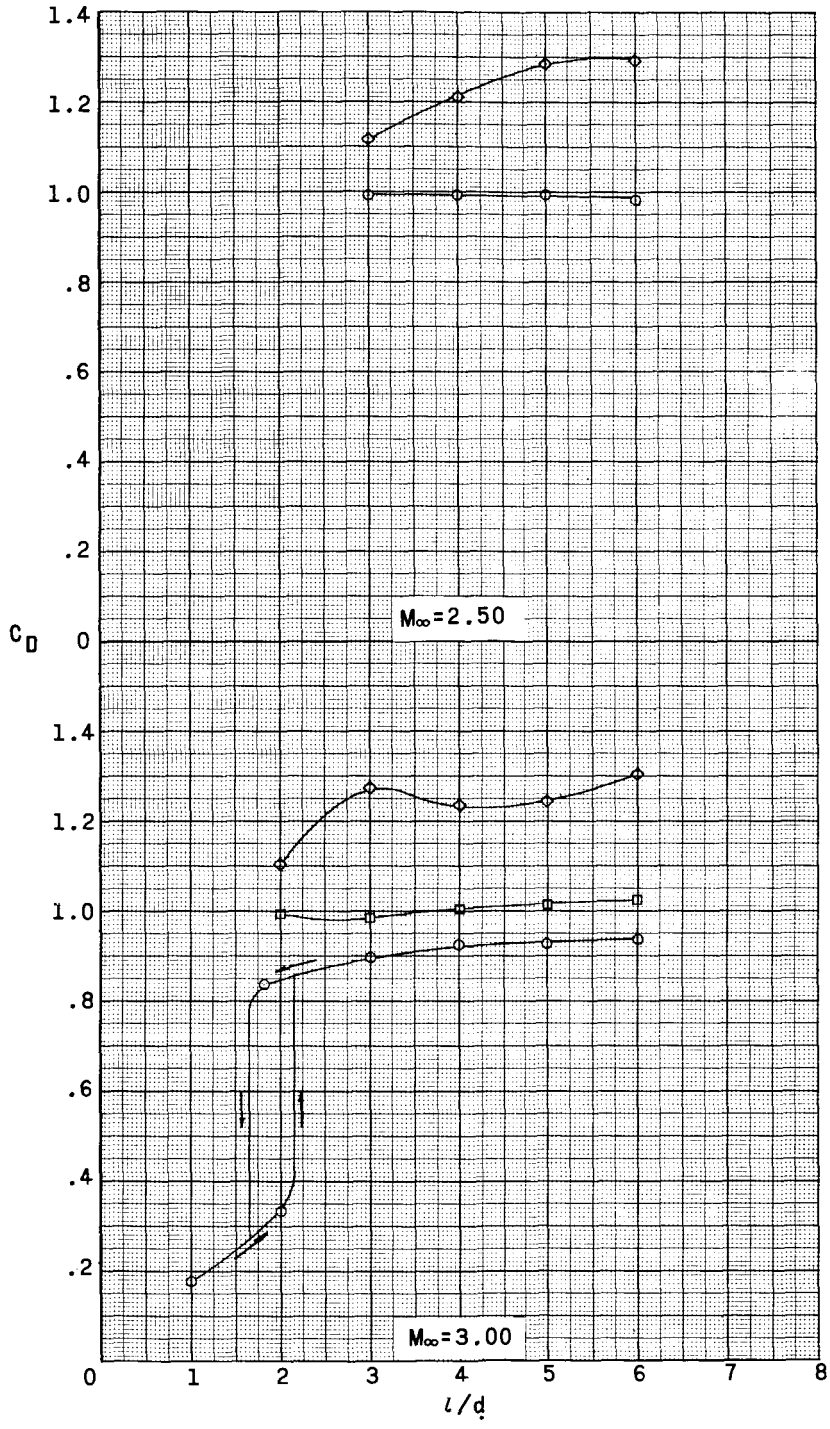

(b) Continued.

Figure 15.- Continued.

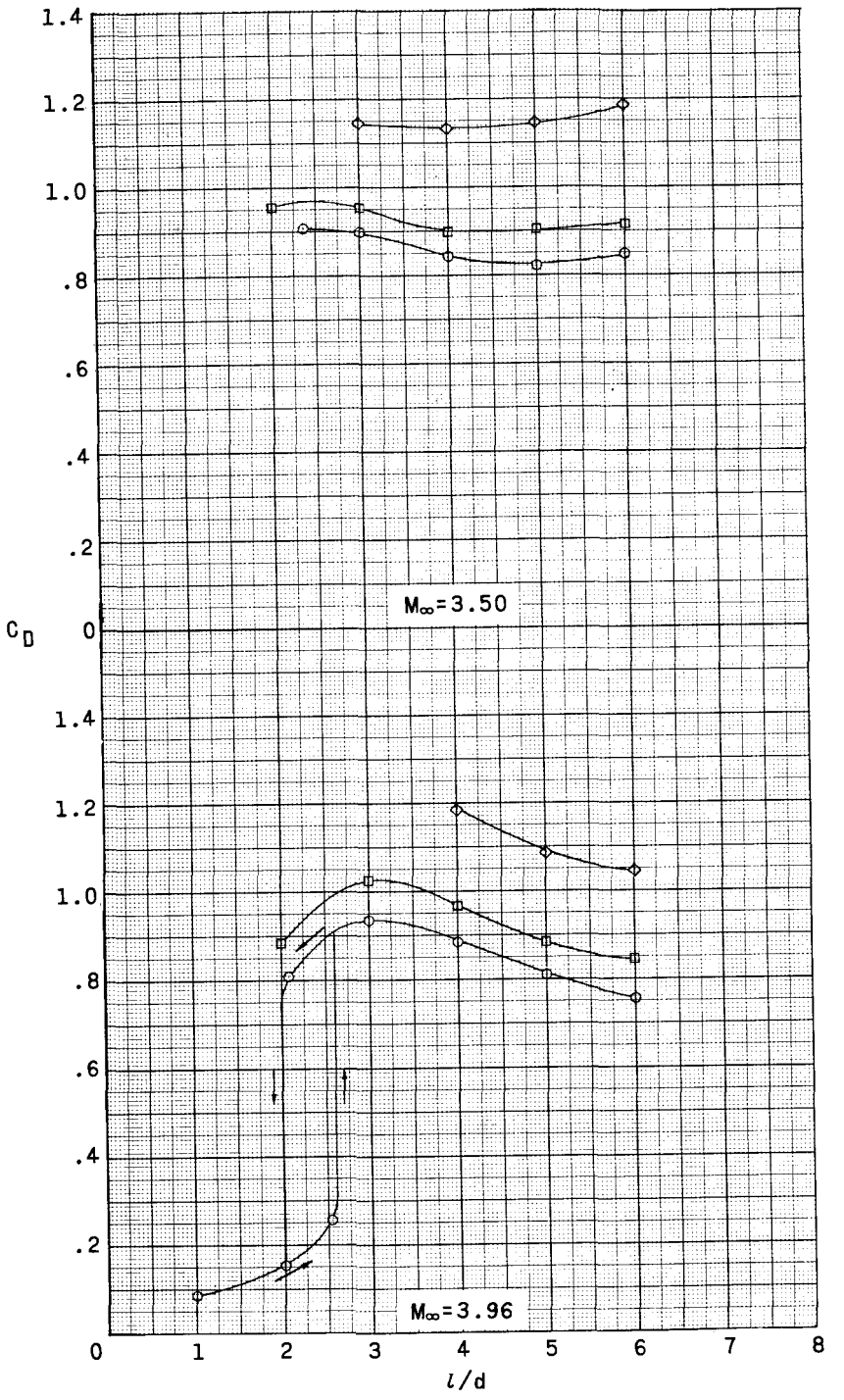

(b) Continued.

Figure 15.- Continued.

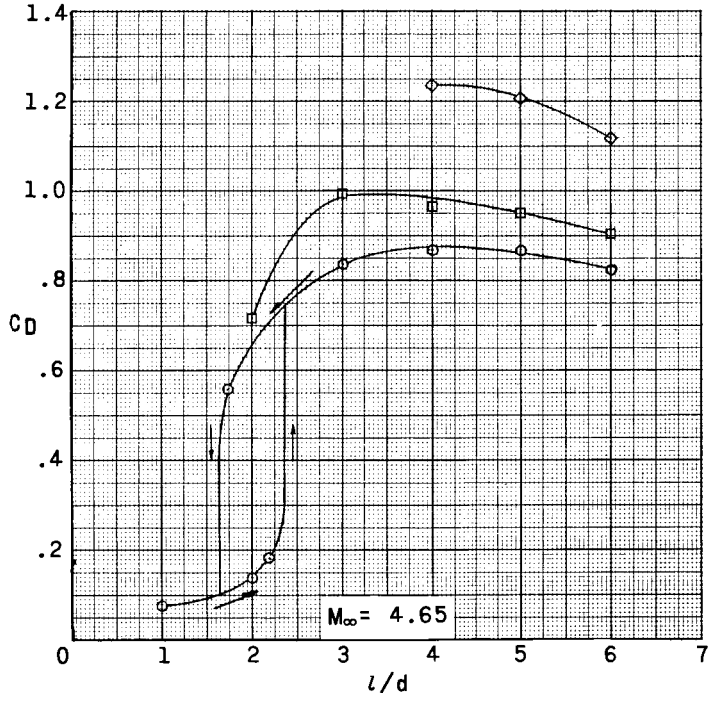

(b) Concluded.

Figure 15.- Concluded.

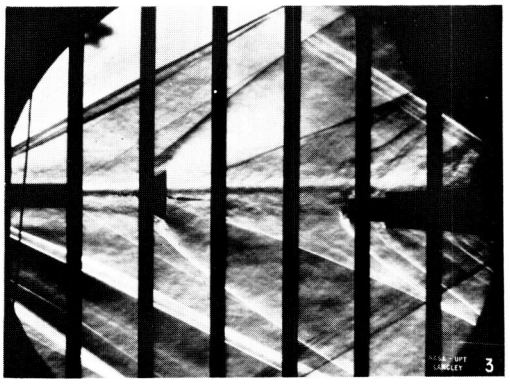

θ = 60°; a = 2.67 ; l/d = 2.0

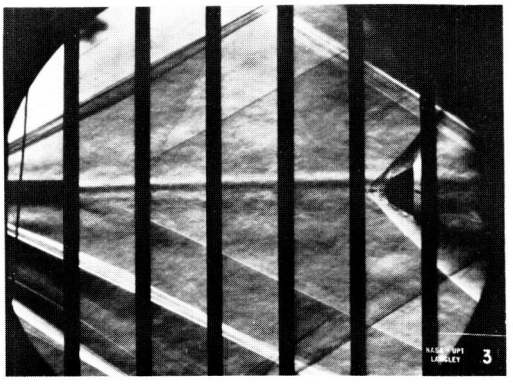

θ = 60°; a = 2.67; l/d = 12.0

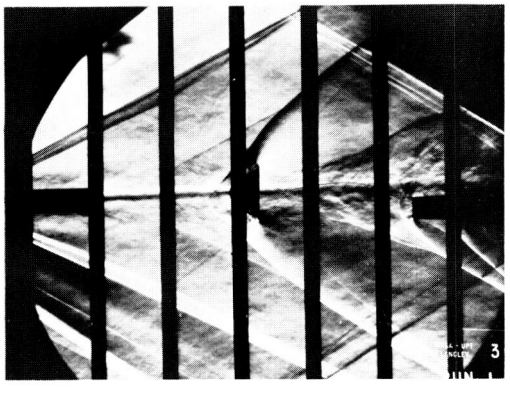

θ = 60°; a = 2.67; l/d = 5.1
(disk-10% increase in diameter)

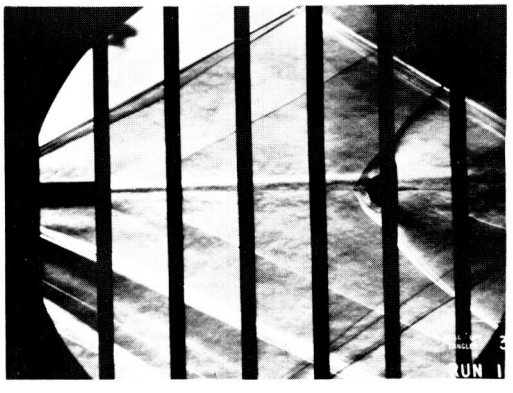

θ = 60°; a = 2.67; l/d = 10.3
(disk-10% increase in diameter)

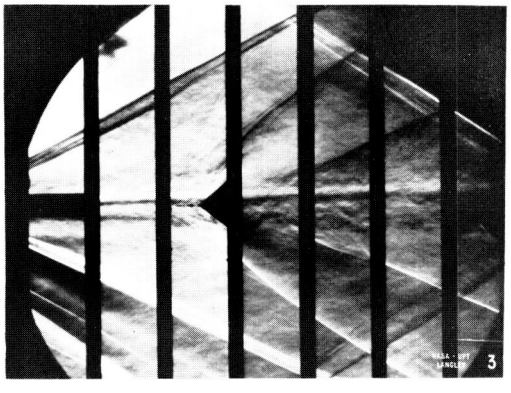

θ = 80°; l/d = 4.0

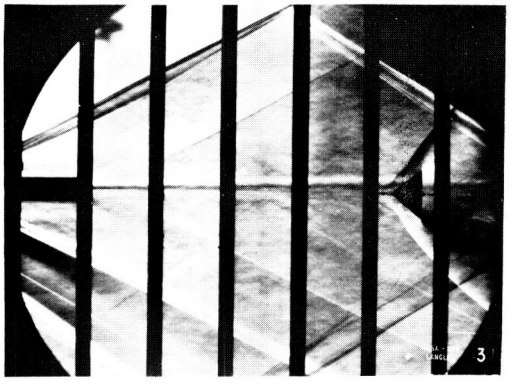

θ = 80°; l/d = 12.0

(a) Space vehicle A. L-63-50

Figure 16.- Typical flow fields of modified 60° and 80° cones in the wake of space vehicles A and B at a Mach number of 2.00.

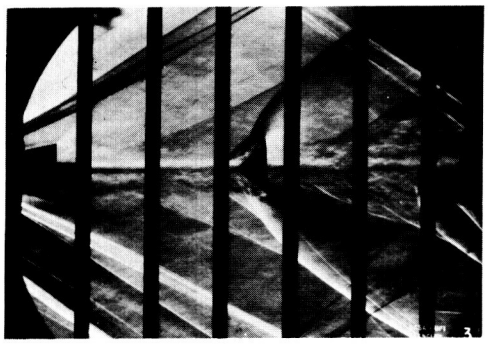

θ = 80°, l/d = 3.2
(disk-5% increase in diameter)

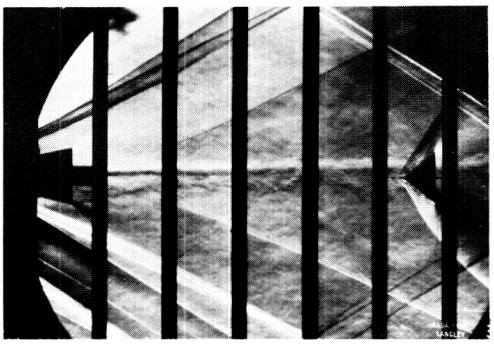

θ = 80°, l/d = 5.8
(disk-5% increase in diameter)

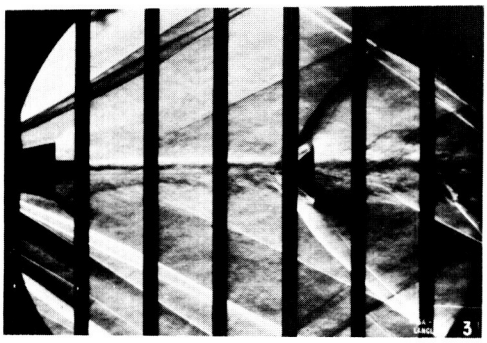

θ = 80°, l/d = 4.0
(disk-10% increase in diameter)

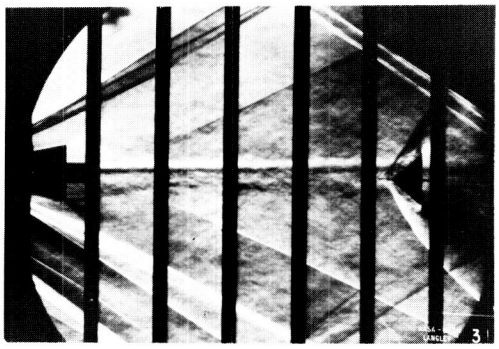

θ = 80°, l/d = 5.7
(disk-10% increase in diameter)

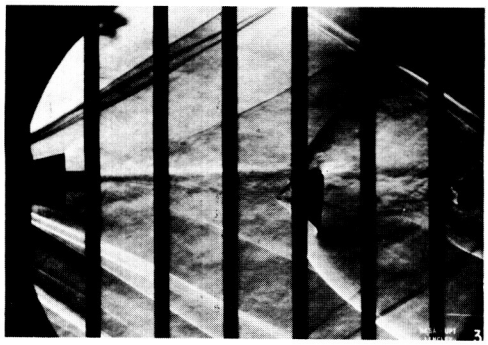

θ = 80°, l/d = 4.0
(disk-15% increase in diameter)

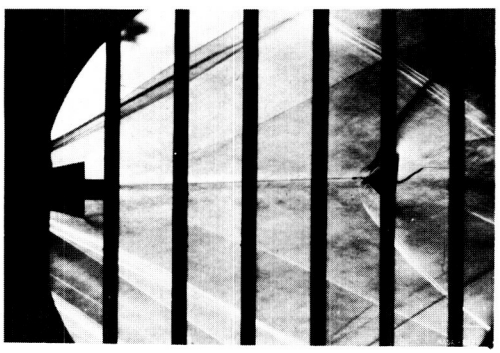

θ = 80°, l/d = 4.9
(disk-15% increase in diameter)

(b) Space vehicle B. L-63-51

Figure 16.- Concluded.

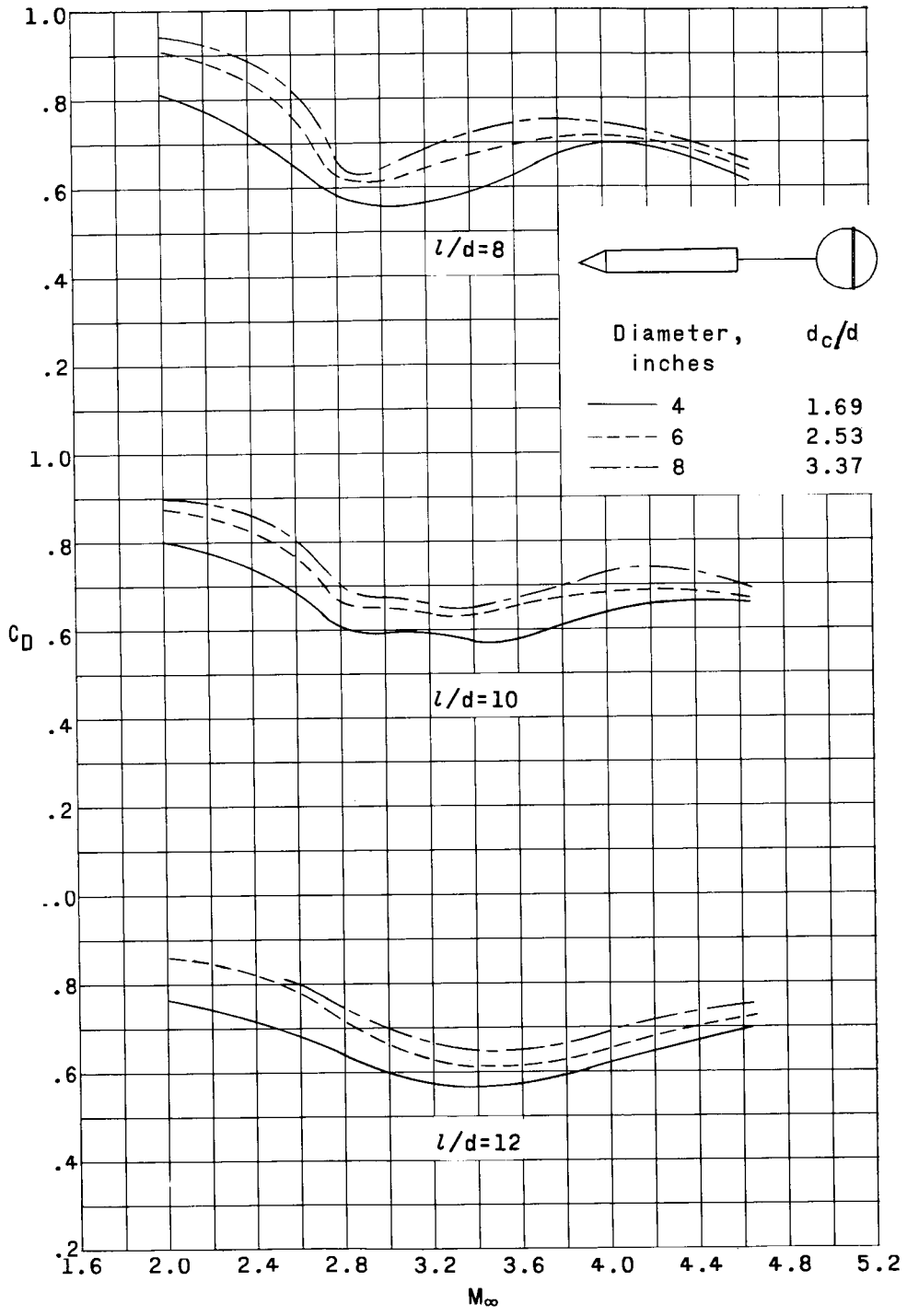

(a) Space vehicle A.

Figure 17.- Variation of drag coefficient with Mach numbers for 4-, 6-, and 8-inch spheres at various tow-cable lengths.

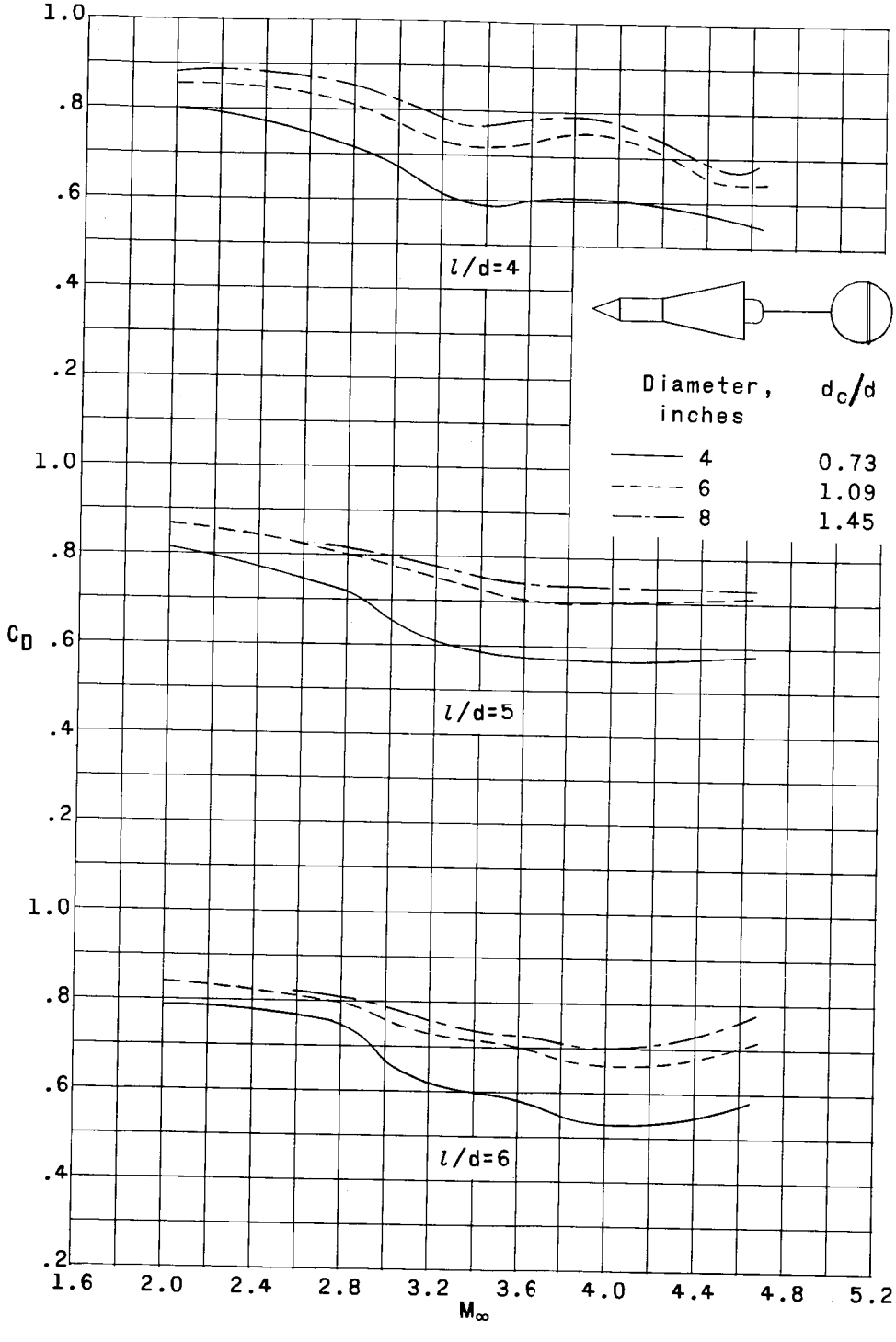

(b) Space vehicle B.

Figure 17.- Continued.

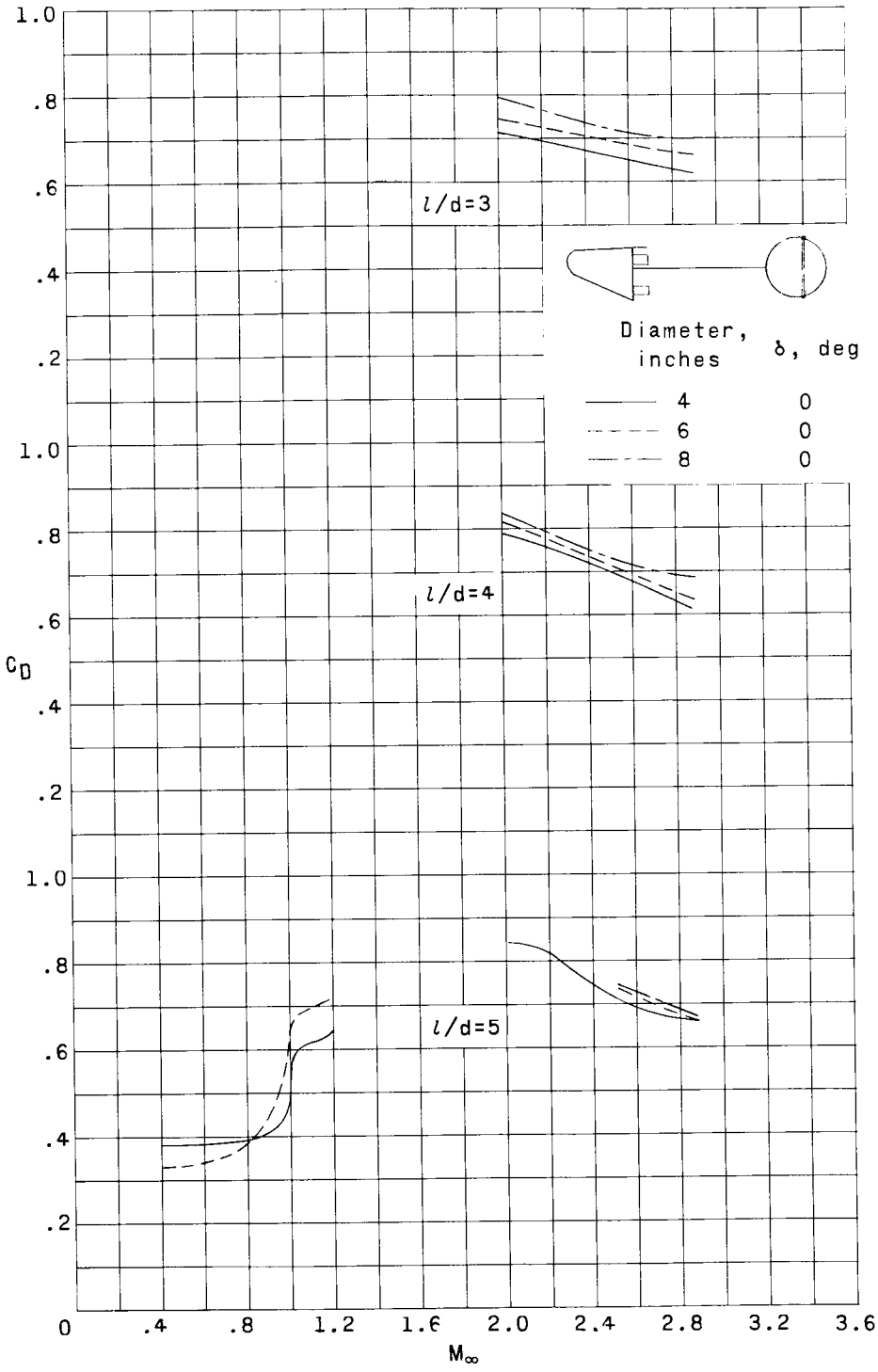

(c) Space vehicle C.

Figure 17.- Continued.

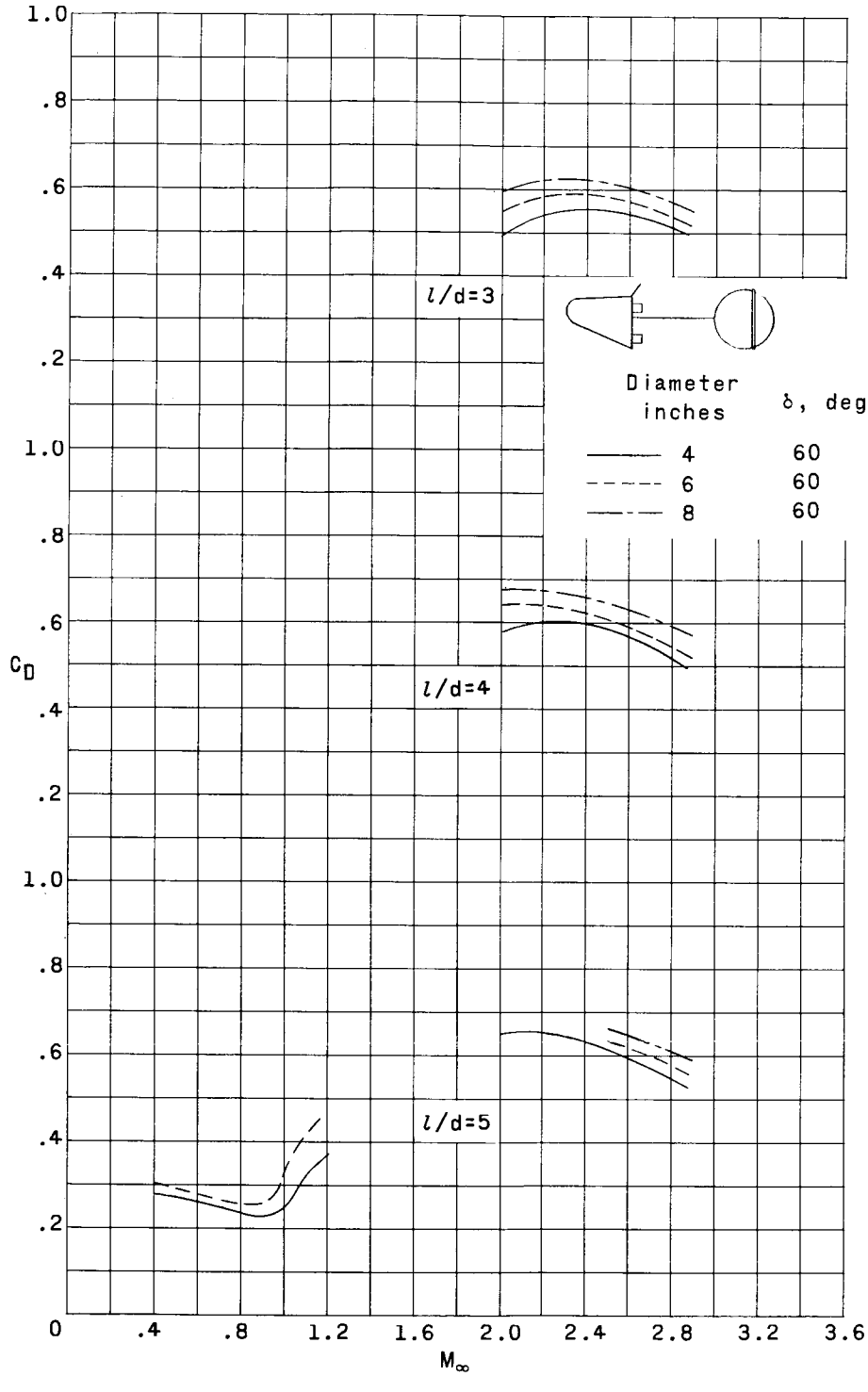

(c) Concluded.

Figure 17.- Concluded.

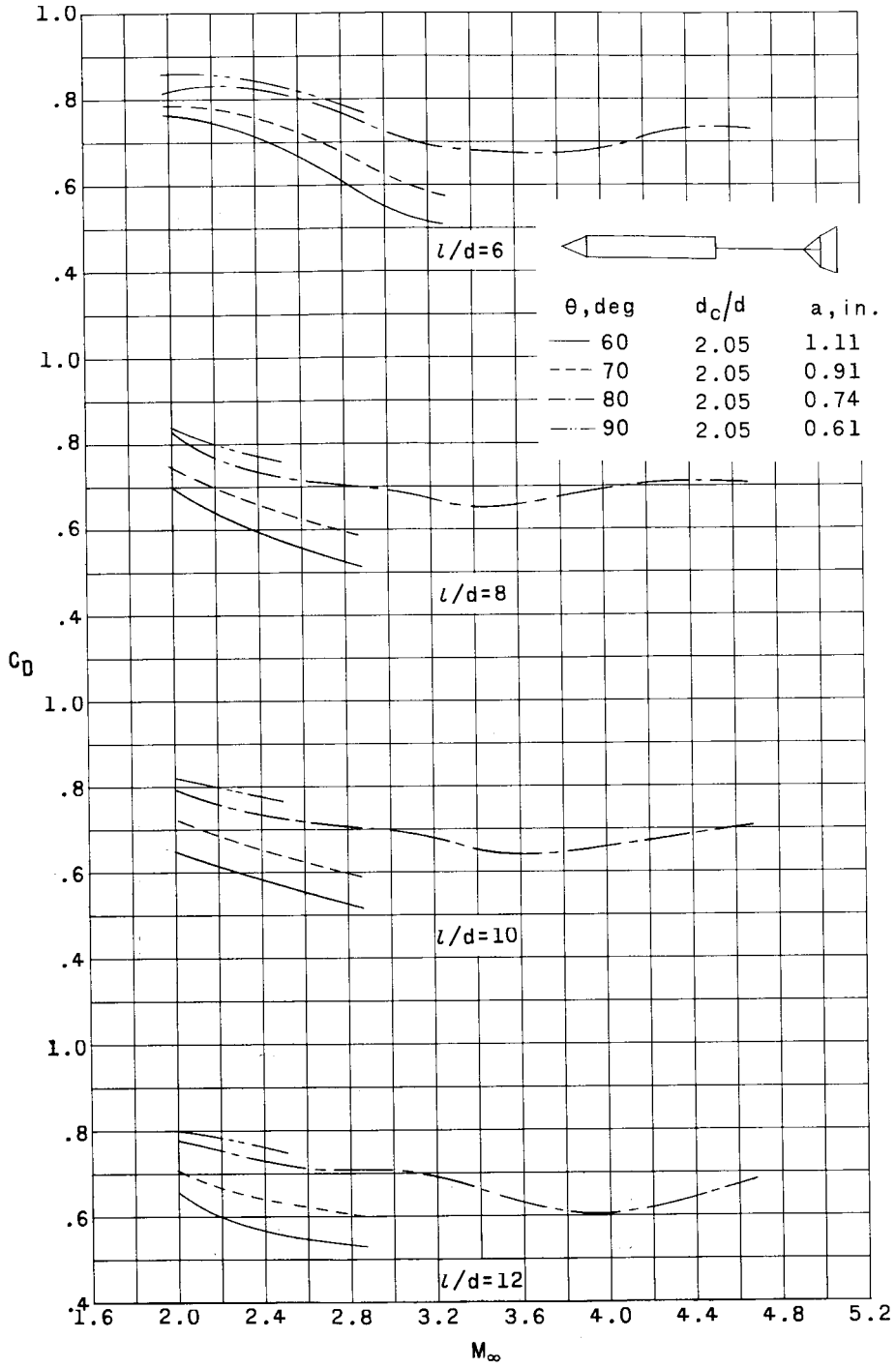

(a) Space vehicle A.

Figure 18.- Variation of drag coefficient with Mach numbers for 60°, 70°, 80°, and 90° conical rings at various tow-cable lengths.

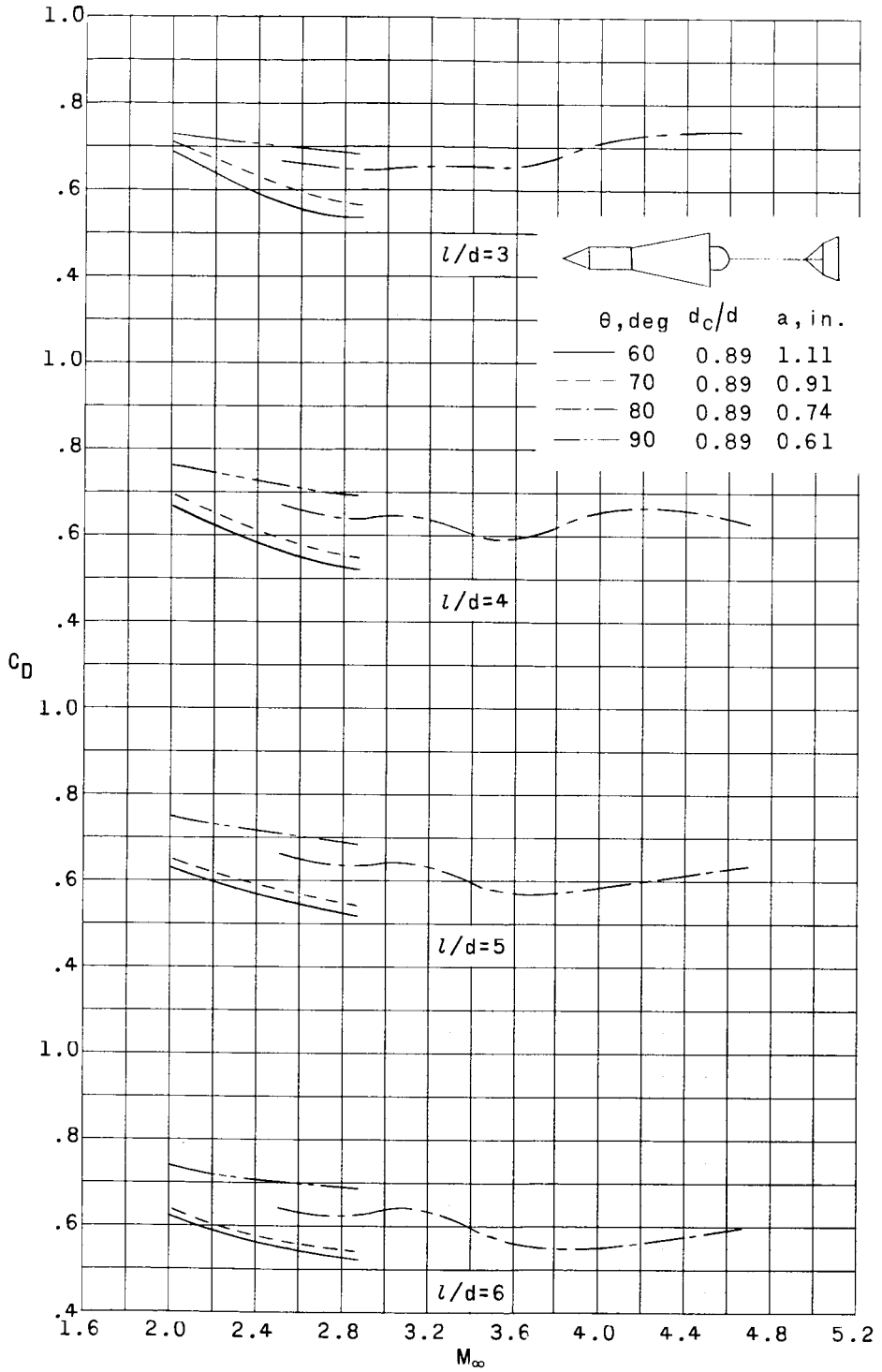

(b) Space vehicle B.

Figure 18.- Continued.

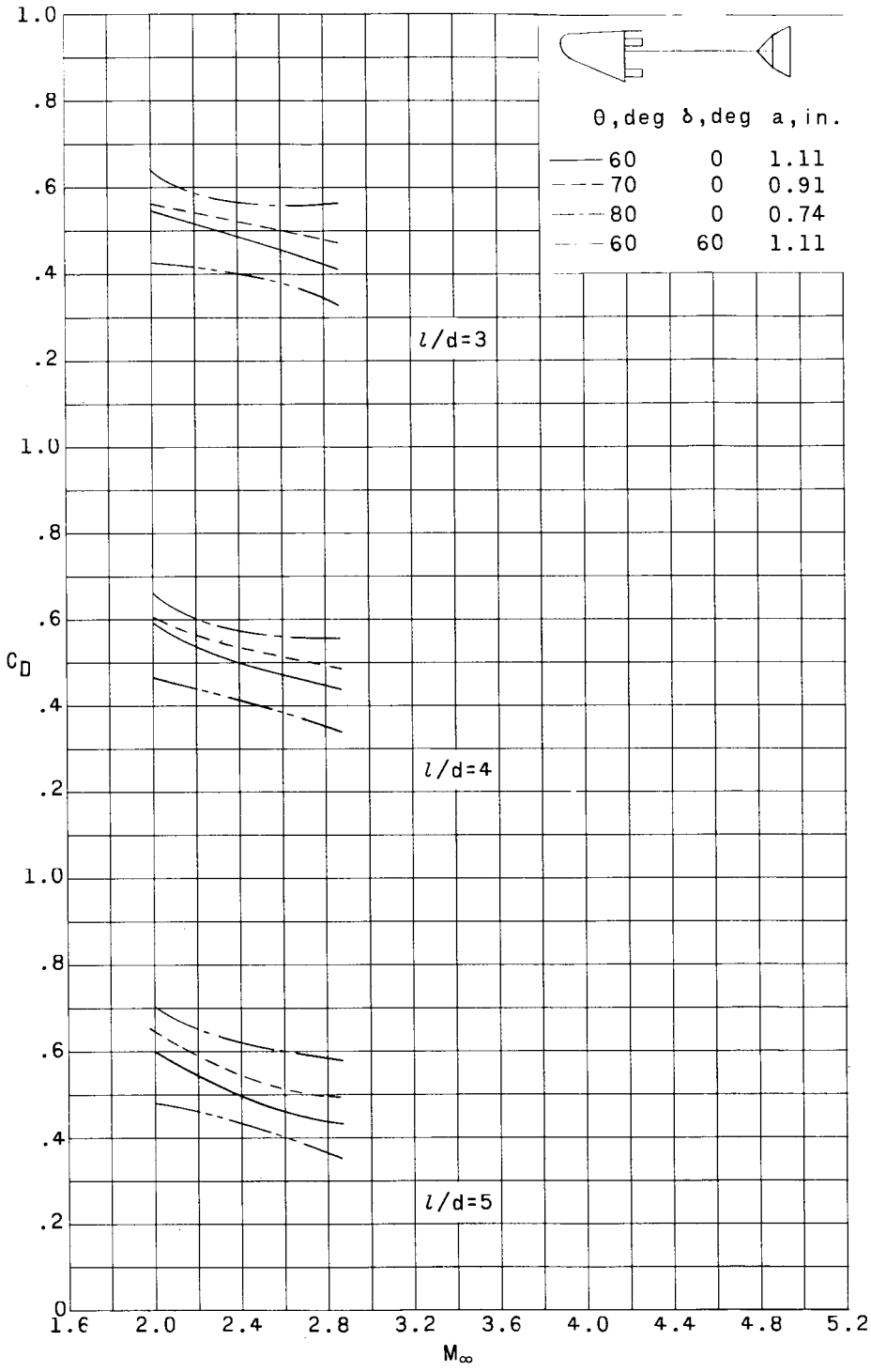

(c) Space vehicle C.

Figure 18.- Concluded.

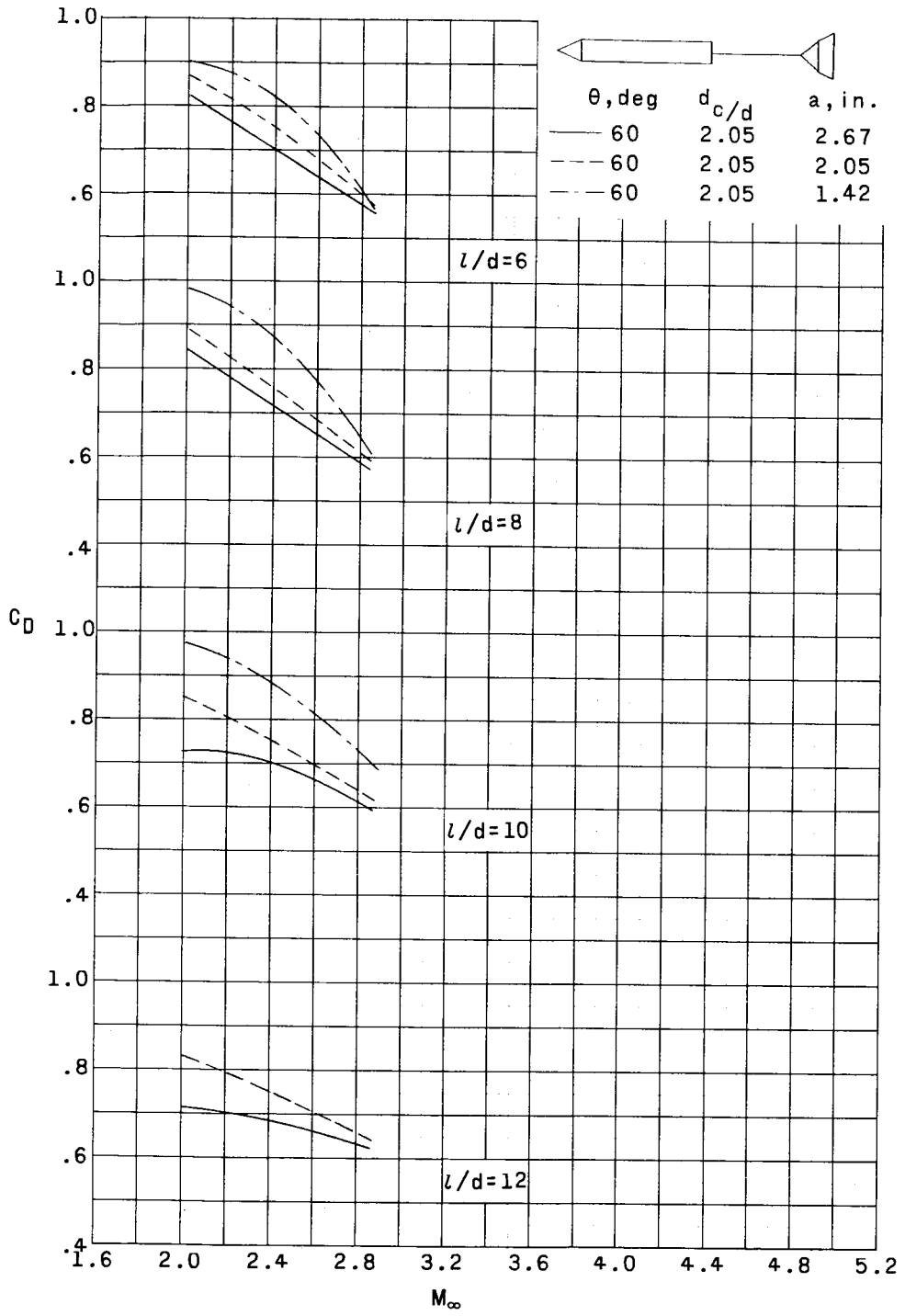

(a) Space vehicle A.

Figure 19.- Variation of drag coefficient with Mach number for 60° modified cones at various tow-cable lengths.

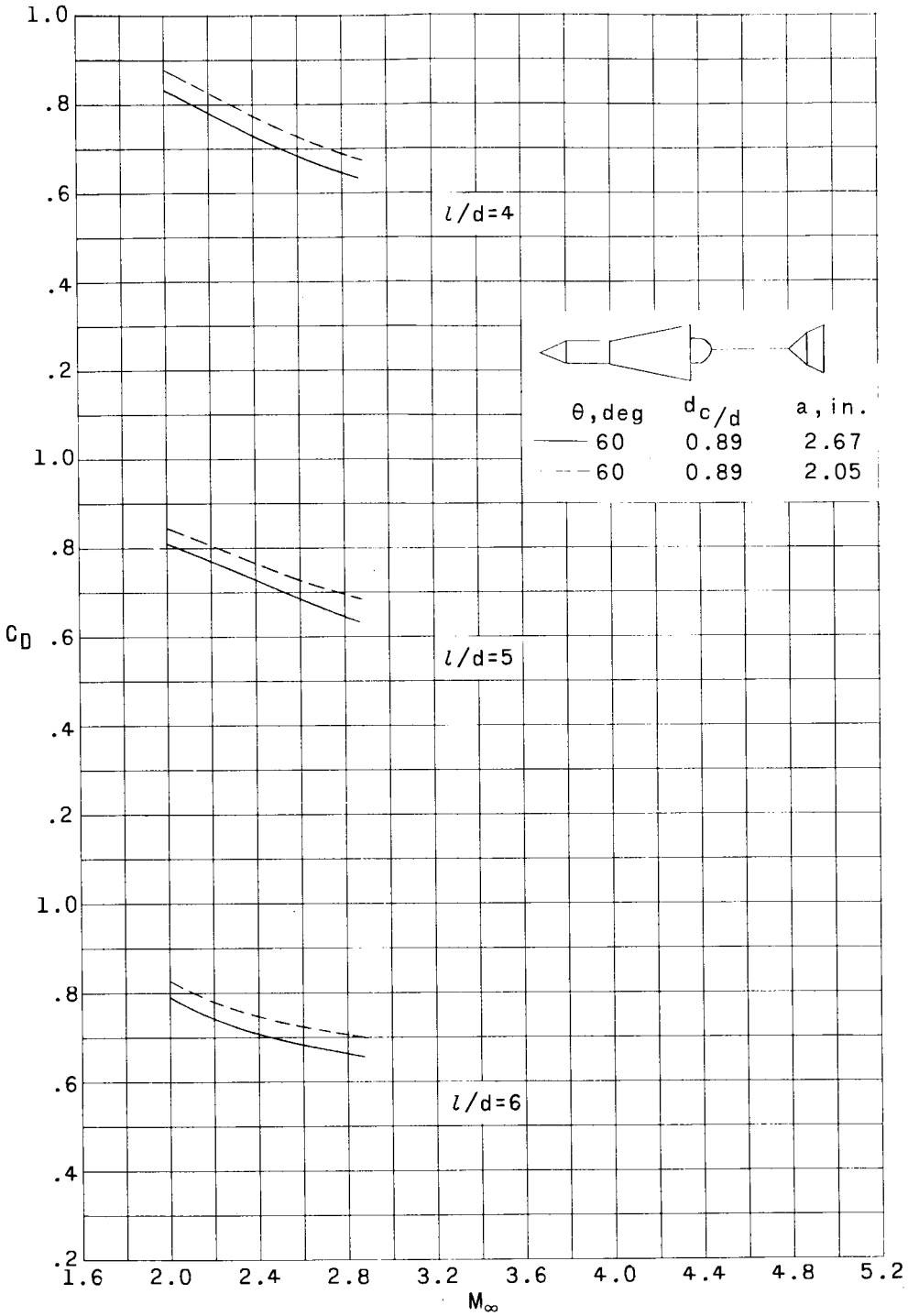

(b) Space vehicle B.

Figure 19.- Continued.

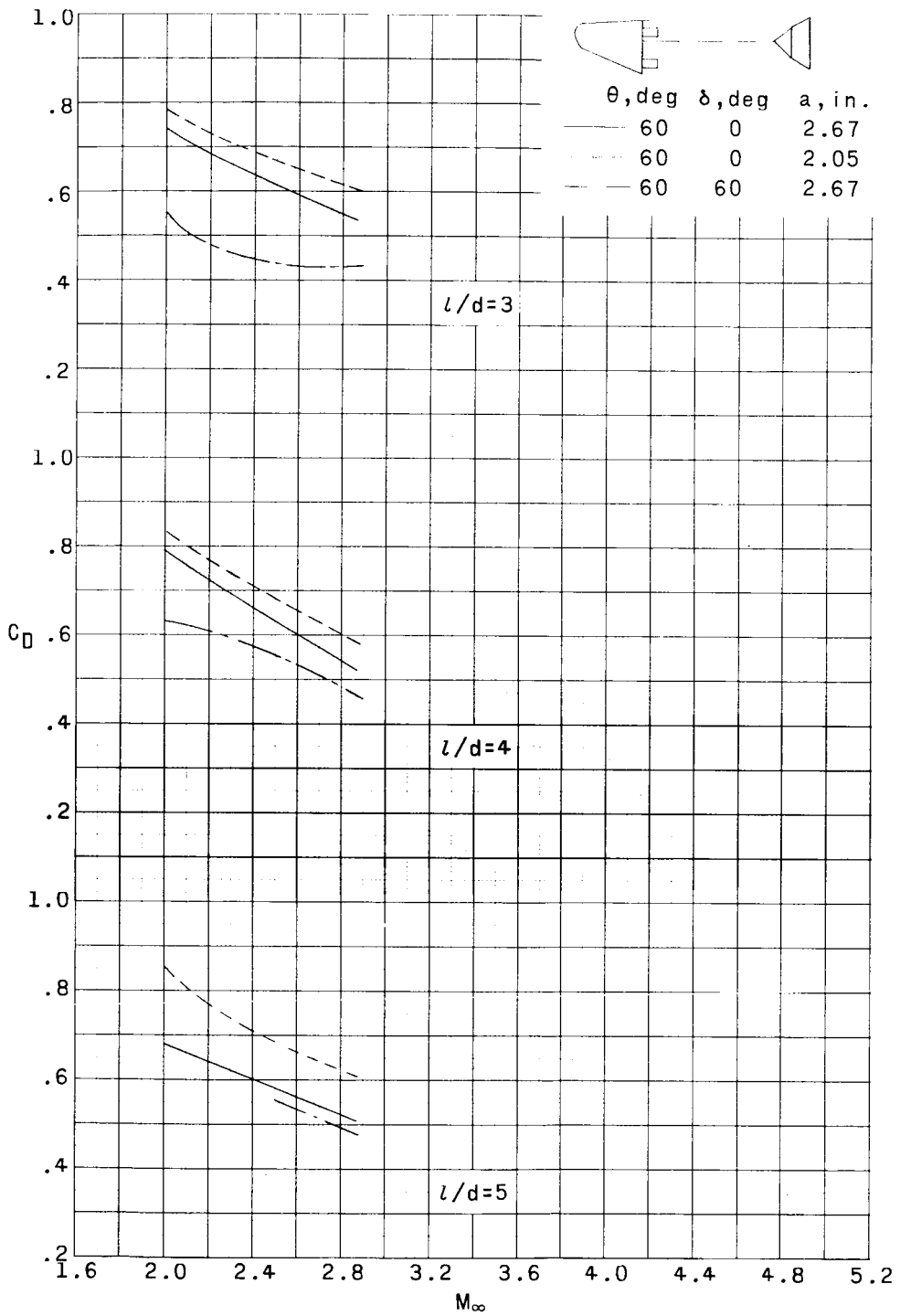

(c) Space vehicle C.

Figure 19.- Concluded.

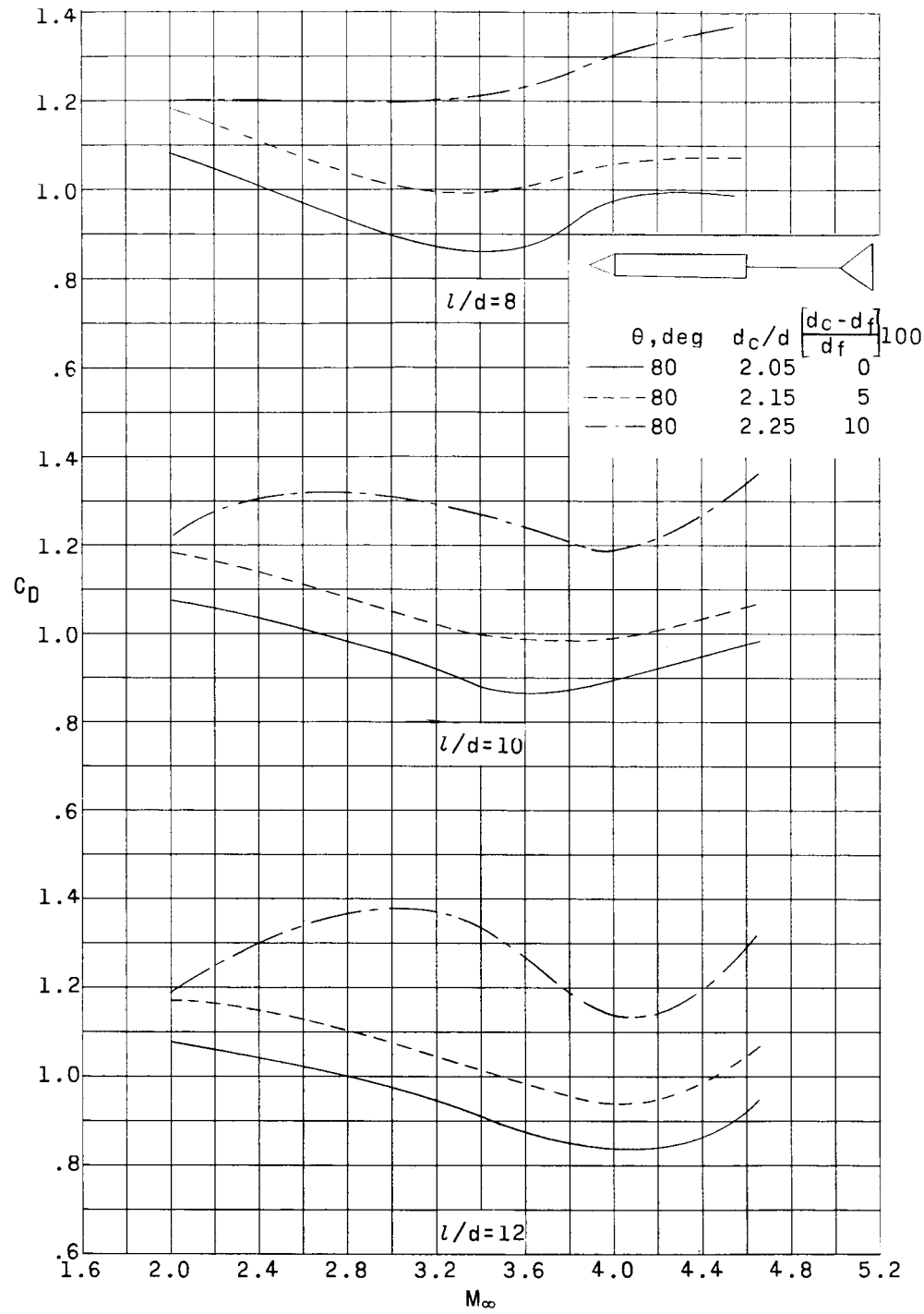

(a) Space vehicle A.

Figure 20.- Variation of drag coefficient with Mach number for 80° modified cone at various tow-cable lengths.

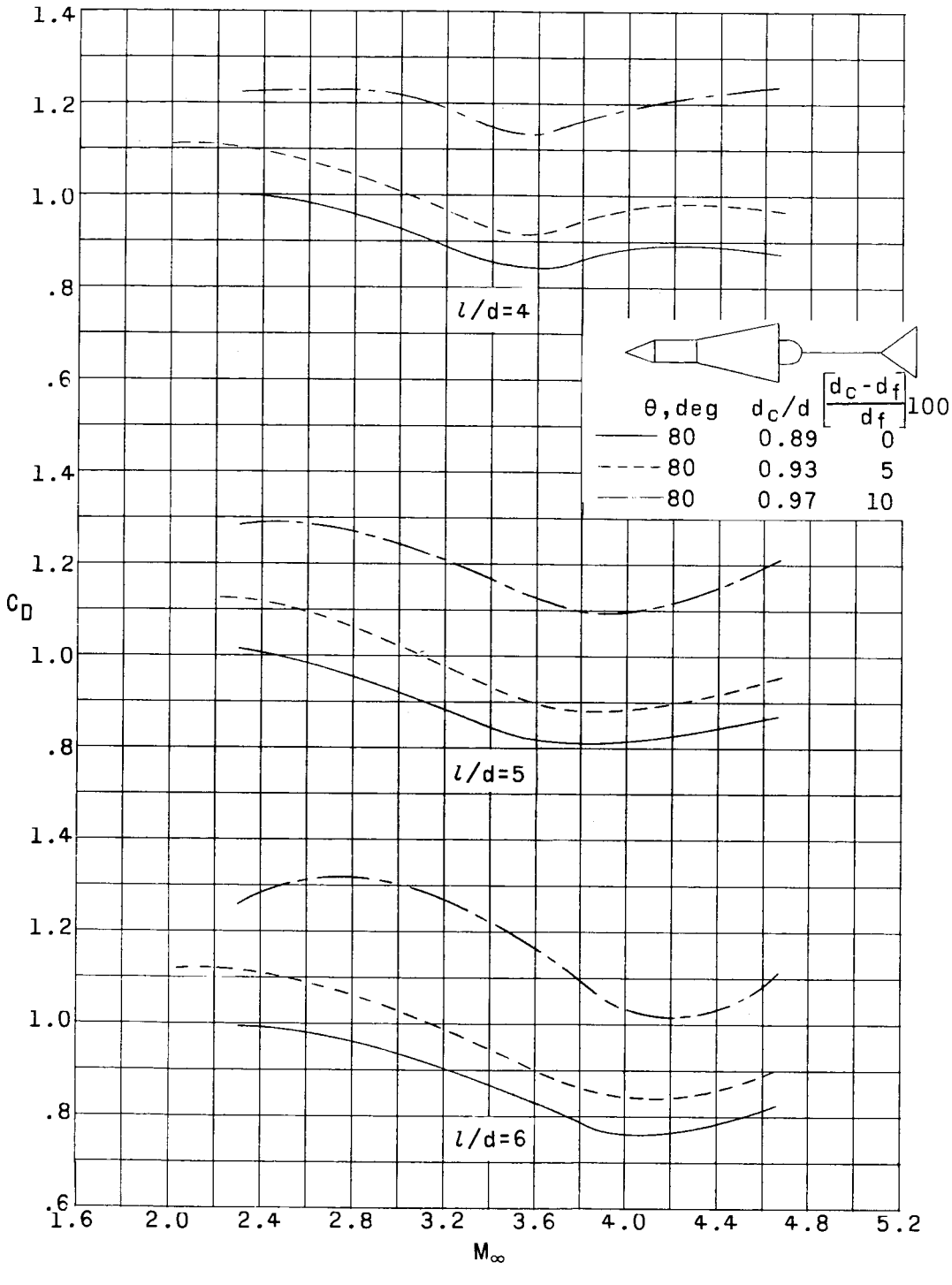

(b) Space vehicle B.

Figure 20.- Concluded.

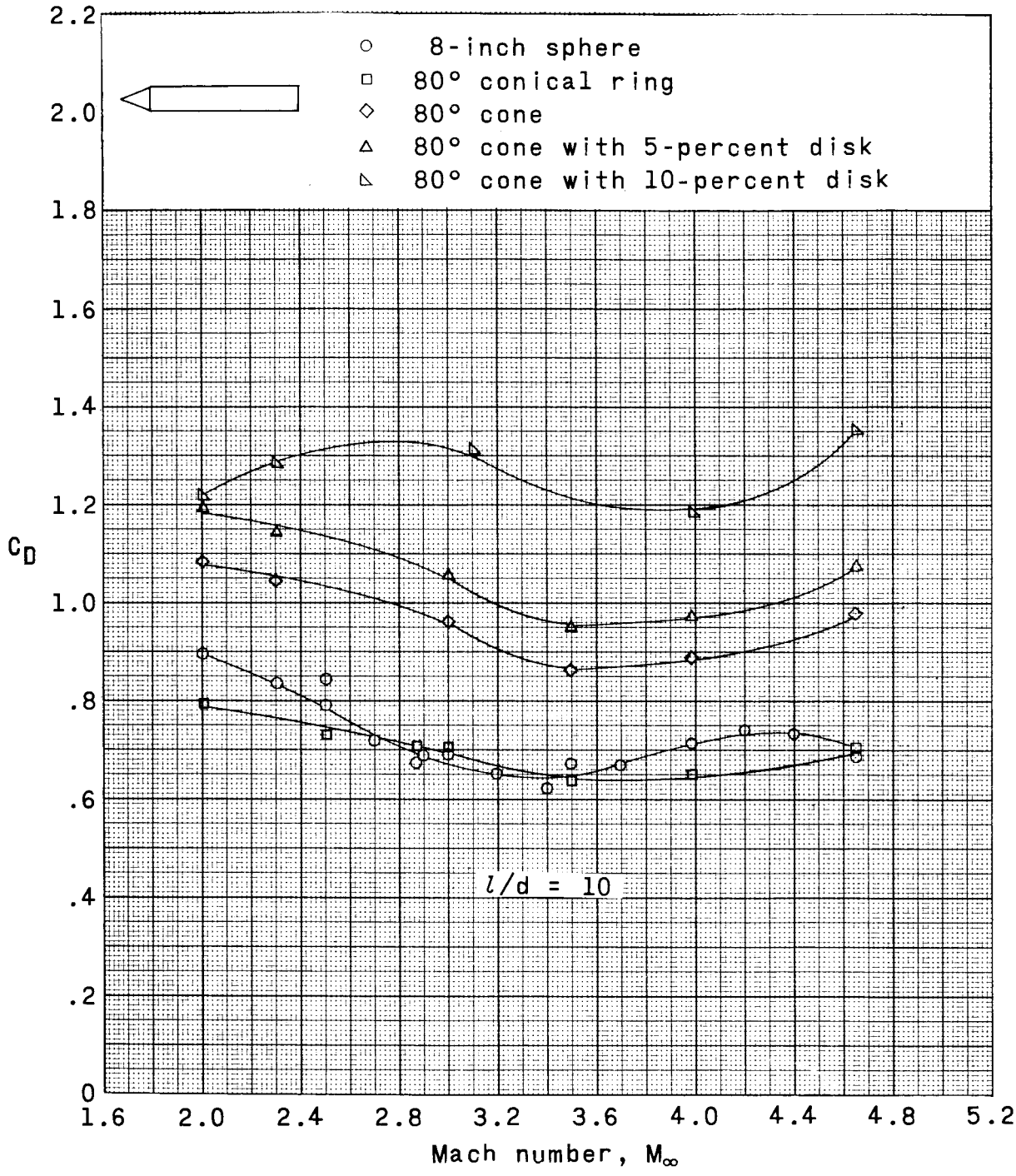

(a) Space vehicle A.

Figure 21.- Comparison of drag coefficients for various stable decelerators through a Mach number range.

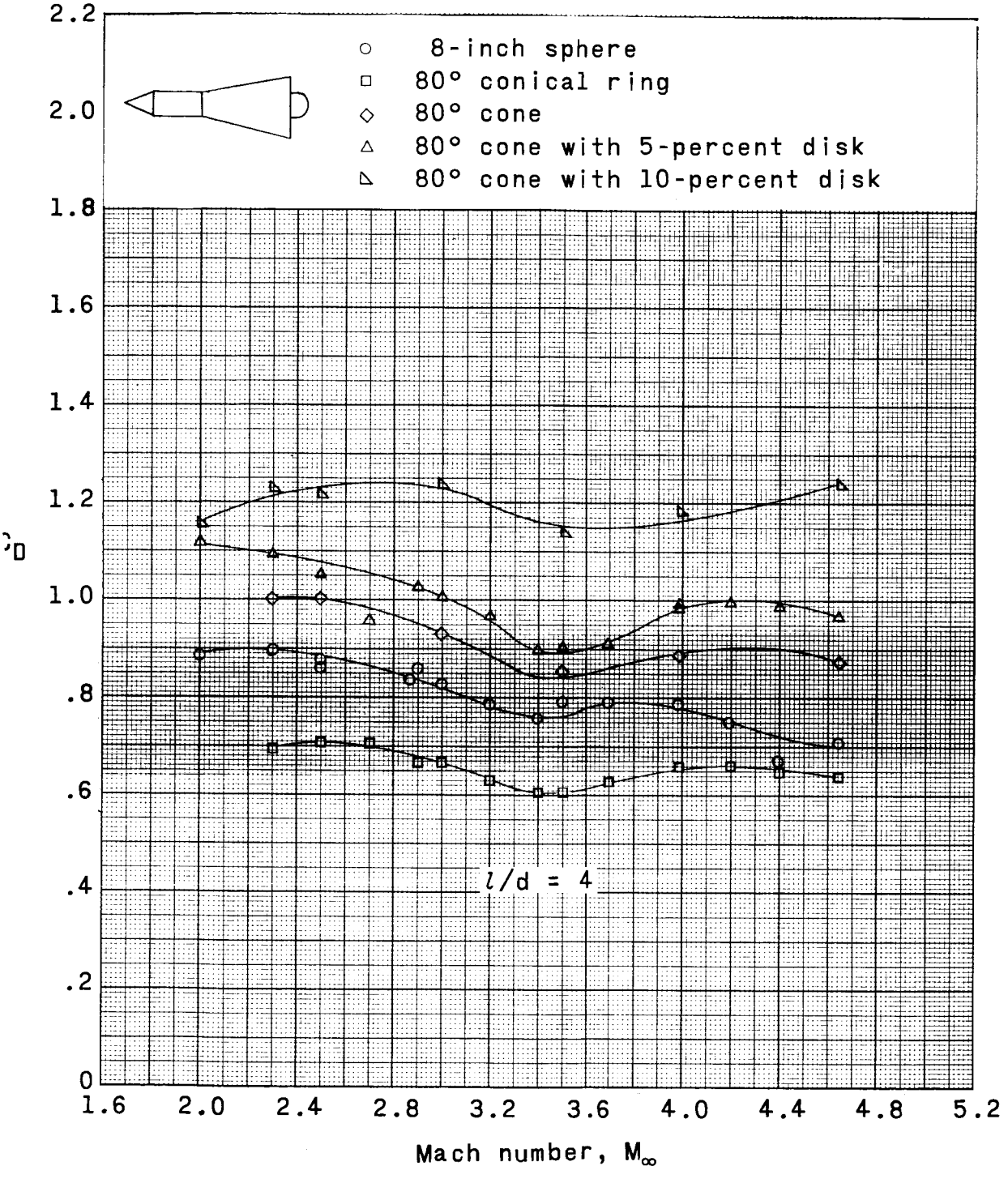

(b) Space vehicle B.

Figure 21.- Concluded.